

Theory of the soft-x-ray edge problem in simple metals: historical survey and recent developments

K. Ohtaka

Laboratory of Applied Physics, Chiba University, Yayoi-cho 1-33, Chiba-shi, 260 Japan

Y. Tanabe

Physics Laboratory, Japan Women's University, Bunkyo-ku, Tokyo 112, Japan

In the first half of this article, theoretical treatments of the infrared divergence involved in the edge problem of soft-x-ray absorption, emission, and photoemission spectra of simple metals are reviewed historically. In the second half, recent developments in the work of the present authors using the Fermi golden rule are described to show that the method permits an analytical treatment and provides exact results for various aspects of the edge problem.

CONTENTS

List of Symbols	930	G. Approaches to an exact solution of the MND problem	949
I. Introduction	931	1. Determinantal formulation of Combescott and Nozières	949
II. The Mahan-Nozières-DeDominicis (MND) Problem	933	2. Dispersion-integral approach of Mahan and co-workers	950
III. Historical Survey of the MND Problem	937	3. Fermi-golden-rule approach of Ohtaka and Tanabe	950
A. Mahan's treatment of exciton effects in a degenerate semiconductor	937	IV. Formulation for $T=0$	952
B. Perturbational treatment with respect to V	938	A. Wave functions before and after the transition	952
1. Mahan's treatment of core-level x-ray photoemission spectra	938	B. Response function for the photoemission spectrum	952
2. XAS and XES as dealt with by Mizuno, Ishikawa, and Ohmura	938	C. X-ray absorption spectrum	954
3. The finite-temperature effect treated by Ferrel	939	D. X-ray emission spectrum	955
C. Exact analytical treatment in terms of phase shift	939	V. Formulation and Results for $T>0$	956
1. Field-theoretical approach of Roulet, Gavoret, and Nozières	939	A. Description of the method	956
2. Asymptotic formulas of Nozières and DeDominicis	939	B. Results	957
3. Extension to the finite-temperature case by Anderson and Yuval	941	VI. Expressions for Moments	958
D. Comments on the results of Nozières and DeDominicis	941	VII. Reduction of Formulas in the Case of a Contact Potential	959
1. Friedel's comment	941	A. Dispersion integrals	959
2. Hopfield's interpretation of the critical exponents	942	B. Expressions for $A(t)$ and $I_0(t)$ at $T=0$	961
E. Anderson's orthogonality theorem	943	C. Expressions for $A(t)$ and $I_0(t)$ at $T>0$	961
1. Anderson's treatment	943	VIII. Edge Behaviors	962
2. Treatments of Rivier and Simanek and of Hamann	943	A. Asymptotic solution of the integral equation	962
3. Extension of Yamada and Yosida	944	B. Behaviors at $T=0$	963
F. Numerical treatments	944	C. Behaviors at finite T	964
1. Treatment of Kotani and Toyozawa	944	D. Critical amplitude and the orthogonality theorem	965
2. Analysis of Grebennikov, Babanov, and Sokolov	945	E. Derivation of power law following Feldkamp and Davis	965
3. Approaches of Schönhammer and Gunnarsson	946	IX. Modification Due to the Presence of a Bound State in the Excited Configuration	966
4. Approach of Swarts, Dow, and Flynn	946	A. Separation into main and secondary bands	966
5. X-ray photoemission spectra as treated by Feldkamp and Davis	947	B. Integrated intensities	967
6. Treatments of Mahan and of von Barth and Grossmann	947	C. Critical exponents	967
7. Numerical renormalization-group approach of Oliveira and Wilkins and Cox <i>et al.</i>	948	D. Critical amplitudes	968
		E. Expression for C_0	969
		X. Other Topics	969
		A. Pairwise expansion of the response functions	969
		B. Approximate formulas based on the single-particle picture	971
		C. Generalized power law	972

XI. Numerical Results	973		
A. Magnitude of C_0 [Eq. (8.43) in the absence of a bound state and Eq. (9.53) in the presence of one]	974	I_A	the excited configuration
B. Critical amplitudes for x-ray photoemission and absorption [Eqs. (9.49)–(9.52)]	975	I_E	integrated intensity of XAS
C. Integrated intensities [Eq. (9.22) for x-ray photoemission and Eq. (9.31) for x-ray absorption spectra]	976	$I(\omega)$	integrated intensity of XES
D. Exact line shape at $T=0$ [Eqs. (4.12), (4.24), (4.25), and (7.30) for photoemission and Eqs. (4.28), (4.42), and (7.31) for XAS]	976	$I_{\text{main}}(\omega)$	x-ray-absorption spectrum or emission spectrum
E. Pairwise series expansion [Eqs. (10.8) and (10.9)]	978	$I_{\text{main}}(t)$	absorption spectrum of the main band
F. Single-particle formulas for XAS [Eqs. (10.14)–(10.20) and Eq. (10.23)]	978	$I_{\text{sec}}(\omega)$	response function yielding $I_{\text{main}}(\omega)$
G. Temporal development of $\mathcal{A}(t)$ and $I_0(t)$ [Eqs. (7.30) and (7.31)]	978	$I_{\text{sec}}(t)$	absorption spectrum of the secondary band
H. Generalized power-law formula [Eq. (10.27) for photoemission and Eq. (10.28) for XAS and XES]	979	$I_0(\omega)$	response function yielding $I_{\text{sec}}(\omega)$
I. Thermal broadening and comparison with experiments on quantum wells [Eqs. (7.38) and (7.39)]	980	$I_0(t)$	spectrum of photoexcited electron or open-line Green's function
XII. Application of the MND Model to Real Systems	984	$I_f(\omega)$	response function for $I_0(\omega)$
XIII. Summary	989	$I_i(\omega)$	final-state rule absorption intensity
Acknowledgments	989	$I_o(\omega)$	initial-state rule absorption intensity
References	989	k	orthogonal final-state rule absorption intensity
		M	index for the band state in the ground configuration
		m	number of band states above the Fermi level
		N	index for the band state below the Fermi level in the ground configuration
		\mathcal{N}	number of band states below the Fermi level
		\mathcal{N}_{eff}	total number of band states ($=N+M$)
		$N(\varepsilon)$	effective total number of band states [$=N(0)W_b$]
		$N(0)$	density of states of the conduction band in the ground configuration
		N_k	density of states of the conduction band at the Fermi level
		$P(\omega)$	$N(\varepsilon_k)$
		$P(t)$	x-ray photoemission spectrum or inverse photoemission spectrum
		$P_{\text{main}}(\omega)$	response function yielding $P(\omega)$
		$P_{\text{main}}(t)$	spectrum of the main photoemission band
		$P_{\text{sec}}(\omega)$	response function yielding $P_{\text{main}}(\omega)$
		$P_{\text{sec}}(t)$	spectrum of the secondary photoemission band
		T	response function yielding $P_{\text{sec}}(\omega)$
		V	temperature or thermal energy kT ($k=1$)
		$V_{kk'}$	minus the contact-type core-hole potential
		W_b	(kk') matrix element of the core-hole potential
		W	total bandwidth of the conduction band ($=D-\bar{D}$)
		w	dipole-moment operator for the total electrons in the system
		w_i	w_{kc} with k dependence neglected
		w_{kc}	dipole-moment operator for the i th electron
		$w_{\kappa c}$	matrix element of dipole-moment operator ($=\langle \varphi_k w_i \varphi_c \rangle$)
		Z	matrix element of dipole-moment operator ($=\langle \psi_\kappa w_i \varphi_c \rangle$)
		α	partition function of conduction electron
		β	$2\delta(0)/\pi$
			critical exponent for XAS and XES

LIST OF SYMBOLS

Some of the symbols and abbreviations that frequently appear in the text are summarized here.

$a_{\kappa k}$	overlap integral between φ_k and ψ_κ
b	index for the one-particle states below the Fermi level in the ground configuration
C_0	prefactor of the orthogonality theorem
D	upper edge of the conduction band measured from the Fermi level
\bar{D}	lower edge of the conduction band measured from the Fermi level
D_c	a cutoff energy of the order of the Fermi energy or the bandwidth
E^0	ground-state energy of N conduction electrons in the ground configuration
E_c^0	ground-state energy including the energy of core electron in the ground configuration
E^{+0}	ground-state energy of N conduction electrons in the excited configuration
E_{Fermi}	Fermi energy measured from the bottom of conduction band ($= \bar{D} $)
f_k	$f(\varepsilon_k)$
$f(\varepsilon)$	Fermi distribution function for the energy ε
$\bar{f}(\varepsilon)$	$1-f(\varepsilon)$
\mathcal{H}	Hamiltonian for the conduction electrons in the ground configuration
\mathcal{H}_c	Hamiltonian for the conduction electrons plus the core electron in the ground configuration
\mathcal{H}^+	Hamiltonian for the conduction electrons in

γ	index for the band state above the Fermi level in the excited configuration	Ψ^0	many-body wave function for the ground state of conduction electrons in the excited configuration
$\delta(\varepsilon)$	phase shift at energy ε of s -like conduction band	Ψ_F	many-body wave function for the excited state of conduction electrons in the excited configuration
$\delta(0)$	phase shift at the Fermi level of s -like conduction band	Ω	photon frequency
δ_k	$\delta(\varepsilon_k)$	ω	photon frequency or energy ($\hbar=1$) measured from the renormalized (unrenormalized in Sec. XI) absorption threshold ($=\Omega-\omega_{\text{th}}^0$)
$\delta_l(\varepsilon)$	phase shift of angular momentum l at energy ε	ω_{th}^0	absorption threshold renormalized by ΔE^0 ($=\Delta E^0-\varepsilon_c$)
Δ	overlap integral between two ground states Φ^0 and Ψ^0 of N conduction electrons ($=\langle \Phi^0 \Psi^0 \rangle$)		
$\Delta\varepsilon$	level spacing at the Fermi level of the conduction band in the ground configuration [$=N(0)^{-1}$]		
ΔE^0	shift of the ground-state energy of N conduction electrons ($=E^{+0}-E^0$)		
ε_c	energy of a core electron relative to the Fermi level		
ε_F	position of the Fermi level [taken as the origin of single-particle energies ($\varepsilon_F=0$) except in Sec. XI]		
ε_κ	energy of the state κ of the conduction band in the excited configuration relative to the Fermi level		
ε_k	energy of the state k of the conduction band in the ground configuration relative to the Fermi level		
ε_λ	energy of the bound state below the conduction band relative to the Fermi level		
η	small positive number of adiabatic switching of the core-hole potential		
κ	index for the band state in the excited configuration		
λ	index for the bound state in the excited configuration		
μ	index for the band state below the Fermi level in the excited configuration		
σ	critical exponent of XPS or the orthogonality theorem		
φ_c	wave function of the core level		
φ_k	orbital for the band state k in the ground configuration		
Φ	many-body wave function of conduction electrons in the ground configuration		
Φ_c	many-body wave function of a state including the core electron in the ground configuration		
Φ^0	many-body wave function for the ground state of conduction electrons in the ground configuration		
Φ_c^0	many-body wave function for the ground state of the ground configuration including core electron		
ψ_κ	orbital for the band state κ in the excited configuration		
Ψ	many-body wave function of conduction electrons in the excited configuration		

I. INTRODUCTION

The study of x-ray-absorption spectra (XAS) and emission spectra (XES) has a long history beginning with the discovery of the x ray by Röntgen in 1895. It has contributed much to the founding of quantum mechanics and to the establishment of many basic concepts in atomic and solid-state physics (Compton and Allison, 1935). As early as the 1930s, it was already recognized that XAS and XES could provide us with valuable information about the structure of atoms and solids. Surprisingly enough, the importance of many-body effects in x-ray spectra was already appreciated at that time (Wentzel, 1925a, 1925b; Richtmeyer, 1936). For example, to interpret some satellite peaks occurring in the lower-energy side of the characteristic K , L , or M emission line, creation of two or more holes in the atomic core levels accompanying the emission was suggested. This implies that, in addition to simple optical processes involving single-particle excitation, complicated processes occur (e.g., Auger and shakeup processes) that can be explained only through the calculation of the transition matrix element by the use of many-electron wave functions. However, the 1930s and 1940s had not yet arrived at a quantitative understanding of the features of the satellite structures, because this entailed the difficult task of handling many-body problems; a full treatment had to wait until the development of sophisticated techniques to include higher-order perturbation effects. Experimentally, the situation was nearly the same: x-ray and soft-x-ray spectroscopy required a good light source, intense as well as tunable and monochromatic, in order to yield data deserving of a detailed theoretical study.

It was not until high-speed computers and field-theoretic techniques were developed on the theoretical side and synchrotron orbital radiation (SOR) came into use on the experimental side that x-ray spectroscopy was revived as an active subject of modern solid-state physics (Tomboulou and Hartman, 1956; Tomboulou, 1957). In his review paper, Paratt (1959) introduced important concepts in the interpretation of XAS and XES data—ejected electron and valence electron configurations, both modified due to the presence of a core hole left behind

after core-electron ejection. Clearly, he had in mind the importance of many-body effects. Indeed, he was considering precisely the final-state interaction in the optical processes, in our terminology, and the concepts he introduced have played central roles in clarifying the Fermi edge anomalies in XAS and XES, investigated so actively ever since.

Although Paratt's paper was written just after the introduction of the BCS theory of superconductivity, the possibility of observing in x-ray spectra the infrared or logarithmic divergence, that is, the edge anomaly due to the presence of long-wavelength excitations across the sharp Fermi level, had not yet been realized. Thus it was only when SOR began to be employed extensively as a light source in the soft-x-ray region (Madden, 1974) and provided us with spectra displaying unambiguous edge anomalies that a consensus developed concerning the edge singularity of XAS and XES, that it was indeed an intrinsic effect connected closely with infrared divergence.

It was Mahan (1967a, 1967b) who showed that the essence of the edge problem was indeed logarithmic divergences in each term of the perturbation series, as a result of the final-state interaction between the core hole and conduction electrons. He predicted a power-law frequency dependence at the threshold of the x-ray photoemission spectra. Independently of Mahan, Mizuno and Ishikawa (1968) also correctly analyzed the XAS and XES data by a perturbation treatment with respect to the strength of the core-hole potential. The analysis of these authors was then extended and refined by Nozières and his collaborators. In particular, Nozières and DeDominicis (1969) succeeded in deriving an exact analytical expression for the exponent of the power-law edge behavior. The edge spectrum of XAS and XES can be written in the form

$$I(\omega) = b\omega^\beta, \quad (1.1)$$

where ω is the frequency measured from the edge or threshold, as defined below in Eq. (2.10). We call β the critical exponent and b the critical amplitude. Nozières and DeDominicis derived an exact expression for β ,

$$\beta = -2[\delta_{l_0}(0)/\pi] + \sum_l 2(2l+1)[\delta_l(0)/\pi]^2, \quad (1.2)$$

where $\delta_l(0)$ is the phase shift of the partial wave l at the Fermi level and l_0 defines the channel excited optically. Equations (1.1) and (1.2) have been important not only for an understanding of the x-ray problem in simple metals, but also for their ability to clarify other fundamental problems in the theory of condensed-matter physics such as the Kondo effect [see, for example, the review by Yosida and Yoshimori (1973)].

Later, Doniach and Sunjić (1970) showed that the theory of Nozières and DeDominicis led to the formula for x-ray photoemission intensity

$$P(\omega) = c\omega^{\sigma-1}, \quad (1.3)$$

where the critical exponent σ is

$$\sigma = \sum_l 2(2l+1)[\delta_l(0)/\pi]^2. \quad (1.4)$$

Since the derivation of Nozières and DeDominicis, the edge problem has been studied with the aim of determining the energy range in which their results have practical and quantitative validity. To put it another way, attempts have been made to obtain expressions for the critical amplitudes b and c in the above formulas or, further, an exact solution of the "MND problem"—so called after Mahan, Nozières, and DeDominicis.

One way to achieve this purpose is to use numerical techniques. This has turned out to be fruitful. For example, Dow and Flynn (1980) and Feldkamp and Davis (1980) were able to determine the amplitude c of the x-ray photoemission formula [Eq. (1.3)] through their attempts to simulate the final-state interaction numerically. Moreover, Oliveira and Wilkins (1981, 1985) and Cox *et al.* (1985) obtained for the first time reliable numerical values for the critical exponents and amplitudes of the edge spectra by using the renormalization-group formalism. Another way is to take a purely theoretical approach to an exact solution. It was Pardee and Mahan (1973) who first showed that the absorption and emission cross sections to and from an electronic state with energy ω above the threshold can be expressed in terms of the "dispersion integrals" defined by ($z = \omega + i0$),

$$X(z) = \exp \left[-\frac{1}{\pi} \int_0^D \frac{\delta(\epsilon)}{z-\epsilon} d\epsilon \right], \quad (1.5)$$

$$\bar{X}(z) = \exp \left[-\frac{1}{\pi} \int_{\bar{D}}^0 \frac{\delta(\epsilon)}{z-\epsilon} d\epsilon \right].$$

The expressions here are given for the case of an s -wave conduction band [$\delta(\epsilon) = \delta_{l=0}(\epsilon)$ in Eq. (1.2)] with the Fermi level taken as the origin of energy, where D and \bar{D} are the upper and lower edges of the conduction band, respectively. The dispersion integrals are the key quantities of the MND problem. Indeed, it can be shown that, in the approximation of putting $\delta(\epsilon)$ equal to $\delta(0)$, $X(z)$ and $\bar{X}(z)$ exhibit a power-law singularity in the limit $\omega \rightarrow 0$ and this eventually leads to the power-law edge behavior.

The soft-x-ray absorption and emission problem initiated by Mahan finds its most complete solution to date in the work of the present authors. This work is complete in the sense that the edge behavior is expressed in an exact analytical form including the prefactor b of Eq. (1.1), an integral equation is derived that yields exact spectra over the whole range of frequency, and, finally, a formulation is also given for the case of finite temperatures. In the view of the present authors, the solution thus obtained seems to have covered almost every aspect of the MND problem and this is the reason we present in Secs. IV–XI an overview of our results.

This review covers a series of papers by the present authors published in *The Physical Review* (Ohtaka and Tanabe, 1983, 1984, 1986, 1989; Tanabe and Ohtaka, 1984, 1985, 1986; Tanabe, 1986) and *Journal of the Physical Society of Japan* (Kita, Ohtaka, and Tanabe, 1987a, 1987b) on the treatments of XAS, XES, and x-ray photoemission spectroscopy in simple metals. We intend to reproduce the main results given therein, together with their brief derivation. However, before presenting them, we shall review, essentially in historical order, important papers by other authors who introduced, developed, and refined the edge problem.

The field of x-ray spectroscopy in the 1960s and early 1970s is reviewed in the book edited by Azároff (1974). In particular, the article by Hedin (1974) on the many-body problem briefly describes the conclusions of Nozières and DeDominicis. With the rapid increase in the use of synchrotron orbital radiation, there have been several review articles on SOR physics in which the MND problem is briefly treated (for example, Brown, 1980; Brown and Doniach, 1980; Bassani and Altarelli, 1983). Among works concentrating especially on the edge problem, we may cite a number of sources. One is Mahan's study (1975) of the earlier treatments, including those of Mahan, Nozières, and DeDominicis. Mahan's textbook on the many-body problem (Mahan, 1981) presents a fairly complete description of the theories of Mahan, Nozières, and DeDominicis as well as those of Combescott and Nozières (1971). In the review of Kotani and Toyozawa (1979) on the final-state interaction, there is a section treating the MND problem as well as their own treatments of incomplete inner shells. The article by Almladh and Hedin (1983) is quite comprehensive, concentrating on many-body aspects of the theory, including the effects of electron correlation on the edge anomaly. The brief review by Wilkins (1982) is also useful on topics related to the exact theory. Very recently, Mahan (1988) reviewed developments in the field since Combescott and Nozières. His review is, however, rather short. On the experimental side, see Brown (1975) and Wertheim and Citrin (1978). The review paper by Citrin *et al* (1979) compares experiments carried out in the 1970s with the MND theories. For more recent experiments, however, no extensive review article seems to be available as far as the authors are aware. We cite here only articles found in the books listed above on synchrotron orbital radiation.

The present article is organized as follows. In Sec. II, the basic outline of the edge problem is presented. Section III is devoted to a review of the important papers prior to our work. At the end of Sec. III, we give a preview of the subsequent sections. Results obtained by the present authors will be given in Secs. IV–X. In Sec. XI, we present some numerical results based on our theories, including an analysis related to the recent optical experiments in n -type semiconducting quantum wells. In Sec. XII, we discuss the MND model in relation to experimental results in real systems. Section XIII offers a final

summary.

Readers who are interested only in the recent developments introduced by the present authors may skip Sec. III, except for its subsection G.3, in which we outline our formulation and briefly summarize our results. Those who are not very interested in the mathematical details of the derivation may skip further and go directly to Sec. XI, after reading Secs. II and III.G.3. For a rough sketch of the approach of the present authors, it will suffice to read only Secs. IV, VII, VIII, and XI. Section XII, where the applicability of the MND model is discussed, will be useful to those interested in the experimental side of the soft-x-ray edge problem.

II. THE MAHAN-NOZIÈRES-DEDOMINICIS (MND) PROBLEM

We briefly recapitulate the soft-x-ray problem, taking the case of XAS as an example. This section also introduces some of the notation used repeatedly in what follows.

Suppose we have a system of $N + 1$ spinless electrons. The freedom of spin may easily be taken into account in the present spin-diagonal final-state interaction. (For the exchange-type final-state interaction, see Sec. XII.) Before the absorption of an x-ray quantum, we have one electron at a core level and N electrons in the conduction band. We call this electron configuration the ground configuration. The Hamiltonian for the conduction electrons of this configuration is given by

$$\mathcal{H} = \sum_k \varepsilon_k a_k^\dagger a_k . \quad (2.1)$$

Here the subscript k specifies the one-particle state of a band electron with energy ε_k and creation (annihilation) operator a_k^\dagger (a_k). When we are considering $(N + 1)$ electrons, including the core electron, we shall use the subscript c . For example, in

$$\mathcal{H}_c = \sum_k \varepsilon_k a_k^\dagger a_k + \varepsilon_c b^\dagger b \quad (2.2)$$

the energy of the core level is ε_c and its creation (annihilation) operator b^\dagger (b). Equations (2.1) and (2.2) represent the initial-state Hamiltonians in the case of absorption. The single-particle wave function, or the orbitals, specified by the index k in the ground configuration, is denoted by φ_k , while that for the core state is denoted by φ_c . For the many-body wave function in the ground configuration, we use the symbol Φ for \mathcal{H} and Φ_c for \mathcal{H}_c . Φ_c is the Slater determinant, with its dimension larger by one than Φ . When there is a need to emphasize the number of electrons, we sometimes use a notation such as $\mathcal{H}(N)$, $\Phi_c(N + 1)$, etc.

The core electron is excited to the conduction band by x-ray absorption. The system is now composed of $N + 1$ conduction electrons with an unoccupied core level. The Hamiltonian for this configuration—the excited configuration—is given by

$$\mathcal{H}^+ = \sum_k \varepsilon_k a_k^\dagger a_k + \sum_{k,k'} V_{kk'} a_k^\dagger a_{k'} . \quad (2.3)$$

This is the final-state Hamiltonian in the case of absorption (in the case of emission, it will be the initial-state Hamiltonian). Very often, a contact-type core-hole potential is assumed for $V_{kk'}$:

$$V_{kk'} = -V . \quad (2.4)$$

The parameter $-V$ defines the strength of the attractive core-hole potential ($V > 0$). The excited-configuration many-body wave function of Eq. (2.3) will be expressed by the symbol Ψ , and the single-particle eigenstates in the excited configuration will be specified by κ with the orbital function ψ_κ . They are obtained by diagonalizing the Hamiltonian equation (2.3). Notations like $\mathcal{H}^+(N+1)$ or $\Psi(N+1)$ will be used to stress the number of electrons involved.

Since the scattering of electrons due to a spherical potential is conveniently dealt with by means of a partial-wave expansion, it is practical to express the band orbital function as a superposition of partial waves. We regard the Hamiltonians \mathcal{H} and \mathcal{H}^+ as standing for the partial wave of s ($l=0$), p ($l=1$), \dots symmetry with a value of $V_{kk'}$ appropriate for that channel. The scalar quantum number k then specifies their eigenstates. When a core electron in the K shell is excited, its final state has p ($l=1$) symmetry, while that in the L shell jumps to the final state with s ($l=0$) or d ($l=2$). Of course, after a core hole is introduced, electrons in the conduction band are all influenced, irrespective of their angular momenta, as in ordinary potential scattering.

In adopting the model Hamiltonians \mathcal{H} , \mathcal{H}_c , and \mathcal{H}^+ , we have made many simplifying assumptions. Although a similar analysis for, say, a separable potential is not impossible, we treat the core-hole potential in this article mostly in the simplest form, given by Eq. (2.4). We are also considering an immobile core hole and neglect completely its recoil during the final-state interaction with conduction electrons. Another simplification is our neglect of the finite lifetime of the core hole and Coulomb correlation among conduction electrons. All these neglected effects must be taken into account in any serious attempt to obtain good agreement between theory and experiment. The Coulomb correlations are especially important in the sense that the actual magnitude of $V_{kk'}$ is determined by screening due to electronic correlation. Although we shall regard the parameter $V_{kk'}$ or $-V$ as a given quantity, standing effectively for the core-hole potential established self-consistently, and neglect the Coulomb effect altogether, its magnitude has to be chosen appropriately in a quantitative treatment.

We emphasize that the idealized form of the MND Hamiltonians, Eqs. (2.1) through (2.3), constitutes the essence of the soft-x-ray problem, especially the edge anomalies due to infrared divergence. We shall return in Sec. XI to these points neglected in the MND model, and attempt to compare the theory with experiment. More-

over, we discuss in some detail in Sec. XII the applicability of the MND model to real systems.

Now let us return to Eqs. (2.2) and (2.3). Consider the ground state Φ_c^0 [$=\Phi_c^0(N+1)$] of the ground configuration for N conduction electrons plus a core electron in their ground state. The state Φ_c^0 is expressed by a $(N+1) \times (N+1)$ Slater determinant. Let the state of the system after photoexcitation be denoted by Ψ_F [$=\Psi_F(N+1)$], with F running over all possible eigenstates of \mathcal{H}^+ [$=\mathcal{H}^+(N+1)$]. The cross section of the photoexcitation is given by the sum over F of the probabilities of a transition from Φ_c^0 to Ψ_F , i.e.,

$$I(\omega) = 2\pi \sum_F |\langle \Psi_F | \mathcal{W} | \Phi_c^0 \rangle|^2 \times \delta(E_F(N+1) - E_c^0(N+1) - \Omega) , \quad (2.5)$$

where Ω is the photon energy ($\hbar=1$ throughout the paper). See Eq. (2.12) for the relation between ω and Ω . In Eq. (2.5), $E_c^0(N+1)$ and $E_F(N+1)$ are $(N+1)$ -particle energies of Φ_c^0 and Ψ_F , respectively, and \mathcal{W} [$=\mathcal{W}(N+1)$] is the dipole-moment operator expressed as

$$\mathcal{W} = \sum_i w_i , \quad (2.6)$$

using the dipole-moment operator w_i for the i th electron. By definition, we may write

$$E_c^0(N+1) = \varepsilon_c + \sum_m \varepsilon_m \equiv \varepsilon_c + E^0 , \quad (2.7)$$

where the subscript m is used for the one-particle state k below the Fermi level and E^0 thus defines the ground-state energy for N electrons in the conduction band in the ground configuration. In the case of finite temperatures, we shall have to consider one-electron states thermally excited above the Fermi level. The symbol $\{b_s\}$ will be employed for them. See Fig. 1 for the notation used for single-particle states of the ground configuration and excited configuration.

The energy $E_F(N+1)$ of Eq. (2.5) is also given by the sum of $(N+1)$ single-particle energies ε_κ for \mathcal{H}^+ ; these are slightly lowered from those of the initial states because of the core attraction, as shown in Fig. 1. As in the case of k , we discriminate κ according to whether the corresponding state is above or below the Fermi level. For states above the Fermi level, we use $\{\gamma_s\}$, and for those below, $\{\mu_s\}$. Since the position of the Fermi level ε_F is not affected even to $O(1/N)$ by the core-hole attraction, it is convenient to measure all the single-particle energies relative to it, so that $\varepsilon_F=0$.

The N -electron ground state $\Psi^0(N)$ in the excited configuration is given by a Slater determinant for the N lowest states below the Fermi level. Its energy is

$$E^{+0} = \sum_\mu \varepsilon_\mu , \quad (2.8)$$

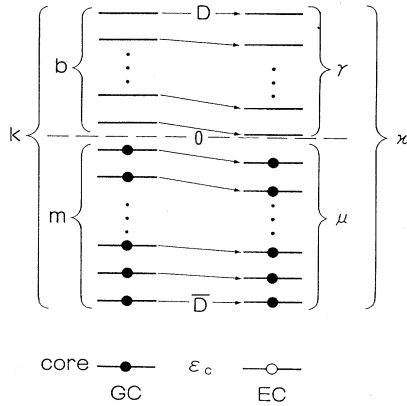


FIG. 1. Level scheme and notation for the single-particle states in the ground configuration (GC) and excited configuration (EC). The Roman and Greek letters are employed for orbitals in the ground and excited configurations, respectively. Different notations are introduced to further distinguish the locations of levels relative to the Fermi level shown by the dashed line. Each level of the ground configuration is shifted downward in the excited configuration by the core-hole attraction. D and \bar{D} are the upper and lower edges of the conduction band, respectively, relative to the Fermi level chosen as the origin of energy.

showing that the N -particle ground-state energy has been changed from E^0 to E^{+0} by the core-hole attraction. Let us call it the relaxation energy ΔE^0 , where

$$\Delta E^0 = E^{+0} - E^0 \tag{2.9}$$

The ground state for $N + 1$ electrons in the excited configuration, i.e., the configuration after photoexcitation, is thus given by adding one extra electron to the level just above the occupied Fermi sea of N electrons. Similarly, the excited states in the excited configuration are obtained by adding the extra electron to a higher level and/or exciting several electrons in the states $\{\mu_s\}$ to the states $\{\gamma_s\}$ above the Fermi level, that is, creating shakeup (electron-hole) pairs. One way of distributing shakeup pairs will yield one excited state of the excited-configuration Hamiltonian \mathcal{H}^+ . Suppose in the state Ψ_F of Eq. (2.5) that there are n electrons excited above the Fermi level, leaving $n - 1$ holes below it. We then obtain

$$\begin{aligned} E_F(N + 1) - E_c^0(N + 1) - \Omega &= \left[\sum \varepsilon_{\gamma_s} - \sum \varepsilon_{\mu_s} + E^{+0} \right] \\ &\quad - (\varepsilon_c + E^0 + \Omega) \\ &= \left[\sum \varepsilon_{\gamma_s} - \sum \varepsilon_{\mu_s} \right] + \omega_{th}^0 - \Omega \\ &= \left[\sum_{s=1}^n \varepsilon_{\gamma_s} - \sum_{s=1}^{n-1} \varepsilon_{\mu_s} \right] - \omega, \end{aligned} \tag{2.10}$$

where the sum is taken over $s = 1, 2, \dots, n$ for ε_{γ_s} and

over $s = 1, 2, \dots, n - 1$ for ε_{μ_s} , as shown in the last equation. Here

$$\omega_{th}^0 = \Delta E^0 - \varepsilon_c \tag{2.11}$$

defines the renormalized threshold energy and

$$\omega = \Omega - \omega_{th}^0 \tag{2.12}$$

is the photon energy measured from the renormalized threshold.

Since the shift of individual level is of the order of $O(1/N)$, ΔE^0 should be of the order of minus the Fermi energy E_{Fermi} measured from the bottom of the conduction band. The transition from the ground state of the ground configuration, $\Phi_c^0(N + 1)$, to that of the excited configuration $\Psi^0(N + 1)$, defines the edge of the absorption band. This is the case of $n = 1$ and γ_1 located just above the Fermi level in Eq. (2.10). In the continuum limit $N \rightarrow \infty$, ε_{γ_1} tends to 0 [remember that the Fermi level is the origin of energies ($\varepsilon_F = 0$)], so that ω_{th}^0 given by Eq. (2.11) defines precisely the absorption threshold, the relaxation energy being just equal to the shift of the threshold frequency.

The ground state of the excited configuration is shown in Fig. 2 for the case in which $V_{kk'}$ and the density of states of the conduction band are such that a localized state appears below the band with bound-state energy $\varepsilon_\lambda (< \bar{D})$. Here we use the index λ to denote the bound state. It is important to note that $N + 1$ electrons are indistinguishable, so that it is meaningless to specify a particular single-particle level as a final state of the photoexcited core electron. Therefore the electron filling the localized level λ may be one that was excited from the core state or may equally be one that was deexcited from the band continuum in the ground configuration. We can only specify a state of the excited configuration, a set of $N + 1$ states as a whole, with the energy of the absorbed photon Ω equal to the difference between the many-

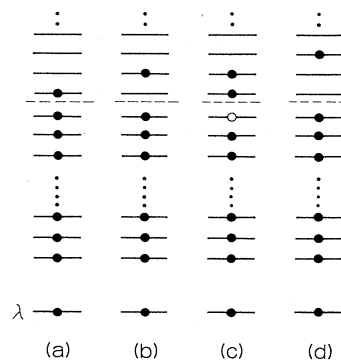


FIG. 2. Examples of the $N + 1$ particle states of the excited configuration when a bound state (denoted by λ) is present. The dashed line indicates the position of the Fermi level for N electrons. State (a) is the ground state, (b) is the lowest among the excited states, and the next lowest states (c) and (d) are degenerate in energy.

particle energies, and not any particular single-particle energies. This is what energy conservation implies in Eq. (2.5).

In Eq. (2.5), the dipole-moment operator \mathcal{W} will be used to express a one-electron transition from the core state through the matrix element $\langle \psi_\kappa | w | \varphi_c \rangle$. The wave functions for the remaining N electrons will then appear in the form of an overlap integral between many-body wave functions. One then wonders how the transition probability (2.5) of the $N + 1$ electron system is related to the vanishing of the overlap Δ between the ground-configuration ground state $\Phi^0 [= \Phi^0(N)]$ and the excited-configuration ground state $\Psi^0 [= \Psi^0(N)]$ of N conduction electrons [the orthogonality catastrophe of Anderson (1967a, 1967b)], which is expressed for spinless s electrons in the limit $N \rightarrow \infty$ as

$$|\Delta|^2 \equiv |\langle \Psi^0 | \Phi^0 \rangle|^2 = C_0 \mathcal{N}_{\text{eff}}^{-\sigma} \tag{2.13}$$

Here

$$\sigma = [\delta(0)/\pi]^2, \tag{2.14}$$

$$\mathcal{N}_{\text{eff}} = N(0)W_b, \tag{2.15}$$

with $N(0)$ the density of states of the conduction band at the Fermi level, $W_b (= D - \bar{D})$ the total bandwidth of the conduction band in question, and $\delta(0)$ the phase shift at the Fermi level. The quantity \mathcal{N}_{eff} is the effective total number of states of the conduction band. It is in general equal neither to \mathcal{N} , the true total number of states, nor to N , the number of states below the Fermi level, nor to M , the number of states above the Fermi level ($\mathcal{N} = N + M$). The theorem is given in a form slightly different from that originally given by Anderson. As will be seen below (Sec. VIII.E), the form (2.13) will prove to be best suited to the MND problem. Note that the phase shift enters in the exponent in the same way as in the critical exponent (cf. the second term of β [Eq. (1.2)] or of σ [Eq. (1.4)] for spinless s electrons). This is why we used the same notation σ as appeared in the x-ray photoemission intensity $P(\omega)$. As concerns the orthogonality theorem, we are naturally interested in an exact analytical expression for the prefactor C_0 . We also hope to discover what kind of correction will be needed in applying the theorem to the case in which a bound state exists in the excited configuration.

The lowest excited state of $(N + 1)$ electrons is shown in Fig. 2(b); here the state γ_1 is occupied together with all the states μ_s below the Fermi level. The next excited state, shown in Fig. 2(c), has two electrons excited above the Fermi level, leaving a hole just below it. This state is degenerate in energy with the state shown in Fig. 2(d). As can be easily imagined, a degeneracy of this type of state increases exponentially with increasing excitation energy because of the combinatorics associated with particle-hole excitations across the Fermi level. Will it

then be possible to calculate the transition probabilities corresponding to each excitation to a respective final state? How are these probabilities related to the overlap Δ ? Does the orthogonality theorem still hold even in the case of low-lying excited final states? If so, how is it possible to obtain a finite intensity for XAS in the limit $N \rightarrow \infty$? How is the intensity expressed analytically? The exact solution to the MND problem should be able to answer all of these questions.

Another class of excited states is shown in Fig. 3, namely, those with an empty bound state. This class also has a continuous spectral density due to the presence of particle-hole excitations, which define an additional absorption band. Let us call this band the secondary band, referring to the spectrum with an occupied localized state as the main band. In Fig. 3(b), we show the lowest-energy state with a hole in the bound state λ , the excitation to which defines the threshold for the secondary band. It lies $|\epsilon_\lambda|$ higher than ω_{th}^0 . The same questions asked before must be answered here. For example, we are interested in expressions for the critical exponents and amplitudes of the secondary band as well as those for the main band.

We have listed some basic questions concerning the soft-x-ray problem, all to be answered in Secs. IV–X. Of course, the answers must be given in the limit $N \rightarrow \infty$. Since the critical exponents of XAS [Eq. (1.2)] and x-ray photoemission [Eq. (1.4)] involve the exponent σ of the

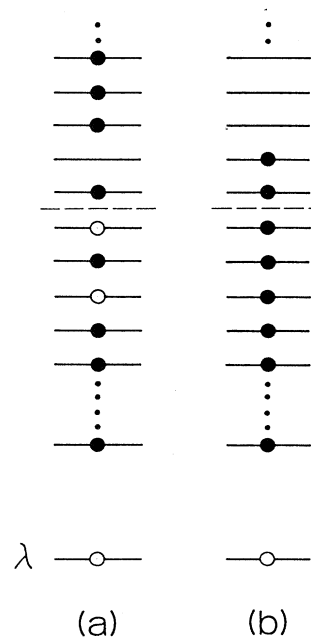


FIG. 3. $(N + 1)$ -particle excited states of the excited configuration giving rise to a secondary absorption band. State (a) is a general state with the bound state λ unoccupied. The final state (b) defines the threshold of the secondary absorption band. The dashed line indicates the position of the Fermi level for N electrons.

orthogonality theorem written for a finite N [finite $N(0)$ in the form of Eq. (2.13)], one might doubt whether or not the amplitude C_0 of the theorem determines the intensity of optical spectra. The temperature effect is also an important open question when we try to compare theory with experiment, as we do in Sec. XI.

The next section is devoted to a historical survey of the work on this problem prior to the publication of the series of papers by the present authors. Although this review is not intended to be comprehensive, we try to cover all those investigations that have made leading contributions to the field.

III. HISTORICAL SURVEY OF THE MND PROBLEM

A. Mahan's treatment of exciton effects in a degenerate semiconductor

The pioneering work on the final-state interaction was done by Mahan (1967a), who examined the exciton effect in a degenerate n -type semiconductor. Here, the attractive potential is due to a mobile hole in the valence band. We assume parabolic conduction and valence bands with electron mass m_e and hole mass m_h . The eigenstates of both are specified by the momentum k . Since an optically created particle-hole pair has zero momentum initially [at the time $\tau = \tau_1$ in the Feynman diagram shown in Fig. 4(a)], it continues to keep zero momentum thereafter. If we could neglect scattering processes involving more than three lines at, say, $\tau = \tau_2$ and $\tau = \tau_3$ in Fig. 4(a), the final-state interaction would be reduced to a one-body potential for a particle with the reduced mass $\mu = m_e m_h / (m_e + m_h)$. This is the ladder approximation. We may then show that each step of the ladder brings in a logarithmic factor, yielding the series

$$\sum_{k=0} [-VN(0)\ln|\omega/D_c|]^k = 1/[1 + VN(0)\ln|\omega/D_c|] \tag{3.1}$$

in the absorption cross section. Here, $-V$ is the scattering matrix element as in Eq. (2.4), $N(0)$ is the density of states for an electron with mass μ and momentum k_F , D_c is the cutoff energy of the order of the Fermi energy E_{Fermi} ($=k_F^2/2\mu$), and ω is the photon energy measured from the absorption edge defined by $E_g + E_{\text{Fermi}}$, where E_g is the energy gap. The logarithmic divergence comes in because the energy denominator vanishes linearly with decreasing energy of the particle-hole pair excitation. This consideration shows that a process containing a zig-zag line, like that at the time $\tau = \tau_2$ [enlarged in Fig. 4(b) to show the momentum assigned to each line], has only a minor contribution as compared to the ladder. Figure 4(c) shows the reason for that: for the excitation energy $[k_1^2 - (-k_2 + \mathbf{q})^2]/2\mu$ to be small with $k_1, k_2 = k_F$, the momentum of the valence hole $-k_1 - \mathbf{q}$ need not necessarily lie near k_F , resulting in a nonvanishing energy

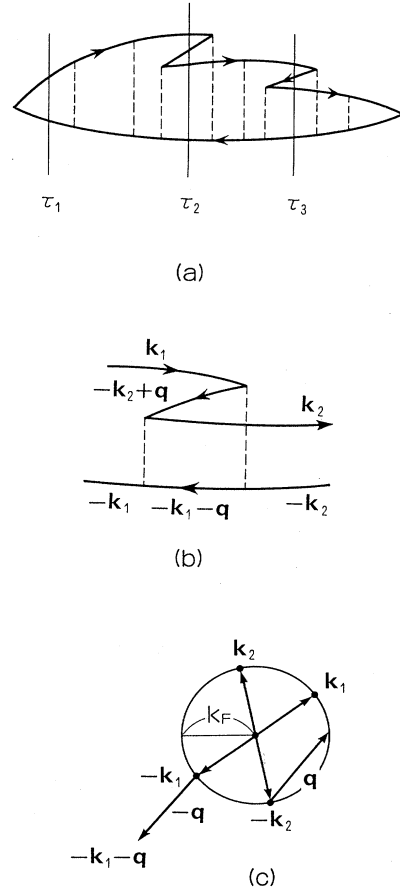


FIG. 4. Interaction between a conduction electron and a valence hole: (a) the general process; (b) enlargement of the portion at $t = \tau_2$. (c) With $|k_1|$, $|k_2|$, and $|-k_2 + \mathbf{q}|$ all close to k_F , the magnitude of the momentum $-k_1 - \mathbf{q}$ will generally deviate from k_F as shown, using a circle with radius k_F .

denominator even at $\omega = 0$. Then in place of $\ln|\omega/D_c|$ in the ladder, we would have a quantity of the order of $\ln|E_{\text{Fermi}}/D_c|$. This reasoning in favor of the ladder approximation shows at the same time a difficulty encountered in the core-electron excitation by the x ray in which $m_h = \infty$. With $(k_1 + \mathbf{q})^2/2m_h = 0$, the "wrong" direction of the vector $-k_1 - \mathbf{q}$ for the hole momentum does not justify the neglect of multiple particle-hole pair excitations.

Mahan has shown that a peak arises near the absorption edge in the ladder approximation. The same approximation has been applied extensively, with some success, in recent treatments of the optical processes in a quasi-two-dimensional system (Bauer and Ando, 1985; Chang and Sanders, 1985; Kleinman and Miller, 1985; Miller and Kleinman, 1985; Schmitt-Rink *et al.*, 1986; Rorison, 1987). It is worth pointing out here that the peak arises mathematically from the pole of Eq. (3.1), in contrast to the infrared peak in the x-ray problem, which comes

from the essential singularity of the response function. The difference shows that, in the case of x rays, a pileup of an infinite number of poles occurs from the contributions neglected in the ladder approximation. Note also that for $|\omega| \sim D_c$, i.e., for a pole of Eq. (3.1) located deep inside the Fermi sea, the ladder approximation fails because of the neglected nonladder terms, which should contribute equally. An estimate of the nonladder contribution as a function of the ratio m_e/m_h and of ω for a hole in the valence band remains to be attempted. This will be a problem of practical interest, because we are able to prepare a system with various values of m_e/m_h fairly easily.

B. Perturbational treatment with respect to V

1. Mahan's treatment of core-level x-ray photoemission spectra

X-ray photoemission spectroscopy measures the intensity of the photoelectrons ejected from a metal by absorbing photons of fixed frequency. If the existence of conduction electrons is neglected, only a sharp line, characterized by a delta-function-like peak, will be observed. Actually, we must take account of the conduction electrons, which change abruptly from their ground configuration to a state in the excited configuration. When the photon energy is high enough for the photoelectron to leave the metal instantly, without being affected by a final-state interaction, the sharp line broadens, with a long tail on its low-energy side. At a frequency ω (> 0) lower than the main peak, the probability $P(\omega)$ of finding an ejected electron, namely, the intensity of the x-ray photoemission, is a direct measure of the probability that the conduction electrons will be excited with an excitation energy ω . This shows that $P(\omega)$ is obtained from the overlap integrals $\langle \Psi_F | \Phi^0 \rangle$ between the two N -electron wave functions of excited- and ground-configuration Hamiltonians. For the ground state $\Psi_F = \Psi^0$ of the excited configuration, this is precisely Δ of the orthogonality theorem, Eq. (2.13). In the sense that the modification due to the ejected photoelectron may be neglected, the treatment of x-ray photoelectron spectra is simpler than that of XAS or XES, in which an excited photoelectron near the Fermi level greatly modifies the spectra. Nevertheless, because of the deep core hole involved, the ladder approximation fails, and we must take into account excitations with many shakeup electron-hole pairs.

Mahan (1967) examined a system whose Hamiltonian \mathcal{H}^+ is given by Eq. (2.3), treating V as a perturbation parameter. By analyzing the logarithmic divergence appearing in a few lower-order terms, he succeeded in deriving the essence of the MND problem: the series of the most divergent terms may be summed up into a closed form leading to the edge behavior described by

$$P(\omega) \propto (\omega/D_c)^{-1+[N(0)V]^2} \quad (\omega > 0) \quad (3.2)$$

to the order of $O(V^2)$, where $N(0)$ is the density of states at the Fermi level of the conduction band. The logarithmic divergence of the series becomes apparent when we rewrite Eq. (3.2) in the form

$$P(\omega) \propto \exp\{-1+[N(0)V]^2 \ln|\omega/D_c|\}. \quad (3.3)$$

The result (3.2) was the first demonstration of the power-law divergence [note that usually $N(0)V < 1$], which triggered a vast number of subsequent theoretical investigations. We note that the exponent $[N(0)V]^2$ of Eq. (3.2) is precisely the first-order term of the critical exponent $\sigma = [\delta(0)/\pi]^2$ of the orthogonality theorem (2.13) [see Eq. (7.15) for the connection of $N(0)V$ with $\delta(0)/\pi$]. The relationship between the critical exponent of x-ray photoemission spectroscopy and the exponent σ of the theorem was clarified by Nozières and DeDominicis (1969). The relation between the critical x-ray photoemission amplitude and the prefactor C_0 of the theorem was examined by Feldkamp and Davis (1980), as well as by the present authors (Tanabe and Ohtaka, 1985; Tanabe, 1986).

2. XAS and XES as dealt with by Mizuno, Ishikawa, and Ohmura

Independently of Mahan, Mizuno and Ishikawa (1968) developed a perturbation theory for a contact-type core-hole potential. They calculated a few lower-order terms of the perturbation series exactly and showed that the sum of the most divergent terms may be written as

$$I(\omega) \propto (|\omega|/D_c)^{-2N(0)V+[N(0)V]^2} \quad (3.4)$$

for XAS ($\omega > 0$) and XES ($\omega < 0$). This expression has, in fact, as an exponent the first term of the correct critical exponent β given by Eq. (1.2), when the phase shift is expanded with respect to V for a spinless s electron.

Moreover, Mizuno and Ishikawa showed that in the case of K emission, the first term of the exponent of Eq. (3.4) vanished; they claimed that the absence of the peaking effect in the observed emission spectrum of Li could be explained by this fact. When $2[N(0)V]$ is replaced by the phase shift $2\delta(0)/\pi$, the result becomes natural, since the photoexcited K electron does not see the contact-type core-hole potential because of the lack of an s -wave part in the final state. To summarize, Mizuno and Ishikawa identified the essential physics of the problem before the analysis of Nozières and DeDominicis.

Ohmura, Ishikawa, and Mizuno extended their treatment further and showed that

(a) XAS is a mirror image of XES only in the immediate vicinity of the edge $\omega=0$ [as expressed by Eq. (3.4)] (Ohmura and Ishikawa, 1973, 1980b; Ohmura *et al.*, 1974), and

(b) away from the edge, both XAS and XES are ex-

pressed better by a generalized power law with an ω -dependent exponent $\beta(\omega)$ (Ishikawa *et al.*, 1973; Ohmura and Ishikawa, 1980a, 1980b):

$$I(\omega) \propto |\omega/D_c|^{\beta(\omega)}. \quad (3.5)$$

Assuming the frequency range $\omega > 0$ for XAS and $\omega < 0$ for XES, we see that the exponent $\beta(\omega)$ has as its first term the exponent $-2N(0)V$. Ohmura and co-workers gave explicit expressions for a few higher-order terms as a series with respect to V .

Remark (a) above follows from the fact that $\beta(\omega)$ is a regular function of ω instead of $|\omega|$, leading to a difference between XAS and XES away from the edge $\omega=0$, unless $\beta(\omega)$ is an even function of ω . By deriving the term linear in ω , Ohmura *et al.* showed that XES had to be sharper in general than XAS. They also did some numerical calculation of the edge spectrum and pointed out the difficulty of deducing the precise value of the critical exponent from the experimental data due to the presence of additional terms in the generalized expression $\beta(\omega)$ (Ohmura and Ishikawa, 1980a).

3. The finite-temperature effect treated by Ferrel

Ferrel attempted a perturbational treatment of x-ray photoemission at a finite temperature T to take into account the effect of a smeared Fermi surface, which leads to blurring of the edge anomalies (Ferrel, 1969). The effect will be appreciable in the frequency range $\omega \sim T$, which implies that it is one of the causes behind the disappearance of the divergence at $\omega=0$. This effect is, however, rather hard to detect in ordinary metals because $T/D \sim 10^{-2}$ even at room temperatures, and usually other effects neglected in the MND Hamiltonians [Eqs. (2.1)–(2.3)], such as a finite lifetime of the core hole, become dominant when the divergence is suppressed. As a result, the temperature effect in x-ray photoemission spectra will be important only when the Fermi energy is comparable to T . As we shall discuss later, such a system is now available, and the examination of the temperature effect on the infrared divergence has become a matter of practical interest.

The result obtained by Ferrel was the leading term with respect to V of the exact expression obtained by Anderson and Yuval (1969). However, the perturbational treatment necessary to extract the most divergent terms was so delicate at finite T that it appeared difficult to extend his calculation to an infinite series and arrive at the result of Anderson and Yuval, who made full use of the Hilbert transform in solving the Dyson equation.

The treatment at finite T is crucial when the theory is applied to the Kondo problem, in which temperature is the main factor affecting the duration time of the final-state interaction (Sec. III.C.3).

C. Exact analytical treatment in terms of phase shift

1. Field-theoretical approach of Roulet, Gavoret, and Nozières

The power-law edge behavior concluded by Mahan and by Mizuno, Ishikawa, and Ohmura was obtained by means of an extrapolation from the results of a few lowest-order terms of the perturbational series. One characteristic of the series with respect to the quantity $\Theta = N(0)V \ln|\omega/D_c|$ is that even if $N(0)V$ is small enough for the series to converge rapidly, the factor $\ln|\omega/D_c|$ causes the series to diverge when $|\Theta| > 1$, namely, just in the neighborhood of the edge $\omega=0$. Thus, although the conclusions of Mahan and Mizuno, Ishikawa, and Ohmura were a correct analytical continuation to the parameter space where $|\Theta| > 1$, a strict mathematical proof was still needed.

Roulet, Gavoret, and Nozières successfully accomplished this (Nozières *et al.*, 1969; Roulet *et al.*, 1969). They noticed that the occurrence of a logarithmic factor in both the particle-hole and hole-hole channels shown in Fig. 5 may be incorporated into a coupled integral equation for a “parquet” diagram. In Fig. 5, the interaction line standing for V , shown by a dashed line in Fig. 4, is replaced by a dot. Therefore Figs. 5(a) and 5(b) show the ladder and zigzag processes, respectively, of Fig. 4. Figure 5(c) shows an example of a complicated parquet diagram constructed from (a) or (b) by inserting internal structures, which themselves are composed of parts yielding logarithms. The repetition of internal structures responsible for the logarithmic divergence characterizes the parquet diagram.

The resulting coupled equation may be solved only to logarithmic accuracy, i.e., in the approximation of putting $\ln|a(\omega/D_c)| \sim \ln|\omega/D_c|$, where a is any constant independent of ω . This amounts to taking account of only the most divergent term in the expression

$$[\ln|a\omega/D_c|]^k = [\ln|a| + \ln|\omega/D_c|]^k \quad (3.6)$$

by discarding the term $\ln|a|$, as did Mahan (1967b) and Mizuno and Ishikawa (1968).

2. Asymptotic formulas of Nozières and DeDominicis

Nozières and DeDominicis made use of the fact that the Hamiltonian \mathcal{H}^+ describes uncorrelated electrons

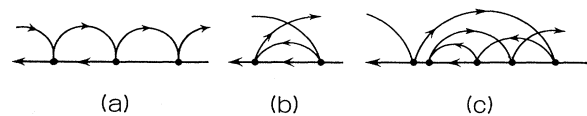


FIG. 5. Particle-hole interaction. The dots here stand for the particle-hole interaction shown by the dashed lines in Fig. 4: (a) Ladder process; (b) zigzag process; (c) a complicated parquet diagram.

moving in a static potential (Nozières and DeDominicis, 1969). If we know the eigenvalues and eigenfunctions of the one-particle Hamiltonian, then the ground state of the many-body Hamiltonian \mathcal{H}^+ is constructed simply by making electrons occupy the N lowest one-particle levels. In a one-particle treatment, the effect of the potential $V_{kk'}$ can be taken into account simply through the phase shift. In particular, we need not worry about the breakdown of the Pauli exclusion principle. That an electron in a state above the Fermi level is able to be scattered into a state below the Fermi level with the matrix element $V_{kk'}$ with $\varepsilon_{k'} > 0$ and $\varepsilon_k < 0$, is guaranteed by the presence of the process represented by the zigzag line of Fig. 4.

One important complication, which constitutes the origin of the difficulty of the MND problem, is that we are not considering a truly static system described by \mathcal{H}^+ , but a system that changes abruptly at $t=0$ from \mathcal{H} to \mathcal{H}^+ . Thus the scattering potential is not static but dynamic.

Nozières and DeDominicis solved the Dyson equation for the Green's function in the time domain, assuming that a core hole existed in the period between 0 and t [for the case of XAS with a contact-type potential (2.4)],

$$\varphi(\tau, \tau'; t, 0) = G_0(\tau, \tau') - V \int_0^t d\tau'' G_0(\tau, \tau'') \varphi(\tau'', \tau'; t, 0), \quad (3.7)$$

where the symbol $(t, 0)$ in φ indicates the time interval over which the core-hole potential operates. The unperturbed Green's function $G_0(\tau, \tau')$ is given by

$$G_0(\tau, \tau') = \begin{cases} -i \sum_b \exp[-i\varepsilon_b(\tau - \tau')] & (\tau > \tau') \\ i \sum_m \exp[-i\varepsilon_m(\tau - \tau')] & (\tau < \tau'). \end{cases} \quad (3.8)$$

All the characteristics of the conduction band are incorporated into the time dependence of G_0 . Nozières and DeDominicis used the long-time form for it in Eq. (3.7):

$$G_0(\tau, \tau') = -N(0) \left[\frac{P}{\tau - \tau'} + \pi \tan\theta \delta(\tau - \tau') \right]. \quad (3.9)$$

Here $\tan\theta \delta(\tau - \tau')$ takes account of the short-time contribution in an approximate way through the quantity θ . The singularity at $\tau = \tau'$ of the unperturbed Green's function reduces the Dyson equation (3.7) to a singular integral equation. The singular edge behavior is traced back to this singularity of the kernel of the Dyson equation. The technique for solving Eq. (3.7) by making use of knowledge of the Hilbert problem is described in the famous book on the topic by Muskhelishvili (1953) and the textbook by Smirnov (1965).

The Green's function $\varphi(t, 0; t, 0)$ describes the evolution of a conduction electron, the core electron photoexcited above the Fermi level, for example, and is sometimes called the open-line contribution, in reference to the form of the Feynman diagram expressing $\varphi(\tau, \tau'; t, 0)$. Let us

denote it as $I_0(t)$:

$$I_0(t) = i\varphi(t, 0; t, 0). \quad (3.10)$$

Another factor that affects the absorption spectrum is the contribution of multiple shakeup excitations, as discussed in Sec. II. It is described by the linked-cluster theorem as

$$P(t) = e^{i\Delta E^0 t} \langle \Phi^0 | e^{i\mathcal{H}t} e^{-i\mathcal{H}^+ t} | \Phi^0 \rangle \\ = e^{i\Delta E^0 t} \exp[\mathcal{L}(t)] \quad (3.11)$$

with

$$\mathcal{L}(t) = \int_0^1 dg \int_0^t d\tau V \varphi_g(\tau, \tau^+; t, 0), \quad (3.12)$$

where g is a coupling constant for the core-hole potential and φ_g is the solution of Eq. (3.7) with V replaced by gV . This contribution is called the closed-loop contribution. Since it takes account only of the background contribution of N electrons, the quantity $P(t)$ determines the x-ray photoemission spectrum. XAS is determined by the product of the two factors, i.e.,

$$I(\omega) = 2\text{Re} \int_0^\infty dt I(t) e^{i\omega t}, \quad (3.13)$$

where

$$I(t) = P(t) I_0(t), \quad (3.14)$$

and where ω_+ is $\omega + i0$ with the frequency ω measured from ω_{th}^0 [Eq. (2.11)]. The long-time behavior of $I_0(t)$ and $P(t)$, derived by Nozières and DeDominicis, is written as

$$P(t) \propto (iD_c t)^{-[\delta(0)/\pi]^2}, \quad (3.15)$$

$$I_0(t) \propto (iD_c t)^{2[\delta(0)/\pi]-1}.$$

Putting these into Eqs. (3.13) and (3.14), we find the famous Nozières and DeDominicis result

$$I(\omega) \propto (\omega/D_c)^{-2[\delta(0)/\pi] + [\delta(0)/\pi]^2}; \quad (3.16)$$

the critical exponent β for XAS defined by Eq. (1.1) is given by

$$\beta = -2[\delta(0)/\pi] + [\delta(0)/\pi]^2, \quad (3.17)$$

which shows that the spectrum of Mizuno and Ishikawa (1968) is, in fact, obtained if we substitute $N(0)V$ for $\delta(0)/\pi$. Further, the exponent $[\delta(0)/\pi]^2$ shows that Mahan's result (Mahan, 1967b) was indeed a first approximation to it. The more realistic form, taking into account the various partial waves and degrees of freedom of spin, was given by Eq. (1.2). For a comparison of the theoretical formula with experiment and an attempt to determine the critical exponent using the Friedel sum rule (Friedel, 1952, 1954), the reader is referred to the review of Citrin *et al.* (1979) and the article of Wilkins (1982). Also, see Sec. XII.

There were several people who questioned the validity of the results obtained by Nozières and DeDominicis.

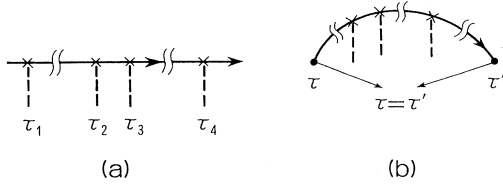


FIG. 6. Scattering process involved in $\varphi(\tau, \tau'; t, 0)$. The symbol inserted between τ_1 and τ_2 , for example, in (a) indicates a long time interval between them. A closed-loop contribution is obtained by putting $\tau = \tau'$ in (b).

One point that is not easy to understand in their results is that the critical exponent is expressed as a function of $\delta(0)$ itself, not in terms of some periodic function of it such as $\sin\delta(0)$. When we consider that the phase shift is determined only with modulus π and that the wave functions at the Fermi level with phase shifts $\delta(0)$ and $\delta(0) + \pi$ are identical, apart from a phase factor, it is rather hard to believe in the correctness of Eq. (3.16). The use of Eq. (3.9), a Green's function that is only asymptotically correct, in the two successive scatterings at τ_2 and τ_3 within a very short time interval [as shown in Fig. 6(a)], or the process of calculating the contribution of the closed-loop diagram by setting τ equal to τ' in $\varphi(\tau, \tau'; t, 0)$ [Fig. 6(b)], looks dubious and tends to undermine one's confidence in the final result. However, these objections later turned out not to be relevant, and the correctness of the edge behavior expressed by Eqs. (3.16) and (3.17) [or Eqs. (1.1) and (1.2) in the general case] has been confirmed and established via several different approaches (for example, Schotte and Schotte, 1969; Hänsch and Ekardt, 1981; Hänsch and Minnhagen, 1982, and of course the one presented in this article).

Moreover, it was not obvious how to apply the Nozières-DeDominicis' approach to the case in which a bound state λ with energy ε_λ lies in the excited configuration below the band bottom. This problem was examined by Combescott and Nozières (1971) by a different approach (Sec. III.G.1).

Since the short-time behavior was not correctly treated in the Nozières-DeDominicis' approach, it was impossible to derive the critical amplitudes for $I_0(t)$ and $P(t)$ by this method, and they remained to be obtained by another approach.

3. Extension to the finite-temperature case by Anderson and Yuval

To apply the idea of Nozières and DeDominicis to the Kondo problem, we need to extend their result to the case of finite temperatures, because, in the Kondo problem, the infrared divergence is cut off by the temperature T , not by ω or t .

Anderson and Yuval solved the Dyson equation (3.7) in the asymptotic region for a finite-temperature case, in which the singular term $1/(\tau - \tau')$ at $T = 0$ [Eq. (3.9)]

was replaced by $\pi T / \sinh \pi T (\tau - \tau')$ (Anderson and Yuval, 1969; Yuval and Anderson, 1970). The key to their success was the idea of generalizing the Hilbert transform originally based on the integral kernel of $1/(\tau - \tau')$ to the finite-temperature case. Considering the complexity encountered in Ferrel's treatment to obtain the leading term, their result was surprisingly simple. It may be summarized as follows: To derive expressions valid for a temperature T , replace the time t in the expressions obtained for $T = 0$ by $\sinh \pi T t / \pi T$ everywhere. Corresponding to the long-time behavior at $T = 0$ given by Eq. (3.15), we thus find at a finite T that

$$\begin{aligned} [I_0(t)]_{T \neq 0} &\propto (iD_c \sinh \pi T t / \pi T)^{2[\delta(0)/\pi] - 1}, \\ [P(t)]_{T \neq 0} &\propto (iD_c \sinh \pi T t / \pi T)^{-[\delta(0)/\pi]^2}. \end{aligned} \tag{3.18}$$

The application of Eq. (3.18) to the Kondo problem by Anderson, Yuval, and Hamann (1970) and by Schotte and Schotte (1971) is beyond the scope of the present review (see, for example, the review of Yosida and Yoshimori, 1973).

D. Comments on the results of Nozières and DeDominicis

1. Friedel's comment

Since the bilinear final-state Hamiltonian Eq. (2.3) can be diagonalized and each many-body final-state Ψ_F can be uniquely determined by assigning the distributions of $N + 1$ electrons in the one-electron orbitals, it is illuminating to consider the optical transition in terms of the Fermi golden rule. The key quantity for this purpose is the overlap integral between the initial orbital φ_k of the conduction band in the ground configuration and the orbital ψ_κ of the excited configuration, using the suffixes k and κ introduced in Sec. II. Let us denote the overlap as

$$a_{\kappa k} = \langle \psi_\kappa | \varphi_k \rangle. \tag{3.19}$$

By analyzing the determinantal form of the many-body transition matrix element expressed in terms of $a_{\kappa k}$, Friedel (1969) showed that the expression for the optical transition probability is made up of terms corresponding to three processes—direct (excitation), replacement, and shakeup. They are shown schematically in Fig. 7. In the direct process [Fig. 7(a)], the core electron is excited to the state γ above the Fermi level with the transition moment $w_{\gamma c}$, while the state of the N background electrons is changed from $\Phi^0 [= \Phi^0(N)]$ to $\Psi^{+0} [= \Psi^{+0}(N)]$ because of the switching of the Hamiltonian from \mathcal{H} to \mathcal{H}^+ . The background effect may be described by the overlap Δ defined by Eq. (2.13) of the orthogonality theorem. Thus, the cross section for the direct process is given by $|\Delta|^2 |w_{\gamma c}|^2$. The replacement process shown in Fig. 7(b) is a two-step process in which the final level γ is occupied by an electron present originally in the state

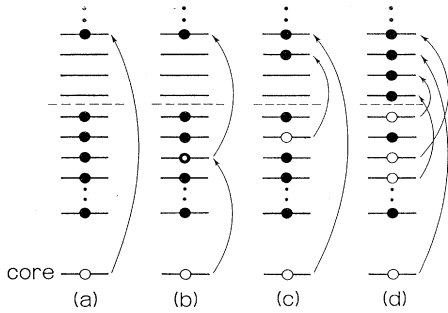


FIG. 7. Several processes that accompany the transition of the core electron to a level above the Fermi level: (a) direct process; (b) replacement process; (c) shakeup process; (d) a general complex process. The dashed line indicates the position of the Fermi level for N electrons.

μ of the conduction band, while the core electron jumps into the hole just created, with the matrix element $w_{\mu c}$. It can easily be seen that this process involves the energy denominator for the excitation from μ to γ , and arbitrariness in the position of μ up to the Fermi level causes the appearance of infrared divergence in the replacement process. It is also interesting to note that the matrix element $w_{\mu c}$ with $\epsilon_\mu < 0$, apparently violating the Pauli exclusion principle, takes part in the optical transition to the state Ψ_F . In the shakeup process, shown in Fig. 7(c), a particle-hole pair excitation occurs across the Fermi level in addition to the core-electron jump to γ . Actually, there are processes much more complex than those described above. An example is given in Fig. 7(d).

Friedel (1969) showed that, to the order of the square of the phase shift, the direct process vanishes by the orthogonality theorem, the replacement process is related to the exponent $2\delta(0)/\pi$, causing the divergent edge peak, and the shakeup processes lead to a powerlaw with the exponent $[\delta(0)/\pi]^2$. By taking account of the multipair excitations discarded in his analysis, he claimed that the critical exponent of Nozières and DeDominicis would be the lowest-order term with respect to $\delta(0)/\pi$ of an expression that is to be given ultimately as a periodic function of the phase shift. Except for this comment, his interpretation of the edge singularity outlined above was qualitatively correct, as we shall see in Secs. IV–VIII. The exact treatment of the present authors described there was indeed stimulated by the work of Friedel.

Friedel also associated the power-law behavior of the spectra with a nonadiabatic screening readjustment of conduction electrons. In the presence of an impurity atom in an otherwise homogeneous system, the scattering potential and the state of each electron are determined in such a way that they satisfy the Friedel sum rule (Friedel, 1952, 1954). This will indeed be the situation in the ground state of the excited configuration described by the Hamiltonian \mathcal{H}^+ given by Eq. (2.3). The temporal evolution of the system from $t=0$, when the impurity is intro-

duced suddenly, up to $t=\infty$, when the system will have been brought finally to the ground state, will be related to the Fourier transform $P(t)$ of the spectral density. The power-law dependence on ω near the edge then implies nonadiabatic readjustment of electrons to the created core hole with a power-law-in-time approach to the new ground state. To summarize, while the screened potential is set up quite quickly with the time constant of the inverse of plasma frequency, the charge fluctuation follows the potential slowly, with a very long power-law tail.

2. Hopfield's interpretation of the critical exponents

Hopfield (1969) proposed the following interpretation for the exponent of the singular power law. Just after the final-state potential has been switched on, the number of electrons around the potential center is wrong in that it violates the Friedel sum rule (Friedel, 1952, 1954). The rule of thumb that Hopfield proposed, without proof, is that the exponent of the time dependence of the response function is given by (-1) times the squared number of conduction electrons for each angular momentum (l, m) , which gather to screen the impurity potential. The time dependence of $P(t)$ given by Eq. (3.15) indeed satisfies this rule, because the excess number of conduction electrons associated with the set of quantum numbers (l, m, s) is $\delta_l(0)/\pi$. In the case of the product $I_0(t)P(t)$ for XAS or XES, the number of displaced conduction electrons in the readjustment is $\{[\delta_{l_0}(0)/\pi]-1\}$ for the channel (l_0, m, s) and $\delta_l(0)/\pi$ for other (l, m, s) with $l \neq l_0$. The term -1 in the former takes care of subtracting the contribution from an optically excited core electron. The result (3.15) is thus reproduced properly according to the rule of thumb. In particular, when there is a bound state in the final state, we find for the time dependence of the photoemission spectrum (for an s -like conduction band)

$$P_{\text{main}}(t) \propto (iD_c t)^{-[\delta(0)/\pi]^2}, \quad (3.20)$$

$$P_{\text{sec}}(t) \propto (iD_c t)^{-[\delta(0)/\pi-1]^2}, \quad (3.21)$$

and for XAS and XES

$$I_{\text{main}}(t) \propto (iD_c t)^{-[\delta(0)/\pi-1]^2}, \quad (3.22)$$

$$I_{\text{sec}}(t) \propto (iD_c t)^{-[\delta(0)/\pi-2]^2}. \quad (3.23)$$

To derive Eq. (3.21), for example, we argue as follows: According to the Friedel sum rule, the number of excess electrons to be accumulated is $\delta(0)/\pi$, including the one occupying the bound state, which leads to Eq. (3.20). Since the secondary band corresponds to the excited states having the bound level unoccupied, the number of conduction electrons to be displaced to form the secondary band becomes $\delta(0)/\pi-1$, leading to Eq. (3.21). In the case of XAS, out of the total $\delta(0)/\pi-1$ electrons to be displaced in the secondary band, one electron is pro-

vided by the core electron, so that the number of displaced conduction electrons amounts to $\delta(0)/\pi - 2$. Thus we have Eq. (3.23).

Hopfield also pointed out that when the overlap integral between ground states with different strengths of impurity potential is involved, it is the difference between the two phase shifts that determines the exponent of the overlap integral. Hopfield's rule of thumb was employed to check the validity of the assumptions made by Combescott and Nozières (1971) in their derivation of the edge behavior in the presence of a bound state in the final state.

E. Anderson's orthogonality theorem

1. Anderson's treatment

The crucial role played by the orthogonality theorem in x-ray absorption, emission, and photoemission was first pointed out by Friedel (1969) and Hopfield (1969). The orthogonality of the two ground-state wave functions may be seen already in the lowest-order perturbation theory, in which the ground-state wave function is modified from Φ^0 to

$$\Psi^0 = S \left[\Phi^0 + \sum_{b,m} \frac{V}{\epsilon_b - \epsilon_m} \Phi_{\bar{m}b} \right], \quad (3.24)$$

where $\Phi_{\bar{m}b}$ stands for the Slater determinant obtained by replacing the state m by b and S is the normalization constant to be determined from

$$|S|^2 \left[1 + V^2 \sum_{b,\bar{m}} \frac{1}{(\epsilon_b - \epsilon_m)^2} \right] = 1. \quad (3.25)$$

If we replace the sum by an integral,

$$\sum_b \rightarrow \int_0^D N(0) d\epsilon, \quad \sum_{\bar{m}} \rightarrow \int_{\bar{D}}^0 N(0) d\epsilon, \quad (3.26)$$

then a logarithmic term $[N(0)V]^2 \ln N$ appears in the second sum, which makes the normalization constant S tend to zero as $N \rightarrow \infty$. Since the value of the overlap $\langle \Phi^0 | \Psi^0 \rangle$ is equal to S from Eq. (3.24), it certainly contains the gist of the orthogonality theorem. Note that the quantity $\ln N$ reflects level spacings of the order of $1/N$ near the Fermi energy.

The original approach of Anderson was a straightforward evaluation of the overlap in its determinantal form in the case of a contact-type impurity potential (Anderson, 1967a, 1967b). The result is given by Eq. (2.13).

The considerations leading to Eq. (3.25) show that the power-law behavior originates from the presence of the Fermi level, which introduces a sharp cutoff in integration procedures, and from the existence of the infinitesimally small excitation energies across the Fermi level. This is the origin of the infrared divergence. In the time-dependent theory there appears a term of the form

$$\sum_{b,m} \{ \exp[-i(\epsilon_b - \epsilon_m)t] - 1 \} / (\epsilon_b - \epsilon_m)^2. \quad (3.27)$$

In the continuous limit ($N \rightarrow \infty$), the sum is turned into an integral. Then a cutoff at an energy of the order of $1/t$ is brought into the energy integral, yielding a logarithmic power-law behavior as a function of t , which, as we have seen, is the origin of the edge singularity.

Attempts to prove orthogonality by means of time-dependent perturbation theory will be reviewed in the next subsection. As we now know, the prefactor C_0 of Eq. (2.13) is an important factor in determining the amplitudes of x-ray spectra near the threshold. Furthermore, the orthogonality theorem puts forward such a fundamental concept that it seems worthwhile to generalize it with respect to the form of the potential and extend it to the case of electrons with correlation. An expression for C_0 was obtained by the present authors (Tanabe and Ohtaka, 1985), and the generalization of the theorem was carried out in a series of papers by Yamada and Yosida (1978a, 1978b, 1979, 1982), as discussed in Sec. III.E.3.

2. Treatments of Rivier and Simanek and of Hamann

The calculation of the overlap integral Δ by a time-dependent method was attempted by Rivier and Simanek (1971). Their formalism is based on the fact that if we switch on the core potential at $t = -\infty$ and make the strength V grow adiabatically to its full value at $t = 0$, the many-body ground state Φ^0 of the Hamiltonian \mathcal{H} given by Eq. (2.1) will eventually, at $t = 0$, evolve into the ground state of \mathcal{H}^+ given by Eq. (2.3). Thus we may write

$$\Psi^0 = T \exp \left[-i \int_{-\infty}^0 dt' \hat{V}(t') \right] \Phi^0, \quad (3.28)$$

apart from a phase factor, where T is the time-ordering operator. The quantity $\hat{V}(t)$ stands for the interaction representation of the adiabatic core-hole potential in the form

$$\hat{V}(t) = -Ve^{\eta t} \sum_{k,k'} a_k^\dagger(t) a_{k'}(t), \quad (3.29)$$

with an infinitesimal positive parameter η to be put to zero, in the final stage of calculation. It then turns out according to the linked-cluster theorem that the overlap Δ is given (apart from a phase factor) by

$$\begin{aligned} \Delta &= \langle \Phi^0 | \Psi^0 \rangle^* \\ &= \exp \left[\int_0^1 dg V \int_{-\infty}^0 d\tau e^{\eta\tau} \varphi_g(\tau, \tau^+; 0, -\infty)^* \right], \end{aligned} \quad (3.30)$$

where φ_g is the Green's function for the potential strength gV . The Dyson equation (3.7) for $\varphi_g(\tau, \tau')$ is then Fourier transformed. It is solved by making use of the analytical properties of the Hilbert transform, as shown by Rivier and Simanek (1971). Unfortunately, they failed to reproduce Anderson's result for σ because

of their incorrect treatment of the parameter η involved in Eq. (3.29).

It was Hamann who obtained the correct result by expanding the solution with respect to the parameter η (Hamann, 1971). He showed that the series for the exponent of Eq. (3.30) reads

$$a_{-1}\eta^{-1} + a_0 + a_1\eta + \cdots \quad (3.31)$$

Since the coefficient a_{-1} proves to be purely imaginary, we have $|\Delta| = \exp(a_0)$ in the limit $\eta \rightarrow 0$. Strictly speaking, Hamann's η expansion was not correct either, since it violates the Gell-Mann and Low theorem¹ (Gell-Mann and Low, 1951). But the well behaved real part of the series (3.31), which starts at η^0 , seems to be valid, and the error lies only in the singular imaginary part. In fact, it can be shown that the correct expression for $|\Delta|$ including the prefactor C_0 can be reproduced by using Hamann's expression of a_0 (Tanabe and Ohtaka, 1985).

3. Extension of Yamada and Yosida

Working from Eq. (3.30) and using the series expansion in powers of η , Yamada and Yosida generalized the orthogonality theorem (Yamada and Yosida, 1978a, 1978b, 1979, 1982). Their extensions were made along the following lines:

(a) Relaxing the restriction on the form of the core-hole potential. Their results apply to non-contact-type potentials, and the results, although expressed formally in terms of the scattering matrix, are given even for a nonspherical potential.

(b) Generalizing the theorem to a system with electron correlation.

(c) Extending the theorem so that we may apply it in calculating the rate for a charged impurity interacting with conduction electrons in a metal to hop from one site to another.

Generalization (a) is by no means trivial, because useful identities associated with the Hilbert transforms of scalar quantities are no longer available once we generalize the Dyson equation in matrix form in trying to incorporate, say, a nonspherical potential. Yamada and Yosida examined the iterative series for the solution of the matrix Dyson equation and proved that the parameter $-V$ of a contact-type core-hole potential is generally replaced by the matrix form of the self-energy part. In the case of (b), the same conclusion is valid if we employ the self-energy part including the electronic correlation. Yamada and Yoshida thereby proved that the exponent σ of the overlap integral could be expressed generally in

¹The result of Hamann for a_{-1} is $a_{-1} = i\Delta E^0$, while the value in accord with the Gell-Mann and Low theorem should be $a_{-1} = i \int_0^1 dg \Delta E^0(g) / g$, where $\Delta E^0(g)$ is the ground-state energy shift for the coupling constant gV .

terms of the same S matrix as appears in the Friedel sum rule (Langer and Ambegaokar, 1961). Procedure (c) was refined by Yamada and collaborators and was used successfully to analyze the temperature dependence of the diffusion constant of positive muons in metal matrices (Yamada *et al.*, 1983, 1985; Kondo, 1984a, 1984b; Yamada, 1984, 1986; Oguchi and Yosida, 1986). See the review by Kondo (1988) on this topic.

F. Numerical treatments

There were several reasons for attempting numerical calculations during the development of the analytical approach: to check the correctness of the theories, which inevitably involved subtlety due to the mathematical complexity of the problem; to determine the magnitudes of quantities so far unattainable by analytical means; to see how far the asymptotic formulas retained their validity, in the frequency range near the threshold, etc.

1. Treatment of Kotani and Toyozawa

Kotani and Toyozawa examined the effect of a core-hole attraction that gives rise to a virtual bound state within a band, mixed by tunneling with (s -like) band states (Kotani and Toyozawa, 1973a). The model system was intended to explain the optical response of a metal involving an incomplete d or f shell. The final-state interaction here is sd mixing triggered by the sudden appearance of a virtual bound state. If intra-atomic Coulomb repulsion $Un_{d\uparrow}n_{d\downarrow}$ of the Hubbard type [not included in the Kotani-Toyozawa (KT) model] is added, the final-state Hamiltonian will be the Anderson Hamiltonian. The Coulomb repulsion was later taken into account by Schönhammer and Gunnarsson (see Sec. III.F.3). Roughly speaking, the model treated by Kotani and Toyozawa is an analog of that introduced by Combescott and Nozières in their treatment of a bound state in the excited configuration, although a marked difference exists, in that a new effect such as the finite width of the virtual state is included.

Kotani and Toyozawa showed that the main XAS band has a power-law edge behavior in general because of the existence of replacement and shakeup excitations across the Fermi level. The exponent of the divergence is still given by Eq. (1.2), where the phase shift of s electrons is now caused by sd mixing. Kotani and Toyozawa found that the exponent derived satisfies Hopfield's rule of thumb (Sec. III.D.2) in all cases investigated of x-ray absorption, emission, and photoemission (Kotani and Toyozawa, 1973a, 1973b, 1974). The secondary band, on the other hand, does not exhibit a power-law edge behavior, in contrast to the Combescott-Nozières (CN) model. It is formed by optical transitions to many-body final states with an empty virtual bound state. Since the hole in the virtual bound state has a finite lifetime due to sd mixing, the band has a blurred step rise expressed by an

arctangent function, which results from convoluting the Lorentzian distribution of the hole with the distribution of an optically excited electron above the Fermi level. When a bound state exists above the Fermi level, it gives rise to a Lorentzian peak in the spectrum. Kotani and Toyozawa examined how these secondary bands are affected by the Fano effect. For more about the KT model, see the review article by Kotani and Toyozawa (1979) and the recent monograph by Kotani (1987). The KT model was subsequently examined using the renormalization group (Oliveira and Wilkins, 1985) and also by the exact analytical approach of Kita and the present authors (1987b).

The numerical treatment of Kotani and Toyozawa (1973b) was intended to check all these theoretical predictions. Their algorithm discretized the whole conduction band into a finite number of states (they used a model with $N = 50$). The final-state Hamiltonian was then diagonalized to obtain eigenvalues and eigenfunctions. This was possible because the Hamiltonian was bilinear. Finally, the many-body transition matrix element was calculated, expressing the many-body states involved by Slater determinants. A complication arose because of the multiplicity of ways to excite a number of particle-hole pairs. Kotani and Toyozawa took account of only one-pair excitations, checking that the corresponding integrated intensities of XAS and XES totaled more than 90% of the theoretical value.

In this way they successfully reproduced their prediction. Some of their results are given in Fig. 8. It shows how the spectra vary with the position ϵ_d of the virtual bound state. It can be seen that the simulation with $N = 50$ reproduces very well the theoretical line shape shown in (a) by the solid curves. This rather surprising phenomenon will be seen again in Sec. III.F.4. The KT model was applied to x-ray photoemission in their third paper (Kotani and Toyozawa, 1974). Most of the subsequent simulations by other authors that were based on a finite number N of conduction electrons employed this KT method.

2. Analysis of Grebennikov, Babanov, and Sokolov

Grebennikov *et al.* (1977a, 1977b) carried out a numerical analysis of the original MND model. Their method was to solve the Dyson equation (3.7) numerically. Since the whole range of t is now in question, a simplified form such as Eq. (3.9) for the Green's function cannot be employed. To take account of every feature of the conduction band, e.g., fine structures in the density-of-state profile, band filling, the position of the Fermi level, etc., it is more advantageous to use $G_0(\omega)$ than $G_0(\tau, \tau')$. They therefore transformed the Dyson equation into a form like that employed by Hamann (1971; Sec. III.E.2) and solved it numerically. To obtain a precise value for the critical exponent, one requires the Green's function for $t = \infty$, and to obtain a reliable in-

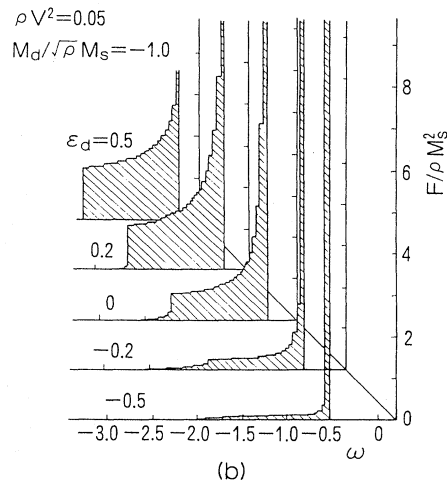
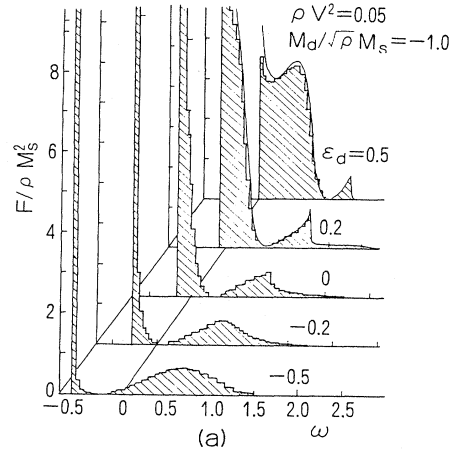


FIG. 8. Typical line shapes obtained by Kotani and Toyozawa (1973b): (a) absorption and (b) emission. The Fermi level, chosen as the origin $\omega=0$, is at the center of the band with a constant density of states ρ . The thresholds are shifted by the relaxation energy. Photon frequency ω is scaled by half the bandwidth, ϵ_d is the position of the d state with an sd mixing parameter V , and $M_d/(\rho^{1/2}M_s)$ is a parameter characterizing the Fano resonance.

tegral kernel one must discretize the conduction band with energy intervals less than $1/t$. Thus the reproduction of the correct value for the critical exponent was a very difficult task in this method.

Grebennikov *et al.* examined over a wide frequency range the behavior of x-ray absorption, emission, and photoemission spectra as a function of the band filling. Some examples are shown in Fig. 9. Their results showed that the usefulness of the approximate formula for spectral intensity obtained from the single-particle cross section depends upon the band filling. We shall discuss the validity of the final-state-rule formula expressed by the final-state single-particle wave function and the initial-state-rule formula involving the initial-state wave function in Sec. III.F.6.

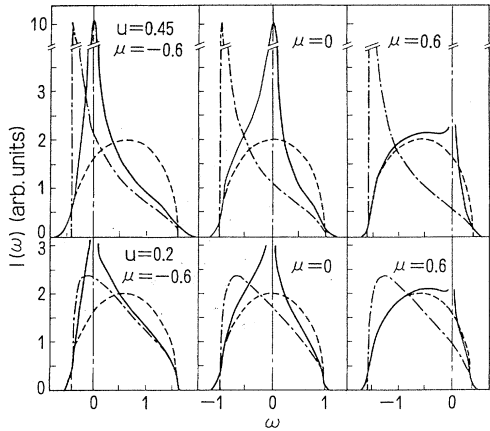


FIG. 9. Variation of a spectrum as a function of the band filling (Grebennikov *et al.*, 1977b). The solid line shows XAS for $\omega > 0$ and XES for $\omega < 0$. The parameter u characterizes the strength of the core-hole potential, μ is the position of the threshold within a band assumed to have a semielliptic density of states with width 2, and ω is measured from the threshold. The dashed curves show the initial-state density of states for the ground configuration; the dot-dashed curves show the spectral density calculated in the presence of a core hole. The dashed curve is seen to be a better approximation for XES for any value of μ . From Grebennikov *et al.* (1977b); reprinted in Wilkins (1982).

Another conclusion to be drawn from the analysis of Grebennikov *et al.* concerns the strength of the XAS and XES secondary absorption band in the presence of a bound state below the conduction band. They showed that the secondary band is so small that it can hardly be observed except for the case of a nearly empty band. One of the reasons for that is the lack of an edge peak at the secondary edge of the absorption and emission spectra, as shown by Eq. (3.23) [$I_{\text{sec}}(t)$ is integrable]. In the case of x-ray photoemission, the secondary band is easier to observe because it shows a divergent edge behavior, as given by Eq. (3.21).

Actually, these characteristics of the secondary band can be deduced by analytical means as will be done in Sec. IX.

3. Approaches of Schönhammer and Gunnarsson

In a series of papers, Schönhammer and Gunnarsson calculated numerically the exact x-ray photoemission spectrum for the model proposed by Kotani and Toyozawa and generalized the KT model in several ways. Their aim was to apply the model to the photoemission spectrum from an atom adsorbed on a metal surface. For that purpose they assumed the Anderson Hamiltonian for the sd mixing, including the intra-atomic Coulomb repulsion.

One of the approaches employed by Schönhammer and Gunnarsson was to discretize the time variable of the Dyson equation, reducing the integral equation to a set of linear coupled equations. This method is thus a more direct way of solving the Dyson equation than that used by Grebennikov *et al.* discussed in Sec. III.F.2. The asymptotic regime of $t = \infty$ was eliminated, by including the finite lifetime of a core hole. Their method therefore provides us with a practical means of obtaining a realistic spectrum by including information on the finite-time region. The second method applied by Schönhammer and Gunnarsson was to solve the Dyson equation by iteration. They showed that the divergence of the resulting Neumann series could be remedied by the Padé approximation, leading to a spectrum in good agreement with that calculated by the first method.

In the absence of the Coulomb correlation (Schönhammer and Gunnarsson, 1977), their results for x-ray photoemission spectra agree essentially with those of Kotani and Toyozawa (1974), if we take account of the differences in the magnitudes of the sd interaction and the finite lifetime of the core hole.

Schönhammer and Gunnarsson (1978a–1978d) extended the KT model to cover coupling with plasmons and the Coulomb repulsion within the adsorbate level. The plasmon coupling model demonstrated how screening charges gather around the core hole as a function of time after the core-hole potential is switched on. The model of Schönhammer and Gunnarsson thus provides us with a rough idea of the time development of a self-consistent core-hole potential that satisfies the Friedel sum rule. The method for treating a model with intra-atomic Coulomb repulsion has been improved and applied recently to explain the optical response observed in some heavy-fermion systems (Gunnarsson and Schönhammer, 1983).

4. Approach of Swarts, Dow, and Flynn

X-ray photoemission spectra from a Fermi sea composed of a finite number of s -wave states were also calculated by Swarts, Dow, and Flynn (1979) and Dow and Flynn (1980). Their method was identical to that employed by Kotani and Toyozawa (1973b) discussed in Sec. III.F.1. These authors were interested in the absolute intensity of the x-ray photoemission especially in the relationship between the prefactor C_0 of the Anderson theorem (2.13) and the critical amplitude c [Eq. (1.3)]. By a simple argument relating the Anderson theorem for a finite system to the x-ray photoemission spectrum of an infinitely large system, they concluded that a definite relationship should exist between C_0 and c (although, unfortunately, the relation they found was not correct).

They also examined how the spectra changed with increasing number N of conduction-band states. As for the integrated photoemission intensity, they found that a larger system improved the numerical result over that of

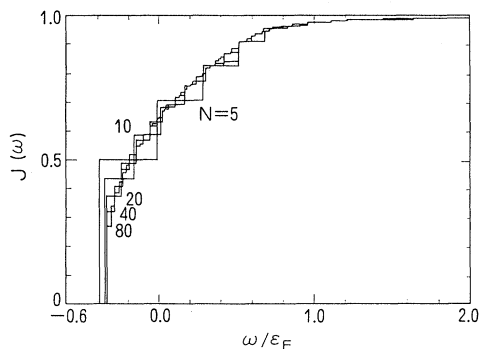


FIG. 10. Integrated x-ray photoemission intensity with increasing N , the number of states below the Fermi level (Dow and Flynn, 1980). The origin $E=0$ is chosen at the unperturbed Fermi level. The threshold is shifted by the relaxation energy.

a smaller one simply by smoothing out the response function found for the latter. This situation is shown in Fig. 10. Since Anderson's theorem appears to imply, in the limit of a large N , a vanishing photoemission probability for transitions to low-lying excited states, it was often argued that a very large number of excited states, not 50 or 100 but, say, on the order of 10^{10} , would be required in order to compensate for the vanishing transition matrix elements due to orthogonality. Figure 10 shows that the actual situation favors numerical calculations, in that even the line shape calculated with N as small as 10 has some resemblance to the exact spectrum. We have already seen that this was also the case in the treatment by Kotani and Toyozawa where $N=50$ seemed sufficient to produce an edge anomaly. Figure 10 obviously shows that the integrated photoemission intensity in the frequency range less than $n\Delta\epsilon$, with $\Delta\epsilon$ the level spacing at the Fermi level, is scaled by $(n/N)^\sigma$. One implication of this is that not only the overlap integral between the ground states of two Fermi seas, as treated by the Anderson theorem but also that between the initial ground state and low-lying excited states should be scaled by the same orthogonality factor $N^{-\sigma}$. That this is indeed so with the scaling factor $(n/N)^\sigma$ was first shown by Feldkamp and Davis (1980).

Another subject examined by Dow and Flynn is the range of validity of the asymptotic power-law formula. They found that the line shape deviated from the Nozières-DeDominicis power-law behavior at $\omega \sim 0.03E_{\text{Fermi}}$ and that precise reproduction of the Nozières-DeDominicis values of the exponent was rather difficult if one discretized the Fermi sea into a finite number of states, say, into 50. They also compared the two line shapes with $\omega > 0$ and $\omega < 0$ and showed that the mirror-image relationship of XAS and XES holds only in the immediate vicinity of the threshold. This is exactly the feature predicted by Ohmura, Ishikawa, and Mizuno (1974).

5. X-ray photoemission spectra as treated by Feldkamp and Davis

X-ray photoemission intensity $P(\omega)$ near the edge was examined analytically by Feldkamp and Davis (1980). For a finite system with a core-hole potential of the contact type and level spacing near the Fermi level $\Delta\epsilon$ [note that $N(0)=1/\Delta\epsilon$], they tried to calculate 2π times the square of the s -wave overlap integral, $2\pi |\langle \Psi_F | \Phi^0 \rangle|^2$, where Ψ_F is an excited state with excitation energy $n\Delta\epsilon (= \omega_n)$ relative to the ground state Ψ^0 . As stated in Sec. II, the calculation grows difficult quickly with increasing n because of the degeneracy. For a conduction band with a uniform level spacing $\Delta\epsilon = W_b/\mathcal{N}$ and $\mathcal{N} = \mathcal{N}_{\text{eff}}$, the calculation was successfully carried out for $n \leq 16$. The result indicated

$$P(\omega_n)\Delta\epsilon = 2\pi C_n \mathcal{N}^{-\sigma} \quad (3.32)$$

with

$$C_n/C_0 = \prod_{k=1}^n [1 + (\sigma - 1)/k] \\ \simeq n^{\sigma-1}/\Gamma(\sigma), \quad (3.33)$$

where C_0 is the prefactor appearing in the Anderson theorem (2.13). The second line shows the extrapolation of the first line for a large n using the gamma function. On the other hand, if the edge spectrum of the x-ray photoemission is assumed to have the form (1.3)

$$P(\omega) = c\omega^{1-\sigma}, \quad (3.34)$$

its discrete version should be obtained by replacing ω by ω_n . Equating it with Eq. (3.32) and using the second line of Eq. (3.33), we then find

$$c = C_0 W_b^{-\sigma} / \Gamma(\sigma). \quad (3.35)$$

The conclusion is that the prefactor C_0 of the orthogonality theorem does determine the intensity of the photoemission. In Sec. VIII.E, we shall give a somewhat detailed derivation of Eq. (3.33) and refine the result of Feldkamp and Davis by showing that if C_0 is defined using \mathcal{N}_{eff} in the orthogonality theorem, as in Eq. (2.13), then Eq. (3.35) holds for any conduction band with arbitrary level spacing.

The proof of Eq. (3.34) and Eq. (3.35) for a general n along the lines adopted by Feldkamp and Davis looks difficult because the calculation up to $n=16$ was already sufficiently cumbersome. However, their result is convincing and strongly suggests the correct form for the critical amplitude of x-ray photoemission. A rigorous proof given by the present authors (Tanabe and Ohtaka, 1985) will be sketched in Sec. IX.D.

6. Treatments of Mahan and of von Barth and Grossmann

In addition to the two numerical approaches—solving the Dyson equation by some means or calculating the

transition probabilities for a finite system by the golden-rule formula—a third approach was developed by Combescott and Nozières (1971), which will be described in the next subsection. By applying the method of Combescott and Nozières, Mahan (1980) calculated the x-ray emission spectrum for a square-well core-hole potential. His main interest lay in examining which of the two rules, the final-state or the initial-state rule, provided a better approximation to the true emission spectrum. In the case of emission, the final-state formula requires the wave functions of the ground-configuration band states to calculate the transition matrix element. For a conduction band with a square-root density of states, Mahan calculated an exact numerical emission spectrum that showed the final-state spectrum to be nearer to the actual XES. His result showed the correctness of the predictions of von Barth and Grossmann (1979) and is in agreement with the analysis of Grebennikov *et al.* (1977a, 1977b), which indicated, as we saw in Fig. 9, that the final-state rule is better in XAS, except in the case of large band filling, and is to be preferred for any extent of band filling in XES.

One interesting remark of Mahan (1980) concerns the integrated intensity I_A and I_E for XAS and XES, respectively. As will be shown later (Sec. VI), there are exact sum rules for XAS and XES at absolute zero temperature:

$$I_A = 2\pi \sum_b |w_{bc}|^2, \quad I_E = 2\pi \sum_\mu |w_{\mu c}|^2. \quad (3.36)$$

Therefore, in the initial-state rule, the sum rule is automatically satisfied. This means, however, that in applying the final-state rule, we need to multiply the overall spectrum by an appropriate factor γ in order for the result to satisfy the sum rule. In Mahan's calculation the factor γ , in fact, leads to much better agreement of the final-state result with the exact (calculated) XES profile. This is shown in Fig. 11 (the lack of divergence in this figure may imply the existence of a rather large numerical error in the near-edge spectrum [see the comment after Eq. (3.41) below]).

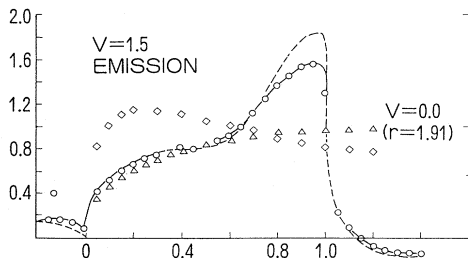


FIG. 11. Comparison of exact spectrum with x-ray emission spectrum according to the final-state rule (Mahan, 1980). The solid curve gives the exact XES, the dashed curve is the exact XES with the orthogonality factor $P(\omega)$ put to unity, while the curve marked by diamonds represents the spectrum obtained by the initial-state rule. The triangles show the final-state rule intensity corrected by multiplying by the factor $r = 1.91$ (see text).

von Barth and Grossmann (1979, 1982) calculated the exact XES spectra both by solving the Dyson equation numerically and by directly calculating the transition matrix element for a system of finite N . In the latter approach, they took account of only the single electron-hole pair excitation, in the same spirit as Kotani and Toyozawa. They used a separable core-hole potential of the form $Vu_k u_{k'}$ with $u_{k'}$ determined from the overlap integral between the core electron and conduction state k . For sodium, they showed that the two methods yielded identical spectra and that the final-state rule gave a better fit to the exact XES than did the initial-state rule (von Barth and Grossmann, 1979). This was indeed the first demonstration of the usefulness of the final-state formula. They also proposed a modified final-state formula that covered, approximately, both the edge anomaly near the threshold and the range far away from the edge (von Barth and Grossmann, 1982).

We shall discuss these approximate formulas in the single-particle picture later in Sec. X.B.

7. Numerical renormalization-group approach of Oliveira and Wilkins and Cox *et al.*

All the numerical treatments discussed above were concerned with the reproduction of overall spectra in a wide frequency range not restricted to the edge region. Unfortunately, they are not able to examine the edge behaviors with sufficient precision.

The renormalization-group (RG) formalism is ideally suited to meeting this need (Oliveira, 1981). It consists of the following steps:

(a) Dividing the conduction band into a finite number of sections with the section points lying at $\Lambda^0, \Lambda^{-1}, \Lambda^{-2}, \dots$, in units of the Fermi energy E_{Fermi} ($\Lambda > 1$), so that the interval becomes infinitesimally small near the Fermi level.

(b) Converting the Hamiltonian of the k representation into that of the new set of orthonormal functions, each being a superposition of the wave functions within each section of the conduction band.

(c) Numerically diagonalizing the Hamiltonian matrix to obtain the eigenvalues and eigenfunctions.

(d) Calculating the optical transition probability using the initial and final Slater determinants for the states obtained in step (c).

Step (a) takes account of the logarithmic singularity in the perturbation series in which a region of the conduction band $[\Lambda^{-l-1}, \Lambda^{-l}]$ in units of the Fermi energy contributes equally, independent of the value of l . For example, a very narrow region, say, $[2^{-10}, 2^{-9}]$ near the Fermi level, matches the broad region $[2^{-2}, 2^{-1}]$ in its contribution to the perturbation series (for the choice $\Lambda=2$). The new set of basis functions is arranged so that the core hole may interact only with the most localized state in the set. This is step (b). But the delocalized wave functions couple to the most localized one through the kinetic-energy term, so we need step (c).

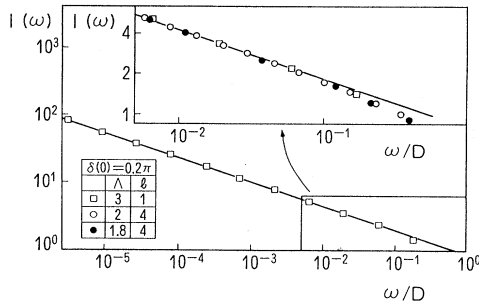


FIG. 12. XAS intensity obtained by the renormalization-group technique (Oliveira and Wilkins, 1981). The solid line corresponds to the theoretical tangent given by Eqs. (1.1) and (1.2). The Fermi level is at the center of the band having a width $2D$ and a constant density of states. The core-hole potential is of a contact type with δ , the phase shift at the Fermi level, chosen to be 0.2π .

Figure 12 shows the result obtained by Oliveira and Wilkins (1981) for a contact potential, in which $\mu(\omega)$ is equal to $I(\omega)$ in our notation. The straight line shows the theoretical prediction of Nozières and DeDominicis, and l is a parameter used in the process of smoothing the numerical line spectra. Note that the Nozières-DeDominicis for the critical exponent is reproduced very well near the edge. In this way, a reliable value for critical exponents was obtained numerically for the first time by use of a renormalization-group formalism.

Cox *et al.* (1985) presented data obtained for x-ray photoemission by the RG formula. As in the case of XAS, the theoretical exponent was reproduced precisely in the range less than $0.01E_{\text{Fermi}}$ from the edge, which grew wider with decreasing potential strength. Their RG value for the critical amplitude will be tested in Sec. X.B.

Oliveira and Wilkins (1985) successfully applied this method to the KT model. They generalized the KT model by adding to it the potential scattering term, as in the original Nozières-DeDominicis model, and demonstrated the capability of the method by producing many reliable quantitative data, including some related to the Fano resonance.

G. Approaches to an exact solution of the MND problem

1. Determinantal formulation of Combescott and Nozières

To treat the effect of a strong final-state attraction giving rise to a bound state, Combescott and Nozières (1971) reproduced the original result of Nozières and DeDominicis by a different method.

The response function $P(t)$ for photoemission spectra has already been given in Eq. (3.11). Combescott and Nozières noticed that $\mathcal{H}^+ [= \mathcal{H}^+(N)]$ is a sum of one-body Hamiltonians $h_i^+ (i = 1, 2, \dots, N)$. It is not difficult to see that $P(t)$ may be put in the form

$$P(t) = e^{i\Delta E_0 t} \det | \lambda_{mm'}(t) | \tag{3.37}$$

with

$$\lambda_{kk'}(t) = \langle \varphi_k | e^{-i(h^+ - \varepsilon_k)t} | \varphi_{k'} \rangle . \tag{3.38}$$

For the response function $I(t)$ of XAS, or the Fourier transform $I(\omega)$ given by Eq. (3.13), it is possible to show that

$$I(t) = P(t)I_0(t) \tag{3.39}$$

with

$$I_0(t) = |w|^2 \sum_{b,b'} e^{i\varepsilon_b t} \left[\lambda_{bb'}(t) - \sum_{m,m'} \lambda_{bm}(t) [\lambda^{-1}(t)]_{mm'} \lambda_{m'b}(t) \right] , \tag{3.40}$$

where $[\lambda^{-1}(t)]_{mm'}$ is the (mm') element of the inverse of the $N \times N$ matrix $(\lambda_{mm'})$. Note that the orbitals φ_k are for the ground-configuration Hamiltonian. Since h^+ is the Hamiltonian for the excited configuration, the calculation of $\lambda_{kk'}$ given by Eq. (3.38) is by no means trivial. For that purpose, Combescott and Nozières made use of the closure property $\sum_{\kappa} |\psi_{\kappa}\rangle \langle \psi_{\kappa}| = 1$ for the excited-configuration band states ψ_{κ} of h^+ :

$$\lambda_{kk'}(t) = \sum a_{\kappa k}^* a_{\kappa k'} \exp[-i(\varepsilon_{\kappa} - \varepsilon_{k'})t] , \tag{3.41}$$

where $a_{\kappa k}$ is the overlap defined by Eq. (3.19) and one of the states in the set κ is the bound state λ . With Eq. (3.41), the set of equations (3.37) and (3.40) now provides a practical means of numerical calculation. In fact, as we

saw in Sec. III.F.6, Mahan (1980) showed by this method the validity of the final-state rule in XES. Although reproduction of the correct long-time behavior was very difficult in the treatment of Combescott and Nozières because of the presence of time-dependent phase factors in Eqs. (3.40) and (3.41), this simple method seems worth re-trying with a modern computer, with respect to the edge anomalies.

The original interest of Combescott and Nozières lay in applying Eqs. (3.37) and (3.40) to an analytical treatment. Although they had to make an assumption concerning the value of the phase shift (which is determined only up to mod π), they succeeded in rederiving the critical exponent of Nozières and DeDominicis and correctly obtaining for the first time the exponents for the main and secondary bands in the presence of a bound state.

These are summarized in Sec. III.D.2 of this review in relation to Hopfield's rule of thumb.

2. Dispersion-integral approach of Mahan and co-workers

The theory that first introduced the dispersion integral Eq. (1.5) into the soft-x-ray problem was offered by Pardee and Mahan (1973). They showed that the critical exponent $2\delta(0)/\pi$ is derived quite naturally if we apply the general Fermi-Watson-Aidzu theorem (Watson, 1954) for a phenomenon taking place near the threshold for the opening of a new scattering channel. They argued that the amplitude $T(\omega)$ for a photon to create a particle-hole pair above the threshold $\omega=0$ may be obtained by solving the Hilbert problem (assuming an s -like channel):

$$\frac{T(\omega+i0)}{T(\omega-i0)} = \begin{cases} \exp[2i\delta(\omega)] & (\omega > 0) \\ 1 & (\omega < 0) \end{cases} \quad (3.42)$$

In other words, $T(z)$ is just equal to $X(z)$ as defined by Eq. (1.3). Considering the fact that the exponent $2\delta(0)/\pi$ in the divergence of XAS and XES originates from the replacement process involving band states μ below the Fermi level (Sec. III.D.1), the form of Eq. (3.42), which has nothing to do with band states below the Fermi level (i.e., $\omega < 0$), looks rather queer.

Penn, Girvin, and Mahan expanded $I_0(t)$ into a pairwise series and showed that Eq. (3.42) holds for the first term of the series and that higher-order terms of multipair excitations involve the quantity $X_+(\omega)$ [$=X(\omega+i0)$] times $\bar{X}_+(\omega)$ defined by Eq. (1.5) for each electron-hole pair (Penn *et al.*, 1981). Judging from the form of the exponents in Eq. (1.5), it is natural that each particle-hole pair in the final state carries one pair of $X_+(\omega)$ and $\bar{X}_+(\omega)$. The reason why the information about the hole below the Fermi level does not appear in Eq. (3.42) is that the product $|X_+(\omega)\bar{X}_+(\omega)|$ is related to the phase shift at energy ω in a simple way [see Eq. (9.35) for $\omega=0$] and hence $|\bar{X}_+(\omega)|$ of the T matrix can be rewritten solely in terms of $|X_+(\omega)|$ and the phase shift $\delta(0)$.

Using a series expansion written in term of $X_+(\omega)$ and $\bar{X}_+(\omega)$, Penn *et al.* (1981) succeeded in obtaining the critical amplitude of $I_0(\omega)$ numerically. In Sec. IV, it will be shown that a closed form for the pairwise series of $I_0(t)$ for both an arbitrary and a contact-type potential can be obtained; an analytical expression of the critical amplitude will be given for a contact-type core-hole potential. The convergence of the pairwise series for $I_0(t)$ is also an interesting subject, which will be discussed in Sec. X.

With regard to the quantity $P(t)$, the pairwise series expansion is naturally much more complicated than that for $I_0(t)$, with the physical quantity of interest appearing in the exponent. Mahan gave the first two terms of the series for the exponent, expressing them explicitly in terms of $X_+(\omega)$ and $\bar{X}_+(\omega)$ (Mahan, 1982). The series

can be given an explicit expression to infinite order and be summed up eventually (Ohtaka and Tanabe, 1983), as will be seen in Sec. IV. However, the extraction of the critical amplitude of $P(t)$ from the resulting expression is much more difficult than that for $T_0(t)$ (Sec. IX.D).

In essence, the treatment of Pardee and Mahan paved the way for an exact solution of the soft-x-ray problem, and with their pairwise series Mahan and collaborators succeeded in obtaining exact results in several respects.

3. Fermi-golden-rule approach of Ohtaka and Tanabe

We are now in a position to describe our own approach towards the exact solution of the MND problem. Before making a start, we give here a brief summary of the following sections, hoping that it will help the reader to have an outline of what follows, in which the mathematics is rather involved. See also the prescription suggested for the reader at the end of Sec. I.

First of all, we calculate the overlap integral between two Slater determinants of the ground- and excited-configuration many-body wave functions. If they are both for the ground states, the overlap integral between them is just Δ of the orthogonality theorem (2.13). Our concern lies in seeing how the overlap changes its form for excited states of the excited configuration and how it is expressed in a unified way for complex excited states having a large number of excited electron-hole pairs. We show that the overlap integral is proportional to the orthogonality factor Δ and that the overlap integral associated with multipair excitation can be expressed using that for the single-pair excitation, as shown, for example, in Eq. (4.11) for two-pair excitation. We give a general expression for the overlap integral valid for any core-hole potential.

These overlap integrals of many-body states determine the photoemission cross section. The problem we are interested in next is whether we can sum the terms in the cross section over the number of excited pairs to obtain the x-ray photoemission spectrum. This will be accomplished by identifying the pairwise series for the cross section with that of a Fredholm determinant. The determinant given by Eqs. (4.19) and (4.20) is nothing but the closed form of the photoemission response function. It is given in t space because energy conservation is taken into account by the Fourier transform. The factor Δ to which each term of the series is proportional is eventually eliminated by the same factor appearing in the denominator of the total sum of overlap integrals, leading finally to a spectrum that is finite even in the limit $N \rightarrow \infty$. It is given by Eqs. (4.24) and (4.25) in a form valid for any core-hole potential. Sections IV.A and IV.B, which are devoted to x-ray photoemission spectroscopy, constitute the basis of our development.

The technique for treating XAS and XES in the remaining part of Sec. IV is similar to that for photoemission, although there is an additional complexity due

to the presence of an extra electron moving to and from the core level. Equation (4.42) with Eq. (4.43) and Eq. (4.47) with Eqs. (4.48)–(4.55) summarize the XAS and XES results, respectively. The response function is composed of two factors, the one $P(t)$ for the shakeup effect and the other $I_0(t)$ for the propagation of the photoelectron. These equations thus provide us with the core-hole propagator and open-line contributions in the formalism of Nazières and DeDominicis, now expressed in a general form valid for any time t and for any core-hole potential.

The response functions at finite temperature are obtained in Sec. V. The need to consider thermal excitation in the ground configuration is the only difference from the treatment of $T=0$. The closed form for the XAS response function is given by Eqs. (5.22)–(5.25). In Sec. VI, the first few moments of the spectrum will be given, including the integrated intensities of the spectrum. The general treatment applicable to any core-hole potential ends there.

The response functions are then analyzed for the case of a contact-type core-hole potential. The reason why further analyses are possible in this case lies in the simplicity of the eigenvalue equation (7.2) for the single-particle energy ε_κ and in the fact that the normalization constant v_κ of the overlap integral (7.3) between the states κ and k depends only on the index κ of the excited-configuration states. These facts enable us to express $X(z)$, $\bar{X}(z)$, and hence all the quantities necessary in the general formulas in terms of the product of the differences between the eigenvalues ε_κ and ε_k . See, for example, Eqs. (7.12) and (7.13) with Eq. (7.8). Explicit results are thus given for a discrete energy scheme. It is shown that in the continuum limit the products turn into the dispersion integrals [Eqs. (7.21) and (7.22)].

To obtain an expression for a particular spectrum, one must calculate an inverse matrix in t space, the quantity F in Eqs. (7.30) and (7.31), for example. For an arbitrary time t , it can only be carried out numerically. In the asymptotic region, i.e., near the edge in frequency space, however, an analytical treatment is possible. This is the theme of Sec. VIII, where we show that solving a Wiener-Hopf integral equation leads to an expression for the critical amplitude, in addition to the Nozières-DeDominicis form for the critical exponent, including the case of $T \neq 0$ [the result, together with those of the secondary bands, is summarized in Eqs. (9.49)–(9.52)]. However, to show that the coefficient C_0 of the orthogonality theorem determines the absolute intensity of the spectrum requires a rather long mathematical treatment, a brief description of which is given in Sec. VIII.E.

In Sec. IX, we treat the case in which there is a bound state in the excited configuration. We may analyze the problem in terms of the basic formulas obtained in Sec. IV by regarding one of the states μ of the excited configuration in, say, Eq. (4.25) as a localized state. The exact edge spectra, including the critical amplitudes for both main and secondary bands, are given by Eqs. (9.49)–(9.52). In Sec. IX.E, the coefficient C_0 of the

orthogonality theorem is examined in the presence of a bound state, and a modification due to the bound state is obtained. In Sec. X, several topics are treated based on the general formulas derived so far. We examine the convergence of the pairwise series of the edge spectrum deduced iteratively from the integral equation (7.32). It will be shown that for a strong core-hole potential an exact edge spectrum cannot be reached iteratively. Moreover, the validity of the generalized power law and the approximate formulas known as final- and initial-state rules will be examined. Their usefulness will be confirmed by comparing them with the exact intensity curve of the MND model.

The theoretical results obtained in Secs. IV–X are studied numerically in Sec. XI. In Figs. 15 and 16, we compare the existing numerical values available for the critical amplitude with our exact analytical expression. In Figs. 28–30, we compare the recent optical experiments in semiconducting quantum wells with the exact solution of the MND model at $T \neq 0$.

To summarize, the basic sections for the formulation are Secs. IV, VII, and VIII. Other sections are devoted to their extension, applications, and numerical demonstration. The main results obtained through our approach are summarized as follows:

(a) Expressions for the pairwise cross sections are given. They include a complete solution for the case of a contact-type core-hole potential, investigated and solved in part by Mahan and collaborators (Mahan, 1980; Penn *et al.*, 1981). The present result is quite general in that it applies at an arbitrary temperature to any core-hole potential, including one inducing the secondary band due to the presence of a bound state in the excited configuration.

(b) For a contact-type core-hole potential, the edge spectra are given their analytical expressions. Mahan's numerical value for the critical amplitude for $I_0(t)$ (Mahan, 1980) is rigorously reproduced by the obtained analytical formula (Ohtaka and Tanabe, 1983), meaning that Mahan almost solved the edge problem for $I_0(t)$ at $T=0$. The present results include those at $T \neq 0$ and for the secondary band. The suggestion of Dow and Flynn (1980) for the relation between C_0 and the intensity of $P(t)$ and the proposed analytical form of the relation by Feldkamp and Davis (1980) are rigorously proved.

(c) Rigorous treatments are given for such topics as the integrated intensities of the secondary band, the expression for the coefficient C_0 of the orthogonality theorem, its modification when a bound state exists in the excited configuration, the radius of convergence of the pairwise series for the edge spectrum with respect to the strength of the core-hole potential, and the validity of the generalized power-law formula and the initial- or final-state formulas for absorption and emission intensities. Except for the last topic, examined already by several authors, these subjects have not yet been investigated in the literature.

Although specific analyses are restricted to the case of a contact-type core-hole potential, a similar development is possible for a separable-type core-hole potential, as will

be seen in Sec. XI.I. This means that we have a rigorous proof for expressions of the critical indices only in these two cases. It is still an open question whether the edge spectra for channels other than s can be described by some version of Eqs. (9.49)–(9.52) in which the s phase shift is replaced by an appropriate one. If we adopt a contact-type core-hole potential with a magnitude determined so as to reproduce the phase shift of the channel in question (the phase-equivalent model potential of Lloyd, 1967), the answer is trivially positive. The result is believed to be meaningful practically, but the error involved is not yet clear mathematically.

We give the various formulas in the discrete energy scheme before considering them in the continuum limit. These formulas are directly applicable to the treatment of the infrared divergence in a finite system (a fine metallic particle, for example) or in a two-dimensional system having a Landau level scheme in a magnetic field. These problems will be treated in the near future.

IV. FORMULATION FOR $T=0$

A. Wave functions before and after the transition

To make the problem clear, we first consider the case of x-ray photoemission and outline how we are going to describe the spectrum. For simplicity, we deal with spinless electrons. For definitions of the notation and symbols not explained here, see Sec. II and the List of Symbols. Readers unfamiliar with x-ray photoemission may find a few paragraphs at the beginning of Sec. III.B.1 helpful.

Before the transition, the system is in the ground configuration of \mathcal{H}_c given by Eq. (2.2), with N electrons in the conduction band and one in the core level. The orbital for the band state k in the ground configuration with its energy ε_k is denoted as φ_k . At absolute zero, the system of N conduction electrons is in the many-electron ground state $\Phi^0 [= \Phi^0(N)]$ in the notation of Sec. II] with its energy $E^0 [= E^0(N)]$, where N lowest levels below the Fermi level are all occupied.

After the transition, that is, after the photoelectron has left the system, N electrons in the conduction band remain in the excited configuration with a hole in the core level. The band orbitals are now greatly modified because of the potential $V_{kk'}$ introduced by the core hole. We denote them as ψ_κ with its orbital energy ε_κ . These are eigenfunctions of a one-electron Hamiltonian h^+ in Eq. (3.38) derived from the many-body Hamiltonian [Eq. (2.3)] for the excited configuration so that there is no guarantee that ψ_κ and φ_k will be orthogonal even when $\varepsilon_\kappa \neq \varepsilon_k$. We may assume, however, that the former functions can be expanded in terms of the latter as

$$\psi_\kappa = \sum_k a_{k\kappa} \varphi_k. \quad (4.1)$$

$$a_{k\kappa} = a_{k\kappa}^* = \langle \psi_\kappa | \varphi_k \rangle. \quad (4.2)$$

The overlap integral $a_{k\kappa}$ already introduced in Eq. (3.19), between the single-particle states in the excited and ground configurations plays a fundamental role in what follows. In the lowest-energy state $\Psi^0 = \Psi^0(N)$, or the ground state of the excited configuration, N orbitals ψ_μ below the Fermi energy ε_F are occupied. Recall Fig. 1 for the symbols for the single-particle states. Because of the nonorthogonality mentioned above, transitions from Φ^0 now become possible, not only to Ψ^0 but also to other excited states of the excited configuration, that is, to the states $\Psi_f^\nu [= \Psi_f^\nu(N)]$, where ν electrons in the levels $\mu_1, \mu_2, \dots, \mu_\nu$ below the Fermi level are excited to the levels $\gamma_1, \gamma_2, \dots, \gamma_\nu$ above it. As implied here, we use the indices γ to indicate the states or levels above the Fermi level according to Fig. 1. The subscript f stands for the set $(\bar{\mu}_1, \dots, \bar{\mu}_\nu; \gamma_1, \dots, \gamma_\nu)$. The bar over μ indicates that a hole has been created at the level μ in the state Ψ^0 . To avoid ambiguity, μ 's and γ 's are supposed to be arranged in ascending order. Our problem now is to calculate quantitatively the transition probabilities for excitations from Φ^0 to Ψ_f^ν .

B. Response function for the photoemission spectrum

We are assuming that the wave function of the photoelectron is hardly affected by the core-hole potential and that the transition matrix element is independent of its energy. Then the intensity of the x-ray photoemission spectrum for the excitation frequency ω measured from the threshold, renormalized by the relaxation energy ΔE^0 , will be proportional to

$$P(\omega) = 2\pi \sum_{\nu, f} \delta(\omega - E_f^{+\nu} + E^0 + \Delta E^0) |\langle \Psi_f^\nu | \Phi^0 \rangle|^2 \quad (4.3)$$

[$E_f^\nu = E_f^\nu(N)$, $E^0 = E^0(N)$], where we have put

$$E_f^{+\nu} - E^0 = \sum_{s=1}^{\nu} \varepsilon_{\gamma_s} - \sum_{s=1}^{\nu} \varepsilon_{\mu_s} + \Delta E^0 \quad (4.4)$$

for the excitation energy $\omega (\hbar=1)$. The relaxation energy ΔE^0 , or the shift of the ground-state energy E^0 in the ground configuration to E^{+0} in the excited configuration, is given by Eq. (2.9).

In order to evaluate $P(\omega)$, we must first calculate the overlap integrals between Ψ^ν and Φ^0 . Let us begin with the case $\nu=0$. Since the wave functions Φ^0 and Ψ^0 are given, respectively, by the Slater determinants as

$$\Phi^0 = |\varphi_1, \varphi_2, \dots, \varphi_N|, \quad (4.5)$$

$$\Psi^0 = |\psi_1, \psi_2, \dots, \psi_N|, \quad (4.6)$$

the overlap integral in question turns out to be

$$\Delta = \langle \Psi^0 | \Phi^0 \rangle = \det \mathbf{A}, \quad (4.7)$$

with the $N \times N$ matrix defined by.

$$(\mathbf{A})_{\mu m} = a_{\mu m} \tag{4.8}$$

in terms of the coefficients $a_{\mu m}$. The overlap Δ is the key quantity of the whole MND problem. The overlap between Ψ_f^1 with $f=(\bar{\mu};\gamma)$ and Φ^0 is then given by the determinant

$$\Delta(\bar{\mu}\gamma) = \det \begin{pmatrix} a_{11} & \cdots & a_{1N} \\ \vdots & & \vdots \\ a_{\gamma 1} & \cdots & a_{\gamma N} \\ \vdots & & \vdots \\ a_{N1} & \cdots & a_{NN} \end{pmatrix} < \mu, \tag{4.9}$$

which is obtained by replacing the μ th row in the determinant Δ by the row vector $(a_{\gamma 1}, a_{\gamma 2}, \dots, a_{\gamma N})$. Note that we have

$$\Delta(\bar{\mu}\gamma)/\Delta = \sum_m a_{\gamma m} (\mathbf{A}^{-1})_{m\mu}. \tag{4.10}$$

Thanks to Jacobi's identity in the theory of determinants (see, for example, Aitken, 1964), all the overlap integrals that appear for $\nu \geq 2$ can be expressed in terms of an overlap of the same type as Eq. (4.9). For example, the overlap $\langle \Psi_f^2 | \Phi^0 \rangle$ with $f=(\bar{\mu}_1, \bar{\mu}_2; \gamma_1, \gamma_2)$ can be expressed as

$$\Delta(\bar{\mu}_1 \bar{\mu}_2 \gamma_1 \gamma_2) = \Delta \det \begin{pmatrix} \Delta(\bar{\mu}_1 \gamma_1)/\Delta & \Delta(\bar{\mu}_1 \gamma_2)/\Delta \\ \Delta(\bar{\mu}_2 \gamma_1)/\Delta & \Delta(\bar{\mu}_2 \gamma_2)/\Delta \end{pmatrix}, \tag{4.11}$$

using Δ and $\Delta(\bar{\mu}\gamma)$. Equation (4.11) may obviously be generalized to the case of an arbitrary value of ν .

For an analytical treatment, it is more convenient to

$$P^{(2)}(t) = |\Delta|^2 \sum_{\gamma_1 < \gamma_2} \det \begin{pmatrix} K(\gamma_1, \gamma_1|t) & K(\gamma_1, \gamma_2|t) \\ K(\gamma_2, \gamma_1|t) & K(\gamma_2, \gamma_2|t) \end{pmatrix} \exp(-i\varepsilon_{\gamma_1} t - i\varepsilon_{\gamma_2} t). \tag{4.18}$$

This may be proved by noting that the determinant on the right-hand side has the form of Gram's determinant, with the definition of $K(\gamma_1, \gamma_2|t)$ given in Eq. (4.17). The determinant can therefore be decomposed into a linear combination of products of two determinants, that is, the determinant given by Eq. (4.10) and its complex conjugate (times appropriate exponential functions), reproducing the expression we started with.

The result (4.18) can also be extended to cases with any value of ν . We then observe that the resulting series (4.13) is a Fredholm series with its kernel given by Eq. (4.17). (See, for example, Courant and Hilbert, 1966). If we denote the number of vacant states in Φ^0 by M , $P(t)$ is expressed as

$$P(t) = |\Delta|^2 D(t) \tag{4.19}$$

in terms of an $M \times M$ Fredholm determinant $D(t)$:

$$D(t) = \det |1 + \mathbf{K}(t)e^{-i\varepsilon t}|, \tag{4.20}$$

work with the Fourier transform of $P(\omega)$. Making use of the expression for the delta function, Eq. (4.3) can be rewritten as

$$P(\omega) = 2\text{Re} \int_0^\infty dt e^{i\omega_+ t} P(t) \tag{4.12}$$

with $\omega_+ = \omega + i0$ and

$$P(t) = \sum_{\nu, f} e^{-i(E_f^\nu - E^0 - \Delta E^0)t} |\langle \Psi_f^\nu | \Phi^0 \rangle|^2 = \sum_{\nu=0} P^{(\nu)}(t), \tag{4.13}$$

where $E_f^\nu = E_f^\nu(N)$. The response function $P(t)$ may also be put in form

$$P(t) = e^{i\Delta E^0 t} \langle \Phi^0 | e^{i\mathcal{H}t} e^{-i\mathcal{H}^+ t} | \Phi^0 \rangle, \tag{4.14}$$

where \mathcal{H} and \mathcal{H}^+ are Hamiltonians for the ground configuration [Eq. (2.1)] and excited configuration [Eq. (2.3)], respectively.

The expressions for $P^{(0)}(t)$ and $P^{(1)}(t)$ are simple,

$$P^{(0)}(t) = |\Delta|^2, \tag{4.15}$$

$$P^{(1)}(t) = |\Delta|^2 \sum_{\gamma} K(\gamma, \gamma|t) e^{-i\varepsilon_{\gamma} t}, \tag{4.16}$$

where $K(\gamma_1, \gamma_2|t)$ is defined by

$$K(\gamma_1, \gamma_2|t) = \sum_{\mu} [\Delta(\bar{\mu}\gamma_1) \Delta(\bar{\mu}\gamma_2)]^* / |\Delta|^2 e^{i\varepsilon_{\mu} t}. \tag{4.17}$$

The expression for $P^{(2)}$ is a little complicated. Perhaps it would be more sensible to give the result here and let interested readers surmise its derivation than to go into the details. We find

where \mathbf{K} is a matrix whose $(\gamma_1 \gamma_2)$ element is given by Eq. (4.17) and ε is a diagonal matrix defined by

$$(\varepsilon)_{\gamma\gamma'} = \varepsilon_{\gamma} \delta_{\gamma\gamma'}. \tag{4.21}$$

Since $P(0)$ is unity by definition, we have

$$D(0) = |\Delta|^{-2}, \tag{4.22}$$

and $P(t)$ may be expressed in the following form (Ohtaka and Tanabe, 1983):

$$P(t) = \exp\{\text{Tr} \ln [1 + \mathbf{K}(\tau)e^{-i\varepsilon\tau}] \Big|_{\tau=0}^{\tau=t}\} \tag{4.23}$$

or

$$P(t) = \exp \left[\int_0^t d\tau A(\tau) \right] \tag{4.24}$$

with

$$A(t) = \text{Tr} \left[\left[\frac{d}{dt} \mathbf{K}(t)e^{-i\varepsilon t} \right] [1 + \mathbf{K}(t)e^{-i\varepsilon t}]^{-1} \right]. \tag{4.25}$$

In order to calculate $A(t)$, we need to know the inverse of the matrix appearing in Eq. (4.25). To obtain it is equivalent to solving a Fredholm integral equation analytically. This is impossible, except for a very large value of t , as we shall see later. As regards the x-ray photoemission problem, let us stop here for the moment and discuss another related subject, the x-ray absorption spectrum.

C. X-ray absorption spectrum

In the case of x-ray absorption, the electron in the orbital φ_c jumps into the conduction band. The state of $N+1$ electrons changes from $\Phi_c^0 [= \Phi_c^0(N+1)]$ in the ground configuration to $\Psi_f^v [= \Psi_f^v(N+1)]$ in the excited configuration, with $v-1$ holes below the Fermi level and v electrons above it, so that $f=(\bar{\mu}_1, \dots, \bar{\mu}_{v-1}; \gamma_1, \dots, \gamma_v)$. We therefore put

$$\Phi_c^0 = |\varphi_1, \dots, \varphi_N, \varphi_c| \tag{4.26}$$

and put, for example, for $v=1$

$$\Psi_f^1 = |\psi_1, \dots, \psi_N, \psi_\tau| \tag{4.27}$$

with $f=(; \gamma)$.

In the same way as in Eq. (4.12), the absorption spectrum $I(\omega)$ may be shown to be given by the Fourier transform of the function $I(t)$:

$$I(\omega) = 2\text{Re} \int_0^\infty dt e^{i\omega t} I(t). \tag{4.28}$$

If we denote by W the dipole-moment operator of the system [Eq. (2.6)], the function $I(t)$ turns out to be defined by

$$\begin{aligned} I(t) &= \sum_{v=1} \sum_f e^{-i(E_f^v - E_c^0 - \omega_{\text{th}}^0)t} |\langle \Psi_f^v | W | \Phi_c^0 \rangle|^2 \\ &= \sum_{v=1} I^{(v)}(t) \end{aligned} \tag{4.29}$$

with

$$E_f^v - E_c^0 = E_f^v(N+1) - E_c^0(N+1) = \sum_{s=1}^v \epsilon_{\gamma_s} - \sum_{s=1}^{v-1} \epsilon_{\mu_s} + \omega_{\text{th}}^0. \tag{4.30}$$

The right-hand side of Eq. (4.29) may also be put in the form

$$I(t) = e^{i\omega_{\text{th}}^0 t} \langle \Phi_c^0 | e^{i\mathcal{H}_c^0 t} W e^{-i\mathcal{H}^+ t} W | \Phi_c^0 \rangle, \tag{4.31}$$

with $\mathcal{H}_c = \mathcal{H}_c(N+1)$ and $\mathcal{H}^+ = \mathcal{H}^+(N+1)$ operating on the $(N+1)$ -electron state Φ_c^0 . For the matrix element of W for $v=1$, we find

$$\langle \Psi_f^1 | W | \Phi_c^0 \rangle = \det \begin{pmatrix} a_{11} & \cdots & a_{1N} & w_{1c} \\ \vdots & & \vdots & \vdots \\ a_{N1} & \cdots & a_{NN} & w_{Nc} \\ a_{\gamma 1} & \cdots & a_{\gamma N} & w_{\gamma c} \end{pmatrix} \tag{4.32}$$

using Eqs. (4.26) and (4.27) with

$$w_{\kappa c} = \langle \psi_\kappa | w | \varphi_c \rangle \quad (\kappa = \gamma, \mu). \tag{4.33}$$

The right-hand side of Eq. (4.32) may be expanded with respect to the last column, and we have

$$\langle \Psi_f^1 | W | \Phi_c^0 \rangle = \Delta p(\gamma), \tag{4.34}$$

where

$$p(\tau) = w_{\gamma c} - \sum_{\mu} [\Delta(\bar{\mu}\gamma) / \Delta] w_{\mu c}, \tag{4.35}$$

so that

$$I^{(1)}(t) = |\Delta|^2 \sum_{\gamma} |p(\gamma)|^2 e^{-i\epsilon_{\gamma} t}. \tag{4.36}$$

The case $v=2$ is a little more involved. However, all the procedures necessary to obtain $I^{(v)}(t)$ for $v>2$ are embodied there, so that it will be worthwhile to sketch the derivation briefly. Within $f=(\bar{\mu}; \gamma_1, \gamma_2)$, we obtain

$$\langle \Psi_f^2 | W | \Phi_c^0 \rangle = \Delta \det \begin{pmatrix} \Delta(\bar{\mu}\gamma_1) / \Delta & p(\gamma_1) \\ \Delta(\bar{\mu}\gamma_2) / \Delta & p(\gamma_2) \end{pmatrix} \tag{4.37}$$

after some manipulation. This then leads to

$$\begin{aligned} I^{(2)}(t) &= |\Delta|^2 \sum_{\gamma_1, \gamma_2} \{ |p(\gamma_1)|^2 K(\gamma_2, \gamma_2 | t) \\ &\quad - p^*(\gamma_1) p(\gamma_2) K(\gamma_1, \gamma_2 | t) e^{-i\epsilon_{\gamma_1} t - i\epsilon_{\gamma_2} t} \} \end{aligned} \tag{4.38}$$

in terms of the matrix elements of K given in Eq. (4.17). The next matrix element for $v=3$ with $f=(\bar{\mu}_1, \bar{\mu}_2; \gamma_1, \gamma_2, \gamma_3)$ may be written as

$$\langle \Psi_f^3 | W | \Phi_c^0 \rangle = \Delta \det \begin{pmatrix} \Delta(\bar{\mu}_1, \gamma_1) / \Delta & \Delta(\bar{\mu}_2, \gamma_1) / \Delta & p(\gamma_1) \\ \Delta(\bar{\mu}_1, \gamma_2) / \Delta & \Delta(\bar{\mu}_2, \gamma_2) / \Delta & p(\gamma_2) \\ \Delta(\bar{\mu}_1, \gamma_3) / \Delta & \Delta(\bar{\mu}_2, \gamma_3) / \Delta & p(\gamma_3) \end{pmatrix}. \tag{4.39}$$

This then enables one to write down the matrix elements of W and, accordingly, an expression for $I^{(v)}(t)$ for any value of v larger than 3. In deriving these results, Jacobi's identity has again played a key role.

In this way, we can show that the series expansion of $I(t)$ may be put in the form

$$\begin{aligned} I(t) &= |\Delta|^2 \left[\sum_{\gamma} |p(\gamma)|^2 e^{-i\epsilon_{\gamma} t} D(t) \right. \\ &\quad \left. - \sum_{\gamma, \gamma'} p^*(\gamma) p(\gamma') D(\gamma, \gamma' | t) e^{-i\epsilon_{\gamma} t - i\epsilon_{\gamma'} t} \right], \end{aligned} \tag{4.40}$$

with $D(t)$ as given previously [Eq. (4.20)] and $D(\gamma, \gamma' | t)$ defined by

$$\begin{aligned}
 D(\gamma, \gamma'|t) &= K(\gamma, \gamma'|t) \\
 &+ \sum_{\gamma_1} \det \begin{bmatrix} K(\gamma, \gamma'|t) & K(\gamma, \gamma_1|t) \\ K(\gamma_1, \gamma'|t) & K(\gamma_1, \gamma_1|t) \end{bmatrix} e^{-i\epsilon_{\gamma_1} t} \\
 &+ \dots
 \end{aligned} \tag{4.41}$$

The expression for $D(\gamma, \gamma'|t)$ is well known in the Fredholm theory of integral equations (Courant and Hilbert, 1966), so that we finally have (Ohtaka and Tanabe, 1983)

$$I(t) = P(t) \cdot I_0(t), \tag{4.42}$$

where $I_0(t)$ is given by

$$I_0(t) = \sum_{\gamma, \gamma'} p^*(\gamma) e^{-i\epsilon_{\gamma'} t} [(1 + \mathbf{K}(t)e^{-i\epsilon t})^{-1}]_{\gamma\gamma'} P(\gamma'). \tag{4.43}$$

The expression for $P(t)$ has already been given in Eqs (4.24) and (4.25). We note that Eq. (4.42), is just Eq. (3.14), first obtained by Nozières and De Dominicis. The expressions for $P(t)$ and $I_0(t)$ given above show that the pairwise series for the cross section may be collected quite generally into an exact closed form.

For an explicit calculation of $I_0(t)$, the same remark as given at the end of the previous subsection applies here. We need to know the inverse of the same matrix as appeared in Eq. (4.25).

D. X-ray emission spectrum

In the case of the x-ray emission spectrum, the system is, in the beginning, in the excited configuration, where we have N conduction electrons in the field of a core hole. Suppose the initial state is the ground state $\Psi^0 [= \Psi^0(N)]$ of the excited configuration, with energy $E^{+0} [= E^{+0}(N)]$ where N levels below the Fermi level are occupied by a core hole. After the transition, the system will be in a state $\Phi_{cf}^n [= \Phi_{cf}^n(N)]$, with energy $[E_{cf}^n = E_{cf}^n(N)]$ in the ground configuration, with $N - 1$ conduction electrons, n holes below the Fermi level, $n - 1$ electrons above it, and one electron occupying the core orbital φ_c . If we use the index m to denote levels below the Fermi level and b for levels above, according to Fig. 1, the subscript f , for example, stands for $(\bar{m}_1, \dots, \bar{m}_n; b_1, \dots, b_{n-1})$.

The response function for x-ray emission spectra whose Fourier transforms defined by Eq. (4.28) give the spectrum $I(\omega)$ can be expressed as

$$I(t) = \sum_{n,f} e^{i(E_{cf}^n - E^{+0} + \omega_{th}^0)t} |\langle \Psi^0 | \mathcal{W} | \Phi_{cf}^n \rangle|^2, \tag{4.44}$$

where

$$\begin{aligned}
 E_{cf}^n - E^{+0} &= E_{cf}^n(N) - E^{+0}(N) \\
 &= \sum_{s=1}^{n-1} \epsilon_{b_s} - \sum_{s=1}^n \epsilon_{m_s} - \omega_{th}^0.
 \end{aligned} \tag{4.45}$$

It is not difficult to see that an equation similar to Eq. (4.31) holds:

$$I(t) = e^{i\omega_{th}^0 t} \langle \Psi^0 | e^{-i\mathcal{H}^+ t} \mathcal{W} e^{i\mathcal{H}_c t} \mathcal{W} | \Psi^0 \rangle \tag{4.46}$$

with $\mathcal{H}^+ = \mathcal{H}^+(N)$ and $\mathcal{H}_c = \mathcal{H}_c(N)$. From here on, the derivation of $I(t)$ parallels that for the case of XAS. We shall therefore give only the final results here. As in Eq. (4.42), we obtain

$$I(t) = P(t) I_0(t). \tag{4.47}$$

Note that $P(t)$ and $I_0(t)$ are different from those given before, although we are using the same notation for both absorption and emission, simply to avoid having too many superscripts and subscripts. The response function for the inverse photoemission is given as

$$P(t) = \exp \left[\int_0^t d\tau A(\tau) \right], \tag{4.48}$$

but with $A(t)$ defined by

$$A(t) = \text{Tr} \left[\left[\frac{d}{dt} \mathbf{K}^0(t) e^{-i\epsilon t} \right] [1 + \mathbf{K}^0(t) e^{-i\epsilon t}]^{-1} \right]. \tag{4.49}$$

Here, $\mathbf{K}^0(t)$ is an $N \times N$ matrix labeled by the indices for the ground configuration, whose $(m_1 m_2)$ element is given by

$$\mathbf{K}^0(m_1 m_2 | t) = \sum [\Delta(|\bar{m}_1 b) \Delta(|\bar{m}_2 b)^* / |\Delta|^2] e^{i\epsilon_b t} \tag{4.50}$$

and

$$(\epsilon)_{mm'} = \epsilon_m \delta_{mm'}. \tag{4.51}$$

The determinant $\Delta(|\bar{m} b)$ is defined as the one obtained from Δ by replacing its m th column by the column vector $(a_{1b}, a_{2b}, \dots, a_{Nb})^{\text{tr}}$, that is,

$$\Delta(|\bar{m}) / \Delta = \sum_{\mu} (A^{-1})_{m\mu} a_{\mu b}. \tag{4.52}$$

We find for $n = 1$ and $f = (\bar{m};)$ that

$$\begin{aligned}
 \langle \Psi^0 | \mathcal{W} | \Phi^1 \rangle &= - \sum \Delta(\bar{\mu} | \bar{m}) w_{\mu c} \\
 &\equiv \Delta p(\bar{m}),
 \end{aligned} \tag{4.53}$$

if we define $\Delta(\bar{\mu} | \bar{m})$ as the negative of the cofactor $\Delta_{\mu m}$ of Δ , so that

$$\Delta(\bar{\mu} | \bar{m}) / \Delta = - (A^{-1})_{m\mu}. \tag{4.54}$$

The quantity $p(\bar{m})$ plays the role of $p(\gamma)$ in the case of absorption. The expression for $I_0(t)$ can be written in terms of $p(\bar{m})$ as

$$I_0(t) = \sum_{m, m'} p(\bar{m})^* e^{-i\epsilon_m t} \{ [1 + \mathbf{K}^0(t) e^{-i\epsilon t}]^{-1} \}_{mm'} P(\bar{m}'). \tag{4.55}$$

Again, the practicability of this method depends upon whether we are able to invert the $N \times N$ matrix as shown on the right-hand side of Eqs. (4.49) and (4.55).

V. FORMULATION AND RESULTS FOR $T > 0$

A. Description of the method

We begin with the case of x-ray absorption at finite temperatures. As in the preceding section, we consider N conduction electrons in the initial (ground) configuration, with the core orbital occupied. At finite T , our initial $N + 1$ electron states are specified by the number of electron-hole pairs and the way they are distributed in the conduction band. Let us denote by $|n\rangle$ the state Φ_{ci}^n of the ground configuration with $i = (\bar{m}_1, \dots, \bar{m}_n; b_1, \dots, b_n)$, where we have n excited electrons at the levels b_1, b_2, \dots, b_n above the Fermi level $\epsilon_F = 0$ and n holes left behind at m_1, m_2, \dots, m_n . In the excited configuration after the absorption, we have $N + 1$ band electrons in the field of a core hole. The final state can be specified by giving the ν occupied levels above the Fermi level as well as the $\nu - 1$ vacant ones below it, so that $|\nu\rangle$ will be used in place of the wave

function Ψ_f^ν with $f = (\bar{\mu}_1, \dots, \bar{\mu}_{\nu-1}; \gamma_1, \dots, \gamma_\nu)$. The energies of the states $\Phi_{ci}^n [= \Phi_{ci}^n(N1)]$ and $\Psi_f^\nu [= \Psi_f^\nu(N + 1)]$ are given, respectively, by

$$E_{ci}^n = E^0 + \sum_{s=1}^n \epsilon_b - \sum_{s=1}^n \epsilon_m + \epsilon_c \tag{5.1}$$

and

$$E_f^{+\nu} = E^{+0} + \sum_{s=1}^{\nu} \epsilon_{\tau_s} - \sum_{s=1}^{\nu-1} \epsilon_{\mu_s} .$$

Taking into account the probability of the occurrence of the state $|n\rangle$ by the Boltzmann factor $\exp(-\beta E_n)$ ($\beta = 1/T$ and $E_n = E_{ci}^n - \epsilon_c$), we find that the response function $I(t)$, whose Fourier transform is the absorption intensity $I(\omega)$ as defined in Eq. (4.28), is now given by

$$I(t) = \sum_{\nu=1} \sum_{n=0} I^{(\nu,n)}(t) \tag{5.3}$$

with

$$I^{(\nu,n)}(t) = \frac{1}{Z} \sum_{\{\gamma\}\{m\}} \frac{\theta_\gamma(t)\theta_m(t^*)}{\nu!n!} \sum_{\{\mu\},\{b\}} \frac{\theta_\mu(t)\theta_b(t^*)}{(\nu-1)!n!} |\langle \nu | W | n \rangle|^2 . \tag{5.4}$$

Note that the factorials have been introduced to compensate for double counting. The factors $\theta(t)$ are defined by

$$\begin{aligned} \theta_\gamma(t) &= \prod_{\gamma=1}^{\nu} e^{-i\epsilon_\gamma t} , \\ \theta_m(t^*) &= \prod_{m=1}^n e^{-i\epsilon_m t^*} , \\ \theta_\mu(t) &= \prod_{\mu=1}^{\nu-1} e^{i\epsilon_\mu t} , \\ \theta_b(t^*) &= \prod_{b=1}^n e^{i\epsilon_b t^*} . \end{aligned} \tag{5.5}$$

The temperature T is introduced into $I(t)$ through the complex time variable t^* defined by

$$t^* = t + i\beta \tag{5.6}$$

and through the partition function Z for the initial (ground) configuration:

$$e^{-\beta E^0} Z = \sum_{\{\epsilon_k\}} \exp[-\beta(\epsilon_{k_1} + \epsilon_{k_2} + \dots + \epsilon_{k_N})] , \tag{5.7}$$

where the sum is to be taken over all possible choices of N states out of the total number of band states \mathcal{N} .

Let us see what the matrix elements of W look like in the simple case of $\nu = 2$ and $n = 1$ so that $f = (\bar{\mu}; \gamma_1, \gamma_2)$ and $i = (\bar{m}; b)$. The result is given as

$$\langle 2 | W | 1 \rangle = \Delta \det \begin{pmatrix} \Delta(\bar{\mu}\gamma_1 |) / \Delta & p(\gamma_1) & \Delta(\gamma_1 | b) / \Delta \\ \Delta(\bar{\mu}\gamma_2 |) / \Delta & p(\gamma_2) & \Delta(\gamma_2 | b) / \Delta \\ \Delta(\bar{\mu} | \bar{m}) / \Delta & p(\bar{m}) & \Delta(| \bar{m} b) / \Delta \end{pmatrix} . \tag{5.8}$$

The sign of the right-hand side of Eq. (5.8) depends, of course, upon the way orbitals are arranged in the Slater determinants involved. We are, however, taking the square of the right-hand side anyway so that what matters here is to see how this result may be generalized to cases with arbitrary values of ν and n , and this is not difficult. On the right-hand side of Eq. (5.8), we see a new type of determinant, defined by

$$\Delta(\gamma | b) / \Delta = a_{\gamma b} - \sum_{m,\mu} a_{\gamma m} (\mathbf{A}^{-1})_{m\mu} a_{\mu b} . \tag{5.9}$$

The determinant $\Delta(\gamma | b)$ is obtained from Δ by adding a new row γ and a new column b , so that it is an $(N + 1) \times (N + 1)$ determinant. If we take the square of the matrix elements of W like Eq. (5.8) and first sum over the indices μ and b , we find that the result can be expressed in terms of the following type of matrix elements besides $p(\gamma)$ and $p(\bar{m})$:

$$\begin{aligned} K(\gamma_1 \gamma_2 | t) &= \sum_{\mu} \Delta(\bar{\mu}\gamma_1 |) e^{i\epsilon_\mu t} \Delta(\bar{\mu}\gamma_2 |)^* / |\Delta|^2 , \\ K(\gamma \ m | t) &= \sum_{\mu} \Delta(\bar{\mu}\gamma |) e^{i\epsilon_\mu t} \Delta(\bar{\mu} | \bar{m})^* / |\Delta|^2 , \\ K(m \ \gamma | t) &= \sum_{\mu} \Delta(\bar{\mu} | \bar{m}) e^{i\epsilon_\mu t} \Delta(\bar{\mu}\gamma |)^* / |\Delta|^2 , \\ K(m_1 \ m_2 | t) &= \sum_{\mu} \Delta(\bar{\mu} | \bar{m}_1) e^{i\epsilon_\mu t} \Delta(\bar{\mu} | \bar{m}_2)^* / |\Delta|^2 ; \end{aligned} \tag{5.10}$$

$$\begin{aligned}
 K^0(\gamma_1 \gamma_2 | t) &= \sum_b \Delta(\gamma_1 | b) e^{i\epsilon_b t^*} \Delta(\gamma_2 | b)^* / |\Delta|^2, \\
 K^0(\gamma m | t) &= \sum_b \Delta(\gamma | b) e^{i\epsilon_b t^*} \Delta(|\bar{m}b|)^* / |\Delta|^2, \\
 K^0(m \gamma | t) &= \sum_b \Delta(|\bar{m}b|) e^{i\epsilon_b t^*} \Delta(\gamma | b)^* / |\Delta|^2, \\
 K^0(m_1 m_2 | t) &= \sum_b \Delta(|\bar{m}_1 b|) e^{i\epsilon_b t^*} \Delta(|\bar{m}_2 b|)^* / |\Delta|^2.
 \end{aligned}
 \tag{5.11}$$

Of these, the first and the last have already been defined [Eq. (4.17) and Eq. (4.50)]. The trouble here is that K and K^0 appear in a correlated way in the result. For example, the coefficient of $|p(\tau_1)|^2$ turns out to be given by

$$\begin{aligned}
 \sum^{(1)} K \begin{pmatrix} \gamma_2 & m \\ \gamma_2 & m \end{pmatrix} &\equiv \det \begin{bmatrix} K(\gamma_2 \gamma_2 | t) & K^0(\gamma_2 m | t^*) \\ K(m \gamma_2 | t) & K^0(mm | t^*) \end{bmatrix} \\
 &+ \det \begin{bmatrix} K^0(\gamma_2 \gamma_2 | t^*) & K(\gamma_2 m | t) \\ K^0(m \gamma_2 | t^*) & K(mm | t) \end{bmatrix}
 \end{aligned}
 \tag{5.12}$$

and this makes summation over ν and n in Eq. (5.3) seemingly rather difficult. There is, however, a mathematical trick for overcoming this difficulty. Let us introduce a complex variable z and put

$$\mathbf{K}_z = \mathbf{K}(t) + z \mathbf{K}^0(t^*). \tag{5.13}$$

Then the right-hand side of Eq. (5.12) may be written as

$$\sum^{(1)} K \begin{pmatrix} \gamma_2 & m \\ \gamma_2 & m \end{pmatrix} = \frac{1}{2\pi i} \int_C \frac{dz}{z^2} \det \begin{bmatrix} K_z(\gamma_2 \gamma_2) & K_z(\gamma_2 m) \\ K_z(m \gamma_2) & K_z(mm) \end{bmatrix}, \tag{5.14}$$

where C is a contour enclosing the origin $z=0$ in the complex z plane.

The trick described above works well for general values of ν and n and allows us to carry out the summation in Eq. (5.3) (Ohtaka and Tanabe, 1984):

$$I(t) = \frac{|\Delta|^2}{Z} \frac{1}{2\pi i} \int_C dz z^{-N-1} \det \mathbf{H}(t) [\mathbf{p}^*(\gamma) e^{-i\epsilon_\gamma t}, \mathbf{p}^*(\bar{m}) z^{-1} e^{-i\epsilon_m t^*}] [\mathbf{H}(t)]^{-1} [\mathbf{p}(\gamma), \mathbf{p}(\bar{m})]^{\text{tr}}, \tag{5.15}$$

where $\mathbf{p}^*(\gamma) e^{-i\epsilon_\gamma t}$ is understood to be a row vector of dimension $M (= \mathcal{N} - N)$ and $\mathbf{p}^*(\bar{m}) e^{-i\epsilon_m t^*}$ is one of dimension N . They are row vectors whose components are specified by the indices γ and m , respectively. The notation $[\dots]^{\text{tr}}$ stands for a transposed row vector, i.e., a column vector of dimension \mathcal{N} . The $\mathcal{N} \times \mathcal{N}$ matrix $\mathbf{H}(t)$ is now given by

$$\mathbf{H}(t) = \begin{bmatrix} 1 + \mathbf{K}_z e^{-i\epsilon_\gamma t} & \mathbf{K}_z z^{-1} e^{-i\epsilon_m t^*} \\ \mathbf{K}_z e^{-i\epsilon_\gamma t} & 1 + \mathbf{K}_z z^{-1} e^{-i\epsilon_m t^*} \end{bmatrix}. \tag{5.16}$$

Note that, in the upper left block, rows and columns are specified by γ , while in the lower right block they are labeled by m . The diagonal matrices ϵ_γ and ϵ_m are defined by

$$\begin{aligned}
 (\epsilon_\gamma)_{\gamma_1 \gamma_2} &= \epsilon_{\gamma_1} \delta_{\tau_1 \tau_2}, \\
 (\epsilon_m)_{m_1 m_2} &= \epsilon_{m_1} \delta_{m_1 m_2}.
 \end{aligned}
 \tag{5.17}$$

It is well known that the partition function Z can also be expressed as a contour integral:

$$e^{-BE^0} Z = \frac{1}{2\pi i} \int_C dz z^{-N-1} \prod_k (1 + z e^{-\beta \epsilon_k}). \tag{5.18}$$

Note that, in the case of x-ray photoemission, we should have for the expression of $P(t)$ only the first factor $\det \mathbf{H}(t)$ in the integrand of Eq. (5.15). Since $P(0)$ has to be unity, Eq. (5.18) then suggests the equality

$$\det \mathbf{H}(0) = |\Delta|^{-2} e^{\beta E^0} \prod_k (1 + z e^{-\beta \epsilon_k}), \tag{5.19}$$

which also can be proved directly.

B. Results

We are now ready to evaluate the contour integrals in Eqs. (5.15) and (5.18). When $N \rightarrow \infty$, this can be done by the method of steepest descent (or, the saddle-point method). It then turns out that the saddle point in the complex z plane is the same for both integrals and is determined from the relation

$$\sum_k (1 + z^{-1} e^{\beta \epsilon_k})^{-1} = N \tag{5.20}$$

if we take the equality (5.19) into consideration. Equation (5.20) implies that z is related to the chemical potential μ through the relation

$$z = e^{\beta \mu}. \tag{5.21}$$

Taking the values at the saddle point, we finally obtain (Ohtaka and Tanabe, 1984)

$$I(t) = P(t) I_0(t) \tag{5.22}$$

with

$$P(t) = \exp \left[\int_0^t d\tau A(\tau) \right], \tag{5.23}$$

where

$$A(t) = \text{Tr} \left[\left[\frac{d}{dt} \mathbf{H}(t) \right] [\mathbf{H}(t)]^{-1} \right] \tag{5.24}$$

and

$$I_0(t) = [\mathbf{p}(\gamma)^* e^{-i\epsilon_\gamma t}, \mathbf{p}(\bar{m})^* z^{-1} e^{-i\epsilon_m t^*}] \times [\mathbf{H}(t)]^{-1} [\mathbf{p}(\gamma), \mathbf{p}(\bar{m})]^{\text{tr}}. \quad (5.25)$$

The value of z given by Eq. (5.21) is to be substituted in these formulas. At $T=0$, these results reduce to those derived in the previous section, because we have $\mu = \epsilon_F$, and all the terms involving $z^{-1} \exp(-i\epsilon_m t^*)$ vanish accordingly.

In retrospect, we realize that the trick in Eq. (5.14) was nothing but the technique used by Fowler (1936) to shift from a treatment in the canonical ensemble (fixed number N of electrons) to one in a grand canonical ensemble. This will be confirmed in the next section, where the temperature dependence of the spectral moments is shown to follow from the Fermi distribution function.

In the case of emission, we can proceed in the same way as above (assuming thermal equilibrium in the excited configuration), and the results may be summarized as follows. For the response function for inverse photoemission $P(t)$, we obtain the same equations (5.23) and (5.24), but with a new definition of an $\mathcal{N} \times \mathcal{N}$ matrix $\mathbf{H}(t)$:

$$\mathbf{H}(t) = \begin{bmatrix} 1 + \mathbf{K}_z e^{-i\epsilon_m t} & \mathbf{K}_z e^{-i\epsilon_\gamma t^*} \\ \mathbf{K}_z e^{-i\epsilon_m t} & 1 + \mathbf{K}_z z e^{-i\epsilon_\gamma t^*} \end{bmatrix} \quad (5.26)$$

where

$$\mathbf{K}_z = \mathbf{K}^0(t) + z^{-1} \mathbf{K}(t^*) \quad (5.27)$$

with

$$t^* = t - i\beta. \quad (5.28)$$

The expression for $I_0(t)$ is given by

$$I_0(t) = [\mathbf{p}(\bar{m})^* e^{-i\epsilon_m t}, \mathbf{p}(\gamma)^* z e^{-i\epsilon_\gamma t^*}] \times [\mathbf{H}(t)]^{-1} [\mathbf{p}(\bar{m}), \mathbf{p}(\gamma)]^{\text{tr}}, \quad (5.29)$$

where $\mathbf{H}(t)$ is, as a matter of course, defined by Eq. (5.26).

VI. EXPRESSIONS FOR MOMENTS

Let us give in this section expressions for the first few moments of the spectrum. The derivation is not difficult but somewhat tedious, so we give here only the relevant results. As mentioned in Sec. V, we can describe the thermal effect solely in terms of the Fermi distribution function.

The zeroth moment, or the integrated intensity, of the spectra (for both XAS and XES) is given by

$$\int_{-\infty}^{\infty} d\omega' I(\omega') = 2\pi I_0(t=0). \quad (6.1)$$

The expressions for $I_0(t=0)$ turn out to be

$$I_0(t=0) = \sum_k |w_{kc}|^2 (1 - f_k) \quad \text{XAS} \quad (6.2)$$

and

$$I_0(t=0) = \sum_\kappa |w_{\kappa c}|^2 f_\kappa \quad \text{XES}, \quad (6.3)$$

where f_k is the Fermi distribution function

$$f_k = f(\epsilon_k) = 1 / (1 + e^{\beta(\epsilon_k - \mu)}). \quad (6.4)$$

As can be seen from Eqs. (5.24) and (5.25), we need quantities like $1 + \mathbf{K}(0)$ in the derivation of results given in this section. See Eqs. (9.23) through (9.25) for details.

The first moment, or the average frequency, is defined as

$$\langle \omega \rangle = \int_{-\infty}^{\infty} d\omega' I(\omega') \omega' / \int_{-\infty}^{\infty} d\omega' I(\omega'). \quad (6.5)$$

The right-hand side can be written as

$$\langle \omega \rangle = iA(t=0) + i\dot{I}_0(t=0) / I_0(t=0). \quad (6.6)$$

The first term represents the average frequency in photoemission or inverse photoemission. For photoemission the expression for $A(t=0)$ is

$$A(t=0) = -i \left[\sum_{\kappa, k} \epsilon_\kappa |a_{\kappa k}|^2 f_k - \sum_k \epsilon_k f_k - \Delta E^0 \right], \quad (6.7)$$

and for inverse photoemission it is

$$A(t=0) = -i \left[\sum_\kappa \epsilon_\kappa f_\kappa - \sum_{\kappa, k} \epsilon_k |a_{\kappa k}|^2 f_\kappa - \Delta E^0 \right], \quad (6.8)$$

i times of which yield $\langle \omega \rangle$ for photoemission and inverse photoemission, respectively. In the cases of XAS and XES we have contributions from the second term on the right-hand side of Eq. (6.6), and the expressions for $I_0(t=0)$ are

$$\begin{aligned} \dot{I}_0(t=0) = & -i \sum_\kappa \epsilon_\kappa \left| \sum_k a_{\kappa k} (1 - f_k) w_{kc} \right|^2 \\ & - i \sum_k \epsilon_k |w_{kc}|^2 f_k (1 - f_k) \quad \text{XAS}, \quad (6.9) \end{aligned}$$

$$\begin{aligned} \dot{I}_0(t=0) = & -i \sum_\kappa \epsilon_\kappa \left| \sum_k a_{\kappa k} f_\kappa w_{\kappa c} \right|^2 \\ & - i \sum_\kappa \epsilon_\kappa |w_{\kappa c}|^2 f_\kappa (1 - f_\kappa) \quad \text{XES}. \quad (6.10) \end{aligned}$$

For the second moment, or the mean-square deviation, we give only the result for photoemission and inverse photoemission, that is,

$$\begin{aligned} \langle \omega^2 - \langle \omega \rangle^2 \rangle = & \int_{-\infty}^{\infty} d\omega' P(\omega') (\omega'^2 - \langle \omega \rangle^2) / \int_{-\infty}^{\infty} d\omega' P(\omega') \\ = & -\dot{A}(t=0). \quad (6.11) \end{aligned}$$

The expressions for $\dot{A}(t=0)$ are somewhat involved. For photoemission it is

$$\begin{aligned} \dot{A}(t=0) = & - \sum_{\kappa, k} \varepsilon_{\kappa}^2 |a_{\kappa k}|^2 f_k - \sum_k \varepsilon_k^2 f_k (1 - f_k) + 2 \sum_{\kappa, k} \varepsilon_{\kappa} \varepsilon_k |a_{\kappa k}|^2 f_k (1 - f_k) \\ & + \sum_{\kappa} \sum_{\kappa'} \left[\sum_k \varepsilon_{\kappa} a_{\kappa k} a_{\kappa' k} f_k \right]^* \left[\sum_{k'} \varepsilon_{\kappa'} a_{\kappa' k'} a_{\kappa k'} f_{k'} \right], \end{aligned} \tag{6.12}$$

and for inverse photoemission

$$\begin{aligned} \dot{A}(t=0) = & - \sum_{k, \kappa} \varepsilon_k^2 |a_{\kappa k}|^2 f_{\kappa} - \sum_{\kappa} \varepsilon_{\kappa}^2 f_{\kappa} (1 - f_{\kappa}) + 2 \sum_{k, \kappa} \varepsilon_{\kappa} \varepsilon_k |a_{\kappa k}|^2 f_{\kappa} (1 - f_{\kappa}) \\ & + \sum_k \sum_{k'} \left[\sum_{\kappa} \varepsilon_{\kappa} a_{\kappa k} a_{\kappa k'} f_{\kappa} \right]^* \left[\sum_{\kappa'} \varepsilon_{\kappa'} a_{\kappa' k} a_{\kappa' k'} f_{\kappa'} \right]. \end{aligned} \tag{6.13}$$

VII. REDUCTION OF FORMULAS IN THE CASE OF A CONTACT POTENTIAL

A. Dispersion integrals

Let us assume that the core-hole potential is of the contact type, that is, the matrix elements $V_{kk'}$ are given by Eq. (2.4):

$$V_{kk'} = -V, \tag{7.1}$$

where V is a positive constant for an attractive potential. This amounts to considering only s waves in the scattering of conduction electrons due to the core-hole potential. However, this assumption allows us to proceed further and leads to expressions for $P(t)$ and $I_0(t)$ that are easy to deal with.

We begin with the (perturbed) eigenvalues ε_{κ} in the excited configuration. It is easy to show that they are determined by the following equation:

$$1 + V \sum_k \frac{1}{\varepsilon_{\kappa} - \varepsilon_k} = 0, \tag{7.2}$$

where ε_k are eigenvalues in the ground configuration and summation is to be taken over all the band states. For one of the values ε_{κ} so determined, the coefficient $a_{\kappa k}$ of the expansion Eq. (4.1) is given by

$$a_{\kappa k} = -v_{\kappa} / (\varepsilon_{\kappa} - \varepsilon_k), \tag{7.3}$$

where v_{κ} is the normalization constant.

Replacing ε_{κ} in Eq. (7.2) by a complex variable z , we define the inverse of the left-hand side as $X_0(z)$, namely,

$$X_0(z) = \left[1 + V \sum_k \frac{1}{z - \varepsilon_k} \right]^{-1}. \tag{7.4}$$

Taking into account the zeros and poles of the rational function $X_0(z)$, we find

$$X_0(z) = \prod_k (z - \varepsilon_k) / \prod_{\kappa} (z - \varepsilon_{\kappa}). \tag{7.5}$$

Note that the normalization constant v_{κ} can be expressed in terms of the residue of $X_0(z)$ at $z = \varepsilon_{\kappa}$:

$$v_{\kappa} = -V \text{Res} X_0(\varepsilon_{\kappa}) \tag{7.6}$$

with

$$\text{Res} X_0(\varepsilon_{\kappa}) = \lim_{z \rightarrow \varepsilon_{\kappa}} [(z - \varepsilon_{\kappa}) X_0(z)]. \tag{7.7}$$

It is convenient to factorize $X_0(z)$ and introduce

$$X(z) = \prod_b (z - \varepsilon_b) / \prod_{\gamma} (z - \varepsilon_{\gamma}), \tag{7.8}$$

to represent the contribution from levels above the Fermi level and

$$\bar{X}(z) = \prod_m (z - \varepsilon_m) / \prod_{\mu} (z - \varepsilon_{\mu}), \tag{7.9}$$

to represent the contribution from below the Fermi level, so that

$$X_0(z) = X(z) \bar{X}(z). \tag{7.10}$$

With these preliminaries, we can calculate the inverse of the matrix \mathbf{A} . When the expression for $a_{\mu m}$ in Eq. (7.3) is used, we note that $(\mathbf{A}^{-1})_{m\mu}$ is, as in Eq. (4.54), essentially a ratio of two determinants that are called Cauchy determinants. The algorithm for this type of determinant is well known, and we obtain

$$(\mathbf{A}^{-1})_{m\mu} = \frac{\text{Res} \bar{X}(\varepsilon_{\mu})}{v_{\mu}} \text{Res} \frac{1}{\bar{X}(\varepsilon_m)} / (\varepsilon_{\mu} - \varepsilon_m). \tag{7.11}$$

With this result, we are able to derive the following expressions for $\Delta(\bar{\mu}\tau)$ etc. (Tanabe and Ohtaka, 1985):

$$\begin{aligned} \Delta(\bar{\mu}\gamma) / \Delta &= V |\bar{X}_{\mu+}| |X_{\gamma+}| / (\varepsilon_{\mu} - \varepsilon_{\gamma}), \\ \Delta(\bar{\mu}|\bar{m}) / \Delta &= V |\bar{X}_{\mu+}| |X_{m+}| / (\varepsilon_{\mu} - \varepsilon_m), \\ \Delta(|\bar{m}b) / \Delta &= V |\bar{X}_{b+}| |X_{m+}| / (\varepsilon_b - \varepsilon_m), \\ \Delta(\gamma|b) / \Delta &= V |\bar{X}_{b+}| |X_{\gamma+}| / (\varepsilon_b - \varepsilon_{\gamma}), \end{aligned} \tag{7.12}$$

where

$$\begin{aligned} |\bar{X}_{\mu+}| &= [-\text{Res} \bar{X}(\varepsilon_{\mu}) / V X(\varepsilon_{\mu})]^{1/2}, \\ |X_{\gamma+}| &= [-\text{Res} X(\varepsilon_{\gamma}) / V \bar{X}(\varepsilon_{\gamma})]^{1/2}, \\ |\bar{X}_{b+}| &= \bar{X}(\varepsilon_b), \\ |X_{m+}| &= X(\varepsilon_m). \end{aligned} \tag{7.13}$$

So far we have assumed that the energy levels of the conduction band are discrete. However, it is sometimes

more convenient to work with a continuous spectrum. We thus give below expressions for quantities defined above in the continuum version (Ohtaka and Tanabe, 1983). The key relation connecting the two versions is

$$\epsilon_\kappa = \epsilon_k - \frac{\delta_\kappa}{\pi} \Delta\epsilon_k, \tag{7.14}$$

which shows that the energy gain of the conduction electron in the change from the ground to the excited configuration is proportional to the level spacing $\Delta\epsilon_k$, and the proportionality constant is given by the phase shift $\delta_\kappa = \delta(\epsilon_\kappa)$ at that energy divided by π . If we put ϵ_κ given by Eq. (7.14) into Eq. (7.2), we obtain an equation for determining the phase shift δ_κ as a function of energy ϵ_κ :

$$1 + V \int_{\bar{D}}^D d\epsilon N(\epsilon) \frac{P}{\epsilon_\kappa - \epsilon} - \pi V N_\kappa \cot\delta_\kappa = 0, \tag{7.15}$$

where we have assumed that the conduction band extends from \bar{D} to D and have put

$$N_\kappa = N(\epsilon_\kappa), \tag{7.16}$$

which is the inverse of $\Delta\epsilon_k$. In deriving Eq. (7.15), we divide the sum on the left-hand side of Eq. (7.2) into two parts—the sum over k with $\epsilon_k \sim \epsilon_\kappa$ and the rest. In the first sum we make use of the partial-fraction expansion for $\cot\delta_\kappa$, and in the second the sum is replaced by the principal value of the integral, as indicated by P in Eq. (7.15). In a similar way, we can derive the expression for $a_{\kappa k}$ of the continuum version:

$$a_{\kappa k} = \delta_{\kappa k} \cos\delta_\kappa - \frac{\sin\delta_\kappa}{\pi N_\kappa} P \frac{1}{\epsilon_\kappa - \epsilon_k} \tag{7.17}$$

with

$$\delta_{\kappa k} = \delta(\epsilon_\kappa - \epsilon_k) / N_\kappa. \tag{7.18}$$

In the continuum limit, $X_0(z)$ is defined by

$$X_0(z) = \left[1 + V \int_{\bar{D}}^D d\epsilon N(\epsilon) \frac{1}{z - \epsilon} \right]^{-1}. \tag{7.19}$$

The expression corresponding to Eq. (7.5) is

$$X_0(z) = \exp \left[-\frac{1}{\pi} \int_{\bar{D}}^D \frac{\delta(\epsilon)}{z - \epsilon} d\epsilon \right], \tag{7.20}$$

so that

$$X(z) = \exp \left[-\frac{1}{\pi} \int_0^D \frac{\delta(\epsilon)}{z - \epsilon} d\epsilon \right], \tag{7.21}$$

$$\bar{X}(z) = \exp \left[-\frac{1}{\pi} \int_{\bar{D}}^0 \frac{\delta(\epsilon)}{z - \epsilon} d\epsilon \right], \tag{7.22}$$

where we have put the Fermi level at $\epsilon_F = 0$. Equations (7.21) and (7.22) are just Eq. (1.5). To prove Eq. (7.20), we take the logarithm of the right-hand side of Eq. (7.5), replace the sums by integrals, and note that the change in

the density of states $N_\kappa - N_k$ is given by the derivative of the phase shift $d\delta(\epsilon)/d\epsilon$ divided by π , according to Eq. (7.14). Partial integration then leads to Eq. (7.20). From Eqs. (7.15) and (7.19), we obtain a useful identity,

$$\sin\delta(\epsilon) / |X_0(\epsilon_+)| = \pi V N(\epsilon), \tag{7.23}$$

where ϵ_+ stands for $\epsilon + i0$, that is, ϵ with a small imaginary part.

We can derive the inverse of the matrix \mathbf{A} either by taking the continuum limit of Eq. (7.11) or by directly inverting $\mathbf{A} = (a_{\mu m})$ using Eq. (7.17), the latter procedure being nothing but solving an integral equation. The result is given by (Ohtaka and Tanabe, 1983)

$$(\mathbf{A}^{-1})_{m\mu} = \frac{|\bar{X}_{\mu+}|}{|\bar{X}_{m+}|} \frac{1}{N_m} \left[\cos\delta_m \delta(\epsilon_m - \epsilon_\mu) + \frac{\sin\delta_m}{\pi} \frac{P}{\epsilon_m - \epsilon_\mu} \right], \tag{7.24}$$

where

$$\begin{aligned} |\bar{X}_{\mu+}| &= \exp \left[-\frac{P}{\pi} \int_{\bar{D}}^0 \frac{\delta(\epsilon)}{\epsilon_\mu - \epsilon} d\epsilon \right], \\ |X_{\gamma+}| &= \exp \left[-\frac{P}{\pi} \int_0^D \frac{\delta(\epsilon)}{\epsilon_\gamma - \epsilon} d\epsilon \right], \\ |\bar{X}_{b+}| &= \bar{X}(\epsilon_b), \\ |X_{m+}| &= X(\epsilon_m). \end{aligned} \tag{7.25}$$

Equations (7.12) for the ratio of the Δ 's are also valid with some modifications in the continuum limit with these "dispersion integrals" in place of Eq. (7.13). The modification required is to replace the inverse of the energy difference in the second equation of Eq. (7.12) as in

$$1/(\epsilon_\mu - \epsilon_m) \rightarrow \frac{P}{\epsilon_\mu - \epsilon_m} - \pi \cot\delta_\mu \delta(\epsilon_\mu - \epsilon_m). \tag{7.26}$$

This is precisely what we have done in deriving Eqs. (7.15) and (7.17) from their corresponding expressions in the discrete scheme. Similar replacement is necessary for $1/(\epsilon_b - \epsilon_\gamma)$ in the fourth equation. [By writing ϵ_γ for ϵ_μ and ϵ_b for ϵ_m in the above, we obtain the expression for $1/(\epsilon_\gamma - \epsilon_b)$.]

Finally, we note that $p(\gamma)$ and $p(\bar{m})$, which appeared in Secs. IV.C and IV.D, take a very simple form,

$$\begin{aligned} p(\gamma) &= |X_{\gamma+}| w, \\ p(\bar{m}) &= |X_{m+}| w, \end{aligned} \tag{7.27}$$

if we neglect the k dependence of w_{kc} and put $w = w_{kc}$. They are valid both in the discrete and in the continuum version. Equation (7.27) for $p(\gamma)$ and $p(\bar{m})$ will be assumed throughout the subsequent sections.

B. Expressions for $A(t)$ and $I_0(t)$ at $T=0$

The result derived in Secs. IV and V are quite general in the sense that they are valid for any type of core-hole potential. However, we must admit that, in terms of practicality, it is not easy to calculate $A(t)$ and $I_0(t)$. More particularly, we have to work simultaneously in frequency and time space to calculate the inverse of the matrix involving \mathbf{K} . Fortunately, in the case of a contact potential, it is possible to work solely in the time space.

We note that energy denominators appear in the expression for $K(\gamma, \gamma'|t)$ when Eq. (7.12) is substituted. Let us replace them by the time integral

$$A(t) = [N(0)V]^2 \int_0^\infty d\sigma \int_0^\infty d\tau \phi(t+\sigma)F(t+\sigma, t+\tau)\bar{\phi}(t+\tau), \tag{7.30}$$

$$I_0(t) = N(0)|w|^2 \int_0^\infty d\sigma \phi(t+\sigma)F(t+\sigma, t+0), \tag{7.31}$$

where $F(t+\sigma, t+\tau)$ is the solution of the integral equation,

$$F(t+\sigma, t+\tau) - \int_0^\infty d\rho \Lambda(t+\sigma, t+\rho)F(t+\rho, t+\tau) = \delta(\sigma-\tau), \tag{7.32}$$

with the kernel Λ defined by

$$\Lambda(t+\sigma, t+\rho) = [N(0)V]^2 \int_0^\infty d\xi \bar{\phi}(t+\sigma+\xi)\phi(t+\rho+\xi). \tag{7.33}$$

In the second argument of F in Eq. (7.31), $+0$ stands for a small positive number.

In the case of XES, we define $\phi(t)$ and $\bar{\phi}(t)$ as

$$\begin{aligned} N(0)\phi(t) &= \sum_m |X_{m+}|^2 e^{-i\varepsilon_m t}, \\ N(0)\bar{\phi}(t) &= \sum_b |\bar{X}_{b+}|^2 e^{i\varepsilon_b t}. \end{aligned} \tag{7.34}$$

Equations (7.30)–(7.33) are also valid for the emission spectrum.

When the energy spectrum is regarded as a continuum, the sums are to be replaced by integrals as in Eq. (3.25), and

$$\begin{aligned} \sum_\gamma &\rightarrow \int_0^D d\varepsilon N(\varepsilon), \\ \sum_\mu &\rightarrow \int_{\bar{D}}^0 d\varepsilon N(\varepsilon). \end{aligned} \tag{7.35}$$

The expressions to be employed for $|X_{\gamma+}|$ etc. are of course given by Eq. (7.25).

$$A(t) = i\eta^0 + [N(0)V]^2 \int_0^\infty d\sigma \int_0^\infty d\tau \Psi(t+\sigma)F(t+\sigma, t+\tau)\bar{\Psi}(t+\tau), \tag{7.38}$$

$$I_0(t) = N(0)|w|^2 \int_0^\infty d\sigma \Psi(t+\sigma)F(t+\sigma, t+0), \tag{7.39}$$

$$\frac{1}{E_+} = -i \int_0^\infty d\tau e^{iE_+ \tau} \tag{7.28}$$

and define two functions $\phi(t)$ and $\bar{\phi}(t)$ for XAS at $T=0$ by

$$\begin{aligned} N(0)\phi(t) &= \sum_\gamma |X_{\gamma+}|^2 e^{-i\varepsilon_\gamma t}, \\ N(0)\bar{\phi}(t) &= \sum_\mu |\bar{X}_{\mu+}|^2 e^{i\varepsilon_\mu t}, \end{aligned} \tag{7.29}$$

where $N(0)$ is the density of states at the Fermi level. Then we can show, after some manipulation, that $A(t)$ and $I_0(t)$ may be put in the following form (Ohtaka and Tanabe, 1983):

C. Expressions for $A(t)$ and $I_0(t)$ at $T > 0$

It turns out that the functions $A(t)$ and $I_0(t)$ for XAS as well as for XES are also given by Eqs. (7.30)–(7.33) if we define $\phi(t)$ and $\bar{\phi}(t)$ by

$$\begin{aligned} \phi(t) &= \sum_\gamma |X_{\gamma+}|^2 e^{-i\varepsilon_\gamma t} + \sum_m |X_{m+}|^2 e^{-i\varepsilon_m t} e^{\beta(\varepsilon_m - \mu)}, \\ \bar{\phi}(t) &= \sum_\mu |\bar{X}_{\mu+}|^2 e^{i\varepsilon_\mu t} + \sum_b |\bar{X}_{b+}|^2 e^{i\varepsilon_b t} e^{-\beta(\varepsilon_b - \mu)} \end{aligned} \tag{7.36}$$

for XAS (Ohtaka and Tanabe, 1984), and

$$\begin{aligned} \phi(t) &= \sum_m |X_{m+}|^2 e^{-i\varepsilon_m t} + \sum_\gamma |X_{\gamma+}|^2 e^{-i\varepsilon_\gamma t} e^{-\beta(\varepsilon_\gamma - \mu)}, \\ \bar{\phi}(t) &= \sum_b |\bar{X}_{b+}|^2 e^{i\varepsilon_b t} + \sum_\mu |\bar{X}_{\mu+}|^2 e^{i\varepsilon_\mu t} e^{\beta(\varepsilon_\mu - \mu)} \end{aligned} \tag{7.37}$$

for XES (Ohtaka and Tanabe, 1989). These functions of course reduce to Eqs. (7.29) and (7.34) at $T=0$. However, they are not so convenient to deal with. First of all, it is not clear at all in this form that the temperature effect should show up eventually in the Fermi distribution functions. Furthermore, it is by no means evident how we should convert the right-hand sides of Eqs. (7.36) and (7.37) into expressions to be employed in the continuum scheme for the energy levels.

If we start from exact expressions for the Δ 's in the continuum scheme, as indicated in the paragraph explaining Eq. (7.26), we can arrive at the correct expressions for $A(t)$ and $I_0(t)$ in that scheme, after considerable manipulation. The final result reads (Ohtaka and Tanabe, 1984)

where $F(t + \sigma, t + \tau)$ is the solution of the integral equation (7.32), with the kernel Λ defined by

$$\Lambda(t + \sigma, t + \rho) = [N(0)V]^2 \int_0^\infty d\xi \bar{\Psi}(t + \sigma + \xi) \Psi(t + \rho + \xi). \tag{7.40}$$

The time-independent quantity η^0 is given by

$$\eta^0 = \Delta E^0 - \frac{i}{2\pi} \int_D^D d\varepsilon \ln[1 + f(\varepsilon)(e^{2i\delta(\varepsilon)} - 1)], \tag{7.41}$$

where $f(\varepsilon)$ is the Fermi distribution function [Eq. (6.4)]. Note that ΔE^0 given by Eq. (2.9) may be expressed as (Fumi, 1955)

$$\Delta E^0 = - \int_D^D d\varepsilon \delta(\varepsilon) / \pi, \tag{7.42}$$

according to Eq. (7.14), so that η^0 vanishes at $T=0$. We also find that the real part of η^0 makes the threshold ω_{th}^0 shift to ω_{th} given by

$$\omega_{th} = \omega_{th}^0 - \text{Re}\eta^0, \tag{7.43}$$

whereas $\text{Im}\eta^0$ plays the role of a damping constant.

The functions $\Psi(t)$ and $\bar{\Psi}(t)$ are defined by

$$\begin{aligned} N(0)\Psi(t) &= \int_D^D d\varepsilon N(\varepsilon) \bar{f}(\varepsilon) e^{-i\varepsilon t} e^{\theta(\varepsilon)}, \\ N(0)\bar{\Psi}(t) &= \int_D^D d\varepsilon N(\varepsilon) f(\varepsilon) e^{i\varepsilon t} e^{\bar{\theta}(\varepsilon)} \end{aligned} \tag{7.44}$$

for XAS, where we have put

$$\bar{f}(\varepsilon) = 1 - f(\varepsilon) \tag{7.45}$$

and

$$\begin{aligned} \theta(\varepsilon) &= \frac{1}{\pi i} \int_D^D d\varepsilon' P \frac{\ln[1 + \bar{f}(\varepsilon')(e^{-2i\delta(\varepsilon')} - 1)]}{\varepsilon - \varepsilon'}, \\ \bar{\theta}(\varepsilon) &= - \frac{1}{\pi i} \int_D^D d\varepsilon' P \frac{\ln[1 + f(\varepsilon')(e^{2i\delta(\varepsilon')} - 1)]}{\varepsilon - \varepsilon'}. \end{aligned} \tag{7.46}$$

For XES, we simply replace the second factor $\bar{f}(\varepsilon)$ and $f(\varepsilon)$ in the integrands of Eq. (7.44) by $f(\varepsilon)$ and $\bar{f}(\varepsilon)$, respectively.

VIII. EDGE BEHAVIORS

A. Asymptotic solution of the integral equation

As will be seen below, with a contact potential, an exact analytic treatment becomes possible near threshold, that is, in the region $\omega \simeq 0$. This applies not only to the exponent of the power law, but also to its amplitude.

Let us begin with the case of XAS at $T=0$ (Ohtaka and Tanabe, 1983). To study the behaviors of the spectra near threshold, we only need to know asymptotic forms of $A(t)$ and $I_0(t)$. From the expressions given in the previous section, we realize that they can be obtained, once we know the asymptotic forms for $\phi(t)$ and $\bar{\phi}(t)$ and succeed in solving the integral equation for $F(t + \sigma, t + \tau)$ for large t .

The first problem is not difficult. We first note for

small values of ε_γ and $|\varepsilon_\mu|$ that we have

$$\begin{aligned} |X_{\gamma+}|^2 &= \varepsilon_\gamma^{-\alpha} |X(0)|^2, \\ |\bar{X}_{\mu+}|^2 &= |\varepsilon_\mu|^\alpha |\bar{X}(0)|^2 \end{aligned} \tag{8.1}$$

approximately, with

$$\alpha = 2\delta(0) / \pi, \tag{8.2}$$

where $\delta(0)$ is the phase shift at the Fermi level, and

$$\begin{aligned} |X(0)|^2 &= D^\alpha \exp \left[\frac{2}{\pi} \int_0^D d\varepsilon \frac{\delta(\varepsilon) - \delta(0)}{\varepsilon} \right], \\ |\bar{X}(0)|^2 &= |\bar{D}|^{-\alpha} \exp \left[\frac{2}{\pi} \int_D^0 d\varepsilon \frac{\delta(\varepsilon) - \delta(0)}{\varepsilon} \right]. \end{aligned} \tag{8.3}$$

Note that we are working in the continuum scheme for the band states. These results may be obtained by rewriting the integrands in the exponent of Eq. (7.25), for example, as $\delta(\varepsilon)/(\varepsilon_\mu - \varepsilon) = \delta(0)/(\varepsilon_\mu - \varepsilon) + [\delta(\varepsilon) - \delta(0)]/(\varepsilon_\mu - \varepsilon)$ and putting $\varepsilon_\mu = 0$ in the second term. The asymptotic forms of $\phi(t)$ and $\bar{\phi}(t)$ are determined by the two equations (8.1) for small values of ε_γ and $|\varepsilon_\mu|$, respectively. Putting $D, |\bar{D}| \rightarrow \infty$ in the definitions of $\phi(t)$ and $\bar{\phi}(t)$ [Eq. (7.29) with Eqs. (7.35)], we obtain

$$\begin{aligned} \phi(t) &= (it)^{-1+\alpha} \Gamma(1-\alpha) |X(0)|^2, \\ \bar{\phi}(t) &= (it)^{-1-\alpha} \Gamma(1+\alpha) |\bar{X}(0)|^2, \end{aligned} \tag{8.4}$$

where $\Gamma(x)$ is the gamma function. This then enables us to write down the asymptotic expression for Λ :

$$\Lambda(t + \sigma, t + \rho) = \frac{\tan\delta(0)}{2\pi} \frac{1}{\sigma - \rho} \left[\left(\frac{t + \rho}{t + \sigma} \right)^\alpha - 1 \right], \tag{8.5}$$

where we have made use of the identity

$$|X(0)|^2 |\bar{X}(0)|^2 = |X_0(z=0+)|^2 \tag{8.6}$$

together with Eq. (7.23).

It is convenient to introduce new variables x and y , defined as follows, in place of $t + \sigma$ and $t + \tau$ to determine the asymptotic form of F :

$$x = t / (t + \sigma), \quad y = t / (t + \tau). \tag{8.7}$$

If we put

$$F(t + \sigma, t + \tau) = t^{-1} x^{1+\alpha} y^{1-\alpha} \bar{F}(x, y), \tag{8.8}$$

it turns out that $\bar{F}(x, y)$ is independent of t and satisfies the integral equation that follows from Eq. (7.32) with Eq. (8.5):

$$\bar{F}(x, y) + \frac{\tan\delta(0)}{2\pi} \int_0^1 dz \frac{1 - (z/x)^\alpha}{x - z} \bar{F}(z, y) = \delta(x - y). \tag{8.9}$$

The asymptotic expressions of $A(t)$ and $I_0(t)$ may also be given by

$$A(t) = -\frac{\delta(0) \tan \delta(0)}{\pi^2} \int_0^1 dx \int_0^1 dy \bar{F}(x, y) / t, \quad (8.10)$$

$$I_0(t) = N_0 |w|^2 \phi(t) \int_0^1 dx \bar{F}(x, 1-), \quad (8.11)$$

in terms of definite integrals involving $\bar{F}(x, y)$. In Eq. (8.11), the first equation of Eq. (8.4) for $\phi(t)$ is to be employed. We observe at this stage that a power law should be valid for both $P(\omega)$ and $I_0(\omega)$. Our next problem is

$$\bar{F}(x, y) = \left[\frac{1}{2\pi i} \right]^2 \int_{l_1} ds_1 U(s_1) x^{-s_1} \int_{l_2} ds_2 V(s_2) y^{s_2-1} / (s_1 - s_2), \quad (8.12)$$

with

$$U(s) = [\Gamma(s - \alpha/2)]^2 / \Gamma(s) \Gamma(s - \alpha), \quad (8.13)$$

$$V(s) = [\Gamma(1 - s + \alpha/2)]^2 / \Gamma(1 - s) \Gamma(1 - s + \alpha),$$

where the straight lines l_1 and l_2 in the complex s plane are drawn parallel to an imaginary axis crossing the real axis at $s_1 = \sigma_1$ and $s_2 = \sigma_2$, respectively, with

$$\text{Max}(\alpha, 0) < \sigma_2 < \sigma_1 < \text{Min}(1 + \alpha, 1), \quad (8.14)$$

assuming $|\alpha| < 1$. Note that $U(s_1)$ [$V(s_2)$] is regular and free from zeros on the right- (left-)hand side of l_1 (l_2). Once the solution $\bar{F}(x, y)$ as given in Eq. (8.12) is obtained, it is not difficult to evaluate the values of the integrals appearing on the right-hand sides of Eqs. (8.10) and (8.11). The resulting asymptotic expressions for $A(t)$ and $I_0(t)$ are given by

$$A(t) = -[\delta(0)/\pi]^2 t^{-1}, \quad (8.15)$$

$$I_0(t) = N(0) |w|^2 [\Gamma(1 - \alpha/2)]^2 |X(0)|^2 (it)^{-1+\alpha}, \quad (8.16)$$

where we have taken Eq. (8.4) into account.

In the case of XES, the edge behavior at $T=0$ can also be examined by first studying the asymptotic forms of $\phi(t)$ and $\bar{\phi}(t)$ relevant to the emission problem [Eq. (7.34)]. They are given by

$$\begin{aligned} \phi(t) &= (-it)^{-1+\alpha} \Gamma(1 - \alpha) |X(0)|^2, \\ \bar{\phi}(t) &= (-it)^{-1-\alpha} \Gamma(1 + \alpha) |\bar{X}(0)|^2. \end{aligned} \quad (8.17)$$

This result implies that $A(t)$ for inverse photoemission is also given by Eq. (8.15), while $I_0(t)$ for XES is given by the complex conjugate of Eq. (8.16), that is, the expression obtained by replacing (it) by $(-it)$ on the right-hand side of Eq. (8.16).

B. Behaviors at $T=0$

Having obtained asymptotic expressions for $A(t)$ and $I_0(t)$ (for both XAS and XES), we are now able to discuss the edge behaviors of the spectra. Let us begin with the

thus to solve Eq. (8.9) for $\bar{F}(x, y)$ to determine the exponent (critical exponent) of the power law for $P(\omega)$ and amplitude (critical amplitude) for $I_0(\omega)$.

It can be shown that the integral equation (8.9) is solvable by means of the Wiener-Hopf technique (see, for example, Smirnov, 1965). Referring the reader to the original paper (Ohtaka and Tanabe, 1983) for the details, we simply give the final expression for the solution $\bar{F}(x, y)$. In terms of the variables x and y , the solution is expressed in the form of a double Mellin transform,

x-ray photoemission spectra. The well-known power law is derived in the following way. We assume Eq. (8.15) to be valid for t greater than a sufficiently large characteristic time t_0 , and put

$$\begin{aligned} P(t) &= \exp \left[\int_0^{t_0} d\tau A(\tau) - \int_{t_0}^t d\tau \frac{\sigma}{\tau} \right] \\ &= C_0 (iW_b t)^{-\sigma}. \end{aligned} \quad (8.18)$$

Here $W_b = D + |\bar{D}|$ is the total bandwidth, the critical exponent σ is given by

$$\sigma = [\delta(0)/\pi]^2, \quad (8.19)$$

and C_0 , which we call the critical amplitude of the photoemission, is defined by

$$\ln C_0 = \lim_{t_0 \rightarrow \infty} \left[\int_0^{t_0} A(\tau) d\tau + \sigma \ln(iW_b t_0) \right]. \quad (8.20)$$

That we can use the same notation C_0 as in the orthogonality theorem (2.13) will be shown in Secs. VIII.E and IX.D. Practically, the limiting value of the right-hand side will be attained for a t_0 which is a few times as large as $1/D$, as will be seen in Sec. XI.G, where we examine the validity of the asymptotic form (8.15).

The Fourier transform $P(\omega)$ of $P(t)$ given by Eq. (8.18) describes the photoemission spectrum near threshold $\omega > 0$. In fact, Eq. (4.12) leads to the Nozières-DeDominicis power law (Ohtaka and Tanabe, 1983; Tanabe and Ohtaka, 1985):

$$P(\omega) = 2\pi C_0 (\omega/W_b)^{\sigma-1} / [W_b \Gamma(\sigma)], \quad (\omega > 0) \quad (8.21)$$

because we have

$$\int_0^\infty dt (it)^{-\sigma} e^{i\omega t} = \omega^{\sigma-1} \Gamma(1 - \sigma) i e^{-i\sigma\pi} \quad (8.22)$$

for $\omega > 0$.

The x-ray absorption spectrum $I(\omega)$ near threshold can be calculated either as the convolution of $I_0(\omega)$ with $P(\omega)$ or directly as the Fourier transform of $I(t) = P(t)I_0(t)$ by means of Eq. (4.28):

$$I_0(\omega) = 2\pi N(0) |w|^2 \Xi(\omega/D)^{-\alpha}, \tag{8.23}$$

$$I(\omega) = 2\pi N(0) |w|^2 C_0 \Xi[\Gamma(1-\alpha)/\Gamma(1-\alpha+\sigma)] \times (\omega/W_b)^\sigma (\omega/D)^{-\alpha}, \tag{8.24}$$

where Ξ is a quantity called the critical amplitude of x-ray absorption by Mahan (1982) and is given by

$$\Xi = D^{-\alpha} |X(0)|^2 [\Gamma(1-\alpha/2)]^2 / \Gamma(1-\alpha). \tag{8.25}$$

For inverse photoemission, we define $P(t)$ as

$$P(t) = C_0 (-iW_b t)^{-\sigma} \tag{8.26}$$

with the same value of C_0 as in Eq. (8.20). This, together with Eq. (8.22), leads to

$$\begin{aligned} \Psi(t) &= (i \sinh \pi T t / \pi T)^{-1+\alpha} [\Gamma(1-\alpha/2)]^2 F(\alpha/2, \alpha/2, 1 | e^{-2\pi T t}) |X(0)|^2, \\ \bar{\Psi}(t) &= (i \sinh \pi T t / \pi T)^{-1+\alpha} [\Gamma(1+\alpha/2)]^2 F(-\alpha/2, -\alpha/2, 1 | e^{-2\pi T t}) |\bar{X}(0)|^2, \end{aligned} \tag{8.28}$$

where $F(a, b, c | z)$ is the hypergeometric function. As we let $T \rightarrow 0$, $\Psi(t)$ and $\bar{\Psi}(t)$ tend correctly to $\phi(t)$ and $\bar{\phi}(t)$, respectively, as given by Eq. (8.4). However, with Eq. (8.28), it is unlikely that we shall be able to evaluate $\Lambda(t + \sigma, t + \rho)$ in a closed form as before. It will be even more unlikely with $F(t + \sigma, t + \tau)$. At best, we can try a power-series expansion of $F(t + \sigma, t + \tau)$ with respect to $\exp[-2\pi T(t + \sigma)]$ and $\exp[-2\pi T(t + \tau)]$. In fact, this primitive method works, and we eventually obtain the following closed (asymptotic) expressions for $A(t)$ and $I_0(t)$:

$$\begin{aligned} A(t) &= i \operatorname{Re} \eta^0 - \pi T \sigma - 2\pi T \sigma e^{-2\pi T t} / (1 - e^{-2\pi T t}) \\ &= i \operatorname{Re} \eta^0 - \pi T t \coth \pi T t, \end{aligned} \tag{8.29}$$

$$I_0(t) = N(0) |w|^2 [\Gamma(1-\alpha/2)]^2 |X(0)|^2 (i \sinh \pi T t / \pi T)^{-1+\alpha}. \tag{8.30}$$

Note that $-\operatorname{Im} \eta^0$ in Eq. (7.38) gives rise to the second term on the right-hand side of Eq. (8.29), whereas the double integral thereof leads to the third term.

The response function $P(t)$ for photoemission then takes the asymptotic form

$$P(t) = e^{i \operatorname{Re} \eta^0 t} C_0 (iW_b \sinh \pi T t / \pi T)^{-\sigma}. \tag{8.31}$$

Here the critical amplitude C_0 is temperature independent with its value given by Eq. (8.20), as shown by Tanabe (1986). Equations (8.30) and (8.31) correspond to Eqs. (3.18) obtained by Anderson and Yuval (1967). We now have their exact forms, including their prefactors. Naturally, Eq. (8.31) tends to Eq. (8.18) as $T \rightarrow 0$. Comparing Eq. (8.18) with Eq. (8.31), we find that, apart from the factor $e^{i \operatorname{Re} \eta^0 t}$, $P(t)$ at a finite temperature T may be obtained by replacing t in the result obtained at absolute zero temperature [see Eq. (8.18)] with $\sinh \pi T t / \pi T$, the result first obtained by Anderson and Yuval (Sec. III.C.3). This is also true with $I_0(t)$ [compare Eq. (8.16)

$$P(\omega) = 2\pi C_0 |\omega/W_b|^{\sigma-1} / [W_b \Gamma(\sigma)] \quad (\omega < 0). \tag{8.27}$$

The expression for $I_0(\omega)$ near threshold for XES is also obtained by replacing ω in Eq. (8.23) by $|\omega|$ for negative ω , so that the edge spectrum for emission is the mirror image of that for absorption.

C. Behaviors at finite T

At finite temperatures, we need asymptotic expressions for $\Psi(t)$ and $\bar{\Psi}(t)$ in order to study the absorption spectra near threshold (Ohtaka and Tanabe, 1984). They are given by

with Eq. (8.30).

The Fourier transform $P(\omega)$ is given by

$$P(\omega) = 2\pi C_0 \omega'^{\sigma-1} p[\omega'/T, \sigma] / W^\sigma \Gamma(\sigma), \tag{8.32}$$

with $\omega' = \omega + \operatorname{Re} \eta^0$, where $p[\omega/T, \sigma]$ is defined by

$$\begin{aligned} \int_0^\infty dt (i \sinh \pi T t / \pi T)^{-\sigma} e^{i \omega t} \\ = \omega^{\sigma-1} p[\omega/T, \sigma] \Gamma(1-\sigma) i (e^{-i \sigma \pi} - e^{-\omega/T}) \end{aligned} \tag{8.33}$$

and given explicitly by

$$p[\omega/T, \sigma] = \frac{e^{\omega/2T}}{2\pi} (2\pi T/\omega)^{\sigma-1} \left| \Gamma \left[\frac{\sigma}{2} + i \frac{\omega}{2\pi T} \right] \right|^2. \tag{8.34}$$

As T tends to zero, $p[\omega/T, \sigma]$ approaches Heaviside's unit function.

Corresponding to Eqs. (8.23) and (8.24), we have

$$I_0(\omega) = 2\pi N(0) |w|^2 \Xi(\omega/D)^{-\alpha} p[\omega/T, 1-\alpha], \tag{8.35}$$

$$I(\omega) = 2\pi N(0) |w|^2 C_0 \Xi[\Gamma(1-\alpha)/\Gamma(1-\alpha+\sigma)] p[\omega'/T, 1-\alpha+\sigma] (\omega'/W_b)^{\sigma-1} (\omega'/D)^{-\alpha}. \tag{8.36}$$

We note that temperature effects enter only through the factors $p[\omega/T, 1-\alpha]$ and $p[\omega'/T, 1-\alpha+\sigma]$, where the frequency ω' is the modified photon frequency, as in Eq. (8.32).

In the case of XES, we have only to replace $i \sinh \pi T t / \pi T$ in Eqs. (8.30) and (8.31) by its complex conjugate $-i \sinh \pi T t / \pi T$. This means that the emission edge spectra are the mirror image of the absorption spectra with respect to the line at $\omega = \omega_{th} = \omega_{th}^0 - \text{Re} \eta^0$.

D. Critical amplitude and the orthogonality theorem

With the discrete scheme for the band energies and $a_{\kappa k}$ given by Eq. (7.3), it is possible to evaluate the overlap integral Δ [Eq. (4.7)] or its square in the following form (Tanabe and Ohtaka, 1985):

$$|\Delta|^2 = \prod_{\mu} X(\varepsilon_{\mu}) / \prod_m X(\varepsilon_m) = \prod_{\gamma} \bar{X}(\varepsilon_{\gamma}) / \prod_b \bar{X}(\varepsilon_b), \tag{8.37}$$

where X and \bar{X} are defined by Eqs. (7.8) and (7.9) and Eq. (7.6) has been used to eliminate the normalization constants. It then follows from Eq. (8.37) that

$$F = -\ln |\Delta|^2 = \sum_{b,m} \ln \left[1 - \frac{\varepsilon_{\mu} - \varepsilon_m}{\varepsilon_{\gamma} - \varepsilon_m} \right] - \sum_{b,m} \ln \left[1 - \frac{\varepsilon_{\mu} - \varepsilon_m}{\varepsilon_b - \varepsilon_m} \right]. \tag{8.38}$$

In taking the summation over b and m on the right-hand side, the excited-configuration energies ε_{γ} and ε_{μ} are to be correlated with the ground-configuration energies ε_b and ε_m by means of Eq. (7.14) (put $k=b$ and $k=m$ for $\kappa=\gamma$ and $\kappa=\mu$, respectively). Now, if the energy dependence of the phase shift is neglected, so that δ_k is put equal to $\delta(0)$, the phase shift at the Fermi level, the sum on the right-hand side can be evaluated in the limit $\Delta \varepsilon_k \rightarrow 0$, and the result turns out to be

$$F_0 = -\ln(1-\sigma) + \sigma \gamma(\sigma) - \sigma \ln(W_b \Delta \varepsilon / D |\bar{D}|) \tag{8.39}$$

with $\Delta \varepsilon [=1/N(0)]$ the level spacing at the Fermi level and $\gamma(\sigma)$ given by

$$\gamma(\sigma) = \gamma + \sum_{k=2}^{\infty} \frac{\zeta(2k-1)-1}{k} \sigma^{k-1}, \tag{8.40}$$

where γ is the Euler constant 0.5772... and $\zeta(s)$ is the Riemann zeta function. The energy dependence of the phase shift introduces the correction

$$F - F_0 = \frac{1}{\pi^2} \int_0^D d\varepsilon \int_{\bar{D}}^0 d\varepsilon' \frac{\delta(\varepsilon)\delta(\varepsilon') - \delta(0)^2}{(\varepsilon - \varepsilon')^2} \equiv \xi. \tag{8.41}$$

Putting Eqs. (8.38), (8.39), and (8.41) together, we obtain

$$|\Delta|^2 = C_0 (\Delta \varepsilon / W_b)^{\sigma}, \tag{8.42}$$

which reproduces the orthogonality theorem of Anderson [Eq. (2.13)]. The result given leads to the following expression for the proportionality constant C_0 :

$$C_0 = (1-\sigma) \left[\frac{W_b^2}{D |\bar{D}|} e^{-\gamma(\sigma)} \right]^{\sigma} e^{-\xi}. \tag{8.43}$$

Since we have used the same notation C_0 for the proportionality constant in Eq. (8.41) and for the critical amplitude in Eq. (8.21), readers may wonder if they are one and the same quantity. That this is really the case can be proved rigorously (Tanabe and Ohtaka, 1985; Tanabe, 1986; Sec. IX.D). However, we shall not go into the details of the general proof here. Instead, we shall see how they are related to each other through the simple derivation of the power law by Feldkamp and Davis (1980).

E. Derivation of power law following Feldkamp and Davis

In Sec. IV.B, we introduced $P(\omega)$ as the Fourier transform of the response function $P(t)$ for x-ray photoemission. In the edge region of a conduction band with discrete energy levels, the intensity of the spectrum for the excitation energy $\omega_n = n \Delta \varepsilon$ ($n=0, 1, 2, \dots$) measured from the threshold will be given by $P(\omega_n) \Delta \varepsilon$, where $\Delta \varepsilon [=N(0)^{-1}]$ is the level spacing at the Fermi level assumed to be constant in this region. Now, from Eq. (4.14) or Eq. (4.20), we find that $P(\omega_n) \Delta \varepsilon$ for small n may be evaluated easily. For example, we have (Tanabe and Ohtaka, 1985)

$$P(0) \Delta \varepsilon = 2\pi |\Delta|^2 \tag{8.44}$$

for $n=0$ and

$$P(\omega_n) \Delta \varepsilon = 2\pi \sum_{\mu, \gamma} |\Delta(\bar{\mu} \gamma)|^2 \tag{8.45}$$

for $1 \leq n < 4$. The summation in the latter equation is to be carried out over pairs of μ and γ such that $\varepsilon_{\gamma} - \varepsilon_{\mu} = n \Delta \varepsilon$. For ε_{γ} and ε_{μ} , we make use of Eq. (7.14), putting $\delta_k = \delta(0)$ and $\Delta \varepsilon_k = \Delta \varepsilon$. For $4 \leq n < 9$, we have to include the contribution from the two electron-hole pair excitations so that

$$P(\omega_n) \Delta \varepsilon = 2\pi \sum_{\mu, \gamma} |\Delta(\bar{\mu} \gamma)|^2 + 2\pi \sum_{\{\mu\}} \sum_{\{\gamma\}} |\Delta(\bar{\mu}_1 \bar{\mu}_2 \gamma_1 \gamma_2)|^2. \tag{8.46}$$

The second summation on the right-hand side of Eq. (8.46) is to be carried out over μ 's ($\mu_1 < \mu_2$) and γ 's ($\gamma_1 < \gamma_2$) such that $\sum_s \varepsilon_{\gamma_s} - \sum_s \varepsilon_{\mu_s} = n \Delta \varepsilon$. As n becomes larger and larger, we have to take more and more multi-electron-hole pair excitations into account.

If we put

$$\begin{aligned} \varepsilon_b &= (b + \frac{1}{2}) \Delta \varepsilon \quad (b=0, 1, 2, \dots), \\ \varepsilon_m &= -(m + \frac{1}{2}) \Delta \varepsilon \quad (m=0, 1, 2, \dots) \end{aligned} \tag{8.47}$$

for the unperturbed energies near the Fermi level $\varepsilon_F=0$, we can derive the expression of $\Delta(\bar{\mu}\gamma|)$ from Eqs. (7.12), (7.13), and (7.23) as follows:

$$\Delta(\bar{\mu}\gamma|)/\Delta = -(\alpha/2) \frac{1}{b+m+1} \times \prod_{k=1}^b \left[1 - \frac{\alpha/2}{k} \right] \prod_{k=1}^m \left[1 + \frac{\alpha/2}{k} \right], \quad (8.48)$$

where the third and fourth factors should be put to unity for $b=0$ and $m=0$, respectively. Equation (8.48) then enables us to evaluate the right-hand sides of Eqs. (8.45) and (8.46) [for the second term of Eq. (8.46), use Eq. (4.11)], and we find

$$P(\omega_n)\Delta\varepsilon = 2\pi|\Delta|^2 \prod_{k=1}^n \left[1 + \frac{\sigma-1}{k} \right] \quad (8.49)$$

for $n < 9$. Actually, Feldkamp and Davis (1980) confirmed this equality up to $n=15$, which corresponds to the excitation of three pairs. Now, if we assume that Eq. (8.49) holds up to $n=\infty$, we obtain

$$P(\omega_n)\Delta\varepsilon = 2\pi C_0 (\Delta\varepsilon/W_b)^\sigma n^{\sigma-1} \Gamma(\sigma) \quad (8.50)$$

for very large n by making use of Eq. (8.42) and the property of the gamma function. This equation is nothing but Eq. (3.32) with \mathcal{N} replaced by \mathcal{N}_{eff} as defined by Eq. (2.15). Dividing both sides by $\Delta\varepsilon$ and putting $\omega=\omega_n=n\Delta\varepsilon$, we arrive at Eq. (8.21) or Eq. (3.34) with Eq. (3.35).

Note that the procedure employed here is free from any restriction on the level spacing of the conduction band (see Sec. III.F.5) and that in this regard the orthogonality theorem is expressed most conveniently in terms of $(W_b/\Delta\varepsilon)^{-\sigma}$, not of $N^{-\sigma}$ as in the original form of Anderson.

IX. MODIFICATION DUE TO THE PRESENCE OF A BOUND STATE IN THE EXCITED CONFIGURATION

A. Separation into main and secondary bands

In order to resolve a spectrum into the main and secondary bands in the presence of a bound state λ with energy ε_λ , the best strategy is to separate all terms containing the factor $e^{i\varepsilon_\lambda t}$ from the rest and then regroup them (Tanabe and Ohtaka, 1984). The factor gives rise to a secondary band that appears $|\varepsilon_\lambda|$ higher than the main band. We restrict ourselves here to photoemission and absorption at $T=0$ (remember that we need never consider the secondary XES band). We may start from Eq. (4.42) with Eqs. (4.24), (4.25), and (4.43) by regarding one of the states μ to be the bound state λ .

In the expression of $P(t)$ reproduced here as

$$P(t) = D(t)/D(0), \quad (9.1)$$

$D(t)$ was given by

$$D(t) = \det |1 + \mathbf{K}(t)e^{-i\varepsilon t}|, \quad (9.2)$$

The definition (4.17) of the $M \times M$ matrix $\mathbf{K} = [K_{\gamma\gamma'}(t)]$ shows that a term with $e^{i\varepsilon_\lambda t}$ is included in every matrix element of \mathbf{K} . Since this is not very convenient, we transform $D(t)$ into a determinant of another matrix involving a new $N \times N$ matrix $\bar{\mathbf{K}}(t)$ as follows:

$$D(t) = \det |1 + e^{i\varepsilon t} \bar{\mathbf{K}}(t)|, \quad (9.3)$$

where the new matrix $\bar{\mathbf{K}}(t)$, whose rows and columns are labeled by μ and μ' , is defined by

$$\bar{K}_{\mu\mu'}(t) = \sum_{\gamma} \Delta(\mu\gamma|)^* e^{-i\varepsilon_\gamma t} \Delta(\mu'\gamma|)/|\Delta|^2. \quad (9.4)$$

The right-hand side no longer contains the factor $e^{i\varepsilon_\lambda t}$. In the transformation leading to Eq. (9.3), we have used the identity

$$\det |1 + \mathbf{A}\mathbf{B}| = \det |1 + \mathbf{B}\mathbf{A}|, \quad (9.5)$$

valid for any two rectangular matrices \mathbf{A} and \mathbf{B} . In the determinant (9.3), the factor $e^{i\varepsilon_\lambda t}$ now appears only in the row $\mu=\lambda$. Thus by expanding it with respect to row λ and column λ , we can single out the factor $e^{i\varepsilon_\lambda t}$ as required:

$$D(t) = D'(t)[1 + e^{i\varepsilon_\lambda t} \Sigma(t)], \quad (9.6)$$

where

$$D'(t) = \det |1 + e^{i\varepsilon t} \bar{\mathbf{K}}'(t)| \\ = \det |1 + \mathbf{K}'(t)e^{-i\varepsilon t}| \quad (9.7)$$

and

$$\Sigma(t) = \bar{K}_{\lambda\lambda}(t) - \sum_{\mu, \mu'} \bar{K}_{\lambda\mu}(t) [1 + e^{i\varepsilon t} \bar{\mathbf{K}}'(t)]_{\mu\mu'}^{-1} e^{i\varepsilon_\mu t} \bar{K}_{\mu'\lambda}(t). \quad (9.8)$$

Here $\bar{\mathbf{K}}'(t)$ stands for a matrix obtained from $\bar{\mathbf{K}}(t)$ with its column λ and row λ deleted. $D'(t)$ is thus the $\lambda\lambda$ cofactor of $D(t)$. In the second line of Eq. (9.7), we have used Eq. (9.5) with the definition

$$K'_{\gamma\gamma'}(t) = \sum_{\mu (\neq \lambda)} \Delta(\mu\gamma|) e^{-i\varepsilon_\mu t} \Delta(\bar{\mu}\gamma')^* / |\Delta|^2. \quad (9.9)$$

From Eqs. (9.1) and (9.6), we obtain

$$P(t) = P_{\text{main}}(t) + P_{\text{sec}}(t) e^{i\varepsilon_\lambda t} \quad (9.10)$$

with

$$P_{\text{main}}(t) = D^*(t)/D(0), \quad (9.11)$$

$$P_{\text{sec}}(t) = D'(t)\Sigma(t)/D(0), \quad (9.12)$$

the first giving rise to the main photoemission band and the second the secondary band.

Similarly, $I_0(t)$ of Eq. (4.43) is decomposed as follows:

$$I_0(t) = I'_0(t) - e^{i\varepsilon_\lambda t} Q(t) \bar{Q}(t) / [1 + e^{i\varepsilon_\lambda t} \Sigma(t)] \quad (9.13)$$

with

$$I'_0(t) = \sum_{\gamma, \gamma'} p(\gamma)^* \{ e^{-i\varepsilon t} [1 + \mathbf{K}'(t) e^{-i\varepsilon t}]^{-1} \}_{\gamma \gamma'} p(\gamma'), \quad (9.14)$$

$$Q(t) = \sum_{\gamma, \gamma'} p^*(\gamma) \{ e^{-i\varepsilon t} [1 + \mathbf{K}'(t) e^{-i\varepsilon t}]^{-1} \}_{\gamma \gamma'} \left[\frac{\Delta(\bar{\lambda} \gamma |)}{\Delta} \right], \quad (9.15)$$

$$\bar{Q}(t) = \sum_{\gamma, \gamma'} \left[\frac{\Delta(\bar{\lambda} \gamma |)}{\Delta} \right]^* \{ e^{-i\varepsilon t} [1 + \mathbf{K}'(t) e^{-i\varepsilon t}]^{-1} \}_{\gamma \gamma'} p(\gamma').$$

Combining Eqs. (9.10) and (9.13), we find

$$I(t) = I_{\text{main}}(t) + I_{\text{sec}}(t) e^{i\varepsilon_\lambda t} \quad (9.16)$$

with

$$I_{\text{main}}(t) = [D'(t)/D(0)] I'_0(t), \quad (9.17)$$

$$I_{\text{sec}}(t) = [D'(t)/D(0)] \Sigma(t) I_1(t), \quad (9.18)$$

where $I_1(t)$ is given by

$$I_1(t) = I'_0(t) - Q(t) \bar{Q}(t) / \Sigma(t). \quad (9.19)$$

Here the energy shift of the ground state in ω_{th}^0 is given by

$$\Delta E^0 = \sum_{\mu} \varepsilon_{\mu} - \sum_{m} \varepsilon_m + (\varepsilon_{\lambda} - D). \quad (9.20)$$

The prime on the second sum indicates that the lowest ε_m of the band states (equal to \bar{D}) is to be removed in accordance with the restriction $\mu \neq \lambda$ in the first sum.

B. Integrated intensities

The integrated intensities of the main and secondary photoemission bands are given by 2π times $P_{\text{main}}(0)$ and $P_{\text{sec}}(0)$. From Eq. (9.6), which shows that

$$D'(0)/D(0) = 1/[1 + \Sigma(0)] \equiv \eta, \quad (9.21)$$

we obtain

$$\begin{aligned} P_{\text{main}}(0) &= 1 - \eta, \\ P_{\text{sec}}(0) &= \eta. \end{aligned} \quad (9.22)$$

The relation between η and the overlap integral $a_{\kappa\kappa}$ is found as follows. Substituting Eq. (4.10) into Eq. (9.4), we obtain

$$\begin{aligned} [1 + \mathbf{K}(0)]_{\mu\mu'} &= \delta_{\mu\mu'} + \sum_{\kappa(>)} \sum_{m, m'} a_{\kappa m} (\mathbf{A}^{-1})_{m\mu} \\ &\quad \times [a_{\kappa m'} (\mathbf{A}^{-1})_{m'\mu'}]^*, \end{aligned} \quad (9.23)$$

the sum over κ being taken over the states above the Fermi level, i.e., over γ . Using the identity

$$\delta_{\mu\mu'} = \sum_{\kappa(<)} \sum_{m, m'} a_{\kappa m} (\mathbf{A}^{-1})_{m\mu} [a_{\kappa m'} (\mathbf{A}^{-1})_{m'\mu'}]^* \quad (9.24)$$

with the sum over κ below the Fermi level (including λ), we can make use of the closure relation

$$\sum_{\kappa(\text{all})} a_{\kappa m} a_{\kappa m'}^* = \delta_{mm'} \quad (9.25)$$

in Eq. (9.23). It then follows that

$$[1 + \mathbf{K}(0)]_{\mu\mu'} = \sum_m (\mathbf{A}^{-1})_{m\mu} (\mathbf{A}^{-1})_{m'\mu'}^*. \quad (9.26)$$

Then, for $\mu = \mu' = \lambda$ in particular, we obtain

$$1 - \eta = [1 + \mathbf{K}(0)]_{\lambda\lambda}^{-1} = \sum_m |a_{\lambda m}|^2 \quad (9.27)$$

or again by the closure relation

$$\eta = \sum_b |a_{\lambda b}|^2. \quad (9.28)$$

The transformation of $I'_0(0)$ and $I_1(0)$ [or $Q(0)$ and $\bar{Q}(0)$] in Eqs. (9.17) and (9.18) proceeds analogously by substituting Eq. (4.35) for $p(\gamma)$. It will suffice here to write down the final results,

$$I'_0(0) = \sum_b |w_{bc}|^2 + (1 - \eta) |Q(0)|^2, \quad (9.29)$$

$$\begin{aligned} Q(0) &= \bar{Q}(0)^* \\ &= - \sum_b a_{\lambda b} w_{bc} / (1 - \eta). \end{aligned} \quad (9.30)$$

The expressions for $I_{\text{main}}(t)$ and $I_{\text{sec}}(t)$ given by Eqs. (9.17) and (9.18) then lead to

$$\begin{aligned} I_{\text{main}}(0) &= (1 - \eta) \sum_b |w_{bc}|^2 + \left| \sum_b a_{\lambda b} w_{bc} \right|^2, \\ I_{\text{sec}}(0) &= \eta \sum_b |w_{bc}|^2 - \left| \sum_b a_{\lambda b} w_{bc} \right|^2. \end{aligned} \quad (9.31)$$

Naturally, the sum conforms to the sum rule Eq. (6.2) at $T=0$.

C. Critical exponents

First we note that

$$\begin{aligned} P_{\text{main}}(t) &= (1 - \eta) D'(t) / D(0) \\ &= (1 - \eta) \exp \left[\int_0^t d\tau A'(\tau) \right], \end{aligned} \quad (9.32)$$

where $A'(\tau)$ is defined by Eq. (4.25) with $\mathbf{K}(t)$ replaced by $\mathbf{K}'(t)$ as defined by Eq. (9.9). Procedures to express $A'(\tau)$ in terms of $|X_{\gamma+}|^2$ and $|\bar{X}_{\mu+}|^2$ may be carried out in the same way as before, keeping the similarity of $\mathbf{K}'(t)$ to $\mathbf{K}(t)$ in mind. We thus obtain Eqs. (7.30) and (7.32) for $A'(\tau)$, in which the asymptotic forms given by Eq. (8.4) for $\phi(t)$ and $\bar{\phi}(t)$ are still valid:

$$\begin{aligned} \phi(t) &= (it)^{-1+\alpha} \Gamma(1-\alpha) |X(0)|^2, \\ \bar{\phi}(t) &= (it)^{-1-\alpha} \Gamma(1+\alpha) |\bar{X}(0)|^2. \end{aligned} \tag{9.33}$$

Here $|X(0)|^2$ is defined by Eq. (8.3), but $|\bar{X}(0)|^2$ is given by

$$|\bar{X}(0)|^2 = |\bar{D}/\varepsilon_\lambda|^2 |\bar{D}|^{-\alpha} \exp \left[\frac{2}{\pi} \int_{\bar{D}}^0 d\varepsilon [\delta(\varepsilon) - \delta(0)]/\varepsilon \right]. \tag{9.34}$$

The extra factor $|\bar{D}/\varepsilon_\lambda|$ appears because of the need to extract the factor $(z - \bar{D})/(z - \varepsilon_\lambda)$ from Eq. (7.9). The revised expression for $|\bar{X}(0)|$ does not, however, affect the remaining calculation, since $|\bar{X}(0)|$ is always coupled with $|X(0)|$ and the relation

$$\begin{aligned} |X(0)|^2 |\bar{X}(0)|^2 &= |X_0(0)|^2 \\ &= [\sin \delta(0) / \pi V N(0)]^2 \end{aligned} \tag{9.35}$$

$$\Sigma(t) = N(0) (-iV\bar{X}_\lambda)^2 \int_0^\infty d\rho \int_0^\infty d\rho' \int_0^\infty d\tau e^{i\varepsilon_\lambda \rho} e^{i\varepsilon_\lambda \rho'} \phi(t + \tau + \rho) F(t + \tau, t + \rho'), \tag{9.38}$$

$$\begin{aligned} \bar{Q}(t) &= Q(-t)^* \\ &= N(0) w (-iV\bar{X}_\lambda) \int_0^\infty d\rho \int_0^\infty d\tau e^{i\varepsilon_\lambda \rho} \phi(t + \tau + \rho) F(t + \tau, t + \rho), \end{aligned} \tag{9.39}$$

where

$$\bar{X}_\lambda = \frac{|\varepsilon_\lambda|}{\nu_\lambda} \exp \left[-\frac{1}{\pi} \int_{\bar{D}}^0 d\varepsilon \frac{\delta(\varepsilon) - \pi}{\varepsilon_\lambda - \varepsilon} \right] \tag{9.40}$$

with

$$\nu_\lambda = \left[\int_{\bar{D}}^D d\varepsilon N(\varepsilon) / (\varepsilon_\lambda - \varepsilon)^2 \right]^{-1/2}, \tag{9.41}$$

the normalization constant for the state ψ_λ . The real fac-

$$\Sigma(t) = N(0) D^{1-\alpha} (VX_\lambda / \varepsilon_\lambda)^2 |X(0)|^2 [\Gamma(1-\alpha/2)]^2 (iDt)^{\alpha-1}, \tag{9.43}$$

$$I_1(t) = N(0) (D/\varepsilon_\lambda)^2 |w|^2 D^{1-\alpha} |X(0)|^2 [\Gamma(2-\alpha/2)]^2 (iDt)^{\alpha-3}. \tag{9.44}$$

With these results inserted into Eqs. (9.12) and (9.18), we see at once that the exponents of the secondary threshold given by Eqs. (3.21) and (3.23) are correctly reproduced (Tanabe and Ohtaka, 1984).

Since the process of expanding $\Sigma(t)$ and $Q(t)\bar{Q}(t)$ into a power series of $(|\varepsilon_\lambda|t)^{-1}$ is obviously well defined, the present calculation (Tanabe and Ohtaka, 1984) is completely free from the ambiguity arising from the modulus π of the phase shift as encountered in the treatment by Combescott and Nozières (1971; see Sec. III.G.1).

D. Critical amplitudes

Now that the exact asymptotic forms for $I'_0(t)$, $\Sigma(t)$, and $I_1(t)$ are available in Eqs. (9.17) and (9.18), the criti-

[Eq. (8.6) with Eq. (7.23)] is now established for the revised $|\bar{X}(0)|$. The conclusion is thus that $P_{\text{main}}(t)$ and $I_{\text{main}}(t)$ have exactly the same forms as Eqs. (8.18) and (8.23), respectively:

$$P_{\text{main}}(t) = C_0 (iW_b t)^{-\sigma} \tag{9.36}$$

and

$$I'_0(t) = N(0) |w|^2 \Gamma(1-\alpha) D \Xi (iDt)^{-1+\alpha}, \tag{9.37}$$

where α is defined by Eq. (8.2) and Ξ by Eq. (8.25). The critical exponents thus reproduce the values given in Eqs. (3.20) and (3.22), obtained by the rule of thumb (Sec. II.D.2).

For the secondary band, we need to evaluate the asymptotic form of $\Sigma(t)$, $Q(t)\bar{Q}(t)$ in Eqs. (9.12), (9.18), and (9.19). In terms of $\phi(t)$ and $F(t + \tau, t + \sigma)$, we find that

tor \bar{X}_λ comes into $\Sigma(t)$ and $Q(t)$ because of the relation

$$\Delta(\bar{\mu}\gamma) / \Delta = \bar{X}_\lambda |X_{\gamma+}| V / (\varepsilon_\lambda - \varepsilon_\gamma). \tag{9.42}$$

The asymptotic forms of $\Sigma(t)$ and $Q(t)$ may be derived by considering the limit $|\varepsilon_\lambda|t \rightarrow \infty$ in Eqs. (9.38) and (9.39). Through integration by parts, we obtain them in the form of a series in powers of the small expansion parameter $(|\varepsilon_\lambda|t)^{-1}$. The leading terms of the series are

cal amplitudes may be obtained from a knowledge only of $P_{\text{main}}(t)$ or $D'(t)/D(0)$. We have already given the correct answer in Eq. (9.36). Our remaining task here is to show that C_0 therein really coincides with the C_0 of the orthogonality theorem (2.13) or (8.42). This was carried out by Tanabe and Ohtaka (1985). We first note that

$$D'(t) = \exp \{ \text{Tr} \ln [1 + \mathbf{K}'(t) e^{-it}] \} \tag{9.45}$$

and

$$D(0) = |\Delta|^{-2} = \exp [-\ln C_0 + \sigma \ln (W_b / \Delta \varepsilon)], \tag{9.46}$$

where we have used Eq. (8.42) for $|\Delta|$. Note that Eq. (8.42) still holds. However, whether Eq. (8.43) is valid or not in the presence of a bound state is an open question,

to be answered in Sec. IX.E. Our aim is to relate $D'(t)/D(0)$ to the factor C_0 in the continuum limit $\Delta\varepsilon \rightarrow 0$. The difficulty here is to transform $D'(t)$ into an expression such that precise cancellation of $(\Delta\varepsilon)^{-\sigma}$ in the ratio $D'(t)/D(0)$ in the limit $\Delta\varepsilon \rightarrow 0$ is readily seen. According to the definition of $\mathbf{K}'(t)$ [Eq. (9.9)], our first task is to evaluate $\Delta(\bar{\mu}\gamma|)/\Delta$ in the discrete scheme. Because of Eq. (9.35), the presence of a bound state does not modify its form given by Eq. (8.48). The next task, to calculate the exponent of Eq. (9.45) for $D'(t)$ with the use of Eq. (8.48), is by no means straightforward. However, we can take advantage of our experience in the derivation of Eqs. (8.29) and (8.30), after expanding $\ln[1 + \mathbf{K}'(t)e^{-i\varepsilon t}]$ into a power series of $e^{-i\varepsilon t}$. We refer the interested reader to the original lengthy proof (Ohtaka and Tanabe, 1984) for details and cite here only the final result, which is quite simple:

$$D'(t) = \exp[-\sigma \ln(1 - e^{-i\Delta\varepsilon t})]. \tag{9.47}$$

This, together with Eq. (9.46), leads to

$$\begin{aligned} p_m &= C_0/[2^\sigma \Gamma(\sigma)(W_b/2)], \\ p_s &= C_0[D/(W_b/2)]^{\alpha-1} N(0) D^{1-\alpha} |X(0)|^2 (V\bar{X}_\lambda/|\varepsilon_\lambda|)^2 [\Gamma(1-\alpha/2)]^2 / \{2^\sigma \Gamma[(1-\alpha/2)^2](W_b/2)\}, \\ \mu_m &= (W_b/2)[D/(W_b/2)]^\alpha p_m \Xi_m B(\sigma, 1-\alpha), \\ \mu_s &= (W_b/2)[D/(W_b/2)]^{\alpha-2} p_s \Xi_s B[(\alpha/2-1)^2, 3-\alpha], \end{aligned} \tag{9.51}$$

with

$$\Xi_m = D^{-\alpha} |X(0)|^2 [\Gamma(1-\alpha/2)]^2 / \Gamma(1-\alpha), \tag{9.52}$$

$$\Xi_s = D^{-\alpha} |X(0)|^2 (\bar{D}/\varepsilon_\lambda)^2 [\Gamma(2-\alpha/2)]^2 \Gamma(3-\alpha)$$

and with $B(x, y) [= \Gamma(x)\Gamma(y)/\Gamma(x+y)]$ the beta function. These results are, of course, for $T=0$. At a finite T , ω on the right-hand side should be replaced by ω' ($=\omega + \text{Re}\eta^0$) and a factor $p[\omega'/T, \dots]$ should be included in Eqs. (9.49) and (9.50) in accordance with the change from Eq. (8.24) to Eq. (8.36).

E. Expression for C_0

We have seen that the coefficient C_0 plays a key role in the analytical expressions for the edge spectra. In the absence of a bound state, it is given its analytical form by Eq. (8.43). We must confirm whether a modification is required in the presence of a bound state. The answer is that there is indeed a correction, and its correct form is given by (Tanabe and Ohtaka, 1985)

$$C_0 = (1-\sigma) \left[\frac{W_b^2}{D|\bar{D}|} e^{-\gamma(\sigma)} \right]^\sigma e^{-\xi} \frac{X(\varepsilon_\lambda)}{X(\bar{D})}, \tag{9.53}$$

where $\gamma(\sigma)$ and ξ are defined by Eqs. (8.40) and (8.41), respectively, and

$$P_{\text{main}}(t) = C_0 (iW_b t)^{-\sigma} \tag{9.48}$$

in the limit $\Delta\varepsilon \rightarrow 0$.

In summary, the critical amplitude of the main photoemission spectrum is given by C_0 of the orthogonality theorem.

We now have analytical expressions for all the critical amplitudes of photoemission and absorption from Eq. (9.48) and Eqs. (9.43) and (9.44). From Eqs. (9.11), (9.12), (9.17), and (9.18), the results of the Fourier transformation are written down here using the reduced frequency defined by $\bar{\omega} = \omega/(W_b/2)$ (Tanabe and Ohtaka, 1985):

$$P_{\text{main}}(\omega) = 2\pi p_m \bar{\omega}^{\sigma-1}, \tag{9.49}$$

$$P_{\text{sec}}(\omega) = 2\pi p_s \bar{\omega}^{(\alpha/2-1)^2-1};$$

$$I_{\text{main}}(\omega) = 2\pi N(0) |w|^2 \mu_m \bar{\omega}^{(\alpha/2-1)^2-1}, \tag{9.50}$$

$$I_{\text{sec}}(\omega) = 2\pi N(0) |w|^2 \mu_s \bar{\omega}^{(\alpha/2-2)^2-1},$$

where

$$\frac{X(\varepsilon_\lambda)}{X(\bar{D})} = \exp \left[-\frac{1}{\pi} \int_0^D d\varepsilon \left[\frac{1}{\varepsilon_\lambda - \varepsilon} - \frac{1}{\bar{D} - \varepsilon} \right] \delta(\varepsilon) \right] \tag{9.54}$$

where $X(z)$ is defined by Eq. (7.21). To see this, we have to return to the first equality of Eqs. (8.37), in which one of μ corresponds to λ in the present case, and the factor $X(\varepsilon_\lambda)$ and its counterpart $X(\bar{D})$ must be treated separately. The remaining factors, involving solely the band states, may be transformed just as in Sec. VI.D. The extracted factor $X(\varepsilon_\lambda)/X(\bar{D})$ can be reduced to the dispersion integral equation (9.54) because of Eqs. (7.21) and (7.22).

Although the critical amplitudes of the main bands are formally identical with Eqs. (8.21) and (8.24), given for the case without a bound state, there are modifications in the expression for C_0 and in the value of $\delta_0(\varepsilon)$ when a bound state is present. For a quantitative estimate of C_0 , therefore, it is important to check beforehand whether or not a bound state exists in the excited configuration.

X. OTHER TOPICS

A. Pairwise expansion of the response functions

In obtaining the spectra at $T=0$ through Eqs. (7.30) and (7.31), a major task is to find a solution for the in-

tegral equation (7.32). One simple way is to carry out an iteration, which gives F in the form of a series in powers of Λ . This procedure is simply the reverse of the process carried out in Sec. IV for a series expansion with respect to the number of excited electron-hole pairs. Since evaluations of lower-order terms of the pairwise series have very often been performed to simulate an exact spectrum, it will be of practical interest to see the validity of the iterative procedure.

We restrict ourselves to the asymptotic region and examine Eq. (8.9), with ξ supplemented as an expansion pa-

rameter:

$$\bar{F}(x,y) + \xi \frac{\tan\delta(0)}{2\pi} \int_0^1 dz \frac{1-(z/x)^\alpha}{x-z} \bar{F}(z,y) = \delta(x-y). \tag{10.1}$$

Later we shall take the limit $\xi=1$. Due to the presence of ξ , the solution of Eq. (10.1) will be slightly modified from that derived previously. We find (Tanabe and Ohtaka, 1986)

$$\bar{F}(x,y) = (1/2\pi i)^2 \int_{l_1} ds_1 U_\xi(s_1) x^{-s_1} \int_{l_2} ds_2 V_\xi(s_2) y^{s_2-1} / (s_1-s_2) \tag{10.2}$$

with

$$U_\xi(s) = \Gamma(s-\rho')\Gamma(s-\rho) / [\Gamma(s-\alpha)\Gamma(s)], \tag{10.3}$$

$$V_\xi(s) = \Gamma(1-s+\rho')\Gamma(1-s+\rho) / [\Gamma(1-s+\alpha)\Gamma(1-s)],$$

where ρ and ρ' are defined by

$$\left. \begin{matrix} \rho \\ \rho' \end{matrix} \right\} = \alpha/2 \pm q/2 \tag{10.4}$$

and

$$\tan q = \sqrt{1-\xi} \tan\delta(0) / [1+\xi \tan^2\delta(0)]^{1/2}. \tag{10.5}$$

When $\xi=1$, the angle q vanishes, and hence $U_\xi(s)$ and $V_\xi(s)$ reduce to $U(s)$ and $V(s)$ respectively, given by Eq. (8.13), as they should.

The functions $A(t)$ and $I_0(t)$ are obtained by inserting Eq. (10.2) into Eqs. (8.10) and (8.11):

$$tA(t) = -[(\alpha/2)^2 - (q/\pi)^2]_{\xi=1}, \tag{10.6}$$

$$I_0(t) = N(0)|w|^2\phi(t) [\Gamma(1-\rho')\Gamma(1-\rho)/\Gamma(1-\alpha)]_{\xi=1} \tag{10.7}$$

These results are still valid for $A'(t)$ and $I_0'(t)$ of the main band in the presence of a bound state.

Equations (10.6) and (10.7) provide us with a pairwise series, if we expand q , ρ , and ρ' as a power series of ξ by using Eqs. (10.4) and (10.5). After a bit of calculation, we find that at $\xi=1$ (Ohtaka and Tanabe, 1986)

$$tA(t) = \sum_{k=0}^{\infty} a^{(k)}, \tag{10.8}$$

$$I_0(t) = N(0)|w|^2\phi(t) \sum_{k=0}^{\infty} b^{(k)}, \tag{10.9}$$

where

$$\begin{aligned} a^{(0)} &= -\delta(0) \tan\delta(0) / \pi^2, \\ a^{(1)} &= \frac{1}{4} [\tan\delta(0) / \pi]^2 \{1 - 2\delta(0) \cot[2\delta(0)]\}, \\ a^{(2)} &= -\frac{1}{4} [\delta(0) \tan\delta(0) / \pi^2]^3 [\pi^2 / 2\delta(0)]^2 \left[\frac{2}{3} - \frac{\cot[2\delta(0)]}{\delta(0)} + 2 \cot^2[2\delta(0)] \right], \\ &\dots; \end{aligned} \tag{10.10}$$

$$\begin{aligned} b^{(0)} &= 1, \\ b^{(1)} &= \frac{\tan\delta(0)}{2\pi} [\psi(1-\alpha) + \gamma], \\ b^{(2)} &= \frac{\tan\delta(0)}{8\pi} [1 - \tan^2\delta(0)] [\psi(1-\alpha) + \gamma] + \frac{1}{2} \left[\frac{\tan\delta(0)}{2\pi} \right]^2 [\psi'(1-\alpha) + \psi(1-\alpha)^2 + 2\psi(1-\alpha)\gamma + \pi^2/6 + \gamma^2], \\ &\dots, \end{aligned} \tag{10.11}$$

and where ψ is the digamma function, ψ' its derivative, and γ the Euler constant.

It is rather hard to obtain the correct value for $tA(t) = -[\delta(0)/\pi]^2$ deductively from the series Eq. (10.9). This is one of the features characterizing the difficulty of the MND problem. However, when all the trigonometric functions are expanded into Taylor series, we find that

$$\sum_{k=1}^n a^{(k)} = -[\delta(0)/\pi]^2 [1 + O(\delta(0)^{2n+2})], \quad (10.12)$$

as verified directly for small values of n .

Now let us examine the radius of convergence of the series (10.3) with respect to the phase shift. The form Eq. (10.5) for $\tan\eta$ as a function of ξ suggests that for the pairwise series for $A(t)$ and $I_0(t)$ to converge at $\xi=1$, it will be necessary that $\tan\delta(0) < 1$, i.e.,

$$\delta(0) < \pi/4. \quad (10.13)$$

This criterion is indeed confirmed by examining the integral representation (not shown here) of the quantities $U_\xi(s)$ and $V_\xi(s)$, which leads to Eq. (10.3). Since we are already too deep in mathematics, however, we stop here without reproducing further analysis. The series given by Eqs. (10.8) and (10.9) will be examined in Sec. XI.E, and the correctness of Eq. (10.13) will be demonstrated there.

B. Approximate formulas based on the single-particle picture

We are interested here in the frequency region away from the edge, say, the region $\omega > 0.2D$, in which the effects of the edge singularities are no longer appreciable. Generally speaking, influences of shakeup pairs can be neglected in a region far away from the edge. This may be seen if we recall Eq. (4.17) for $K(\gamma, \gamma'|t)$ together with Eq. (5.10), which indicates that $K(\gamma, \gamma'|t) \rightarrow 0$ as $\varepsilon_{\gamma'}, \varepsilon_{\gamma'} \rightarrow \infty$. However, a quantitative estimate of the shakeup effects is difficult because it depends on the potential strength. Here we make use of the numerical studies of Kotani and Toyozawa (1973b; see Sec. III.F.1) and von Barth and Grossmann (1979, 1982; see Sec. III.F.6), in which neglect of multipair excitations has been shown to be generally good away from the edge, and we set $(1 + \mathbf{K}e^{i\varepsilon t})^{-1} = 1$ in $I_0(t)$ and $A(\tau) = 0$ in $P(t)$. The latter will be confirmed to be good in Sec. XI.G for the short-time region of t satisfying $t < 10/D$, which just corresponds to the frequency range of interest.

Suppose we are thus in the frequency range where

$$\begin{aligned} I(\omega) &= 2\pi \sum_{\gamma} |p(\gamma)|^2 \delta(\varepsilon_{\gamma} - \omega) \\ &\equiv I^{(0)}(\omega). \end{aligned} \quad (10.14)$$

Note that the formula still incorporates an important many-body effect through the replacement process (Sec. III.D.1).

As candidates for the single-particle absorption formulas, let us examine the following three rules (at $T=0$, and for $\omega > 0$):

(a) Initial-state rule,

$$\begin{aligned} I_i(\omega) &= 2\pi \sum_b |w_{bc}|^2 \delta(\varepsilon_b - \omega) \\ &= 2\pi |w|^2 \sum_b \delta(\varepsilon_b - \omega). \end{aligned} \quad (10.15)$$

(b) Final-state rule,

$$\begin{aligned} I_f(\omega) &= 2\pi \sum_{\gamma} |w_{\gamma c}|^2 \delta(\varepsilon_{\gamma} - \omega) \\ &= 2\pi |w|^2 \sum_{\gamma} \left| \sum_k a_{\gamma k} \right|^2 \delta(\varepsilon_{\gamma} - \omega). \end{aligned} \quad (10.16)$$

(c) Orthogonalized final-state rule,

$$I_{of}(\omega) = 2\pi |w|^2 \sum_{\gamma} \left| \sum_b a_{\gamma b} \right|^2 \delta(\varepsilon_{\gamma} - \omega). \quad (10.17)$$

Here we have set $w_{kc} = w$ for simplicity. We see that $I_i(\omega)$ is just proportional to the density of states of the conduction band. In the second line of $I_f(\omega)$, ψ_{γ} is expanded in terms of φ_k [Eq. (4.1)]. The orthogonalized final-state rule was introduced first by Davis and Feldkamp (1981); in it ψ_{γ} is approximated so as to be orthogonal to the unperturbed states φ_m below the Fermi level. Since the index b labels the states above the Fermi level, $I_{of}(\omega)$ shows a logarithmic divergence when we let $\omega (= \varepsilon_{\gamma}) \rightarrow 0$.

Using Eq. (7.17) for a contact-type core-hole potential, we obtain

$$I_i(\omega) = 2\pi |w|^2 N_{\gamma}, \quad (10.18)$$

$$I_f(\omega) = 2\pi |w|^2 N_{\gamma} (\sin\delta_{\gamma}/\pi V N_{\gamma})^2, \quad (10.19)$$

$$I_{of}(\omega) = 2\pi |w|^2 N_{\gamma} \left[\cos\delta_{\gamma} - \frac{\sin\delta_{\gamma}}{\pi N_{\gamma}} \sum_b \frac{P}{\varepsilon_{\gamma} - \varepsilon_b} \right]^2, \quad (10.20)$$

with $N_{\gamma} = N(\varepsilon_{\gamma})$, $\delta_{\gamma} = \delta(\varepsilon_{\gamma})$, and $\varepsilon_{\gamma} = \omega$.

Now let us express $p(\gamma)$ in several apparently different forms, though all are equivalent (Ohtaka and Tanabe, 1986). The first is its definition, Eq. (4.30):

$$p(\gamma) = w_{\gamma c} - \sum_{\mu} w_{\mu c} \Delta(\bar{\mu}\gamma)/\Delta. \quad (10.21)$$

The second is given by substituting Eq. (4.1) into $w_{\gamma c}$ and $w_{\mu c}$ of Eq. (10.21). It then follows that

$$p(\gamma) = w \sum_b \left[a_{\gamma b} - \sum_{\mu} a_{\mu b} \Delta(\bar{\mu}\gamma)/\Delta \right]. \quad (10.22)$$

The third is Eq. (7.27), expressed in terms of the dispersion integrals (7.21) and (7.22):

$$\begin{aligned} p(\gamma) &= w |X_{\gamma+}| \\ &= w \exp \left[-\frac{P}{\pi} \int_0^D d\varepsilon \delta(\varepsilon)/(\varepsilon_{\gamma} - \varepsilon) \right]. \end{aligned} \quad (10.23)$$

The form Eq. (10.21) shows that, provided we can neglect its second term, $I(\omega)$ reduces to $I_i(\omega)$. This will actually be the case if the band filling is small ($\bar{D} \simeq 0$), since the index μ is used for states with $\bar{D} < \varepsilon_\mu < 0$. The form Eq. (10.22) reveals the general usefulness of the formula $I_{of}(\omega)$, because away from the edge with $\varepsilon_\gamma, \varepsilon_b \rightarrow D$, the second term becomes small. Equation (10.23), on the other hand, shows that $I_i(\omega)$ becomes good in the case of large band filling ($D \simeq 0$) where, because of $\delta_\gamma \rightarrow 0$ for $\varepsilon_\gamma \simeq D$, the dispersion integral becomes practically γ -independent and N_γ determines the line shape.

To sum up, we may say that preference for the initial-state or final-state rule in x-ray absorption is to be decided by the position of the Fermi level. This was demonstrated in the numerical studies of Grebennikov *et al.* (1977a, 1977b; see Sec. III.F.2) and pointed out first by Wilkins (1982). This feature will be shown also in our numerical study in Sec. XI.F (Ohtaka and Tanabe, 1986).

The case of emission is a little different. Here we have in place of Eq. (10.14)

$$I^{(0)}(\omega) = 2\pi \sum |p(\bar{m})|^2 \delta(\varepsilon_m - \omega), \quad (10.24)$$

with [see Eqs. (7.25) and (7.27)]

$$p(\bar{m}) = w |X_{m+}| \\ = w \exp \left[-\frac{1}{\pi} \int_0^D d\varepsilon \delta(\varepsilon) / (\varepsilon_m - \omega) \right]. \quad (10.25)$$

When $D \rightarrow 0$ (large band filling), $|X_{m+}|$ is practically m independent, since $\delta(\varepsilon) = 0$ for $0 < \varepsilon < D$, making Eq. (10.36) tend to the final-state rule (corresponding to the band states in the ground configuration). For a smaller band filling, on the other hand, $|X_{m+}|$ is m dependent in general. One is tempted by this to conclude in favor of the initial-state rule. But in the case of emission we have no counterpart for Eqs. (10.21) and (10.22), and we must calculate the ω dependence of Eq. (10.25) actually. This was indeed what Mahan (1980) and von Barth and Grössman (1979, 1982) did to conclude that the final-state rule describes XES much better than the initial-state rule (Sec. III.F.6).

C. Generalized power law

The results summarized in Eqs. (9.49)–(9.52) are the leading terms of the singular edge behavior. The applicability of these formulas is gradually lost as we move farther and farther from the edge region.

One way we can attempt to obtain a formula having a wider range of validity is to assume the following form for the energy dependence of the phase shift:

$$\delta(\varepsilon) = \delta(0) + \delta'(0)\varepsilon. \quad (10.26)$$

Whether the approximation is good or not, of course, depends on the profile of the density of states. We shall see in Sec. XI.H that for a semielliptic density of states Eq. (10.26) holds over a wide frequency range.

In our derivation of Eqs. (9.49)–(9.52), the key relation was Eq. (8.48). We noted there that only the phase shift at the Fermi level comes into play [$\alpha = 2\delta(0)/\pi$]. By making use of Eq. (10.26), we can improve Eq. (8.48) so that it may contain $\delta(\varepsilon_m)$ and $\delta(\varepsilon_b)$ instead of $\delta(0)$ and so that it has wider applicability with respect to the states μ and γ . The intensities of the spectra may then be obtained by following the approach of Feldkamp and Davis (1980). Higher-order terms in the ω dependence of the critical exponent may be examined in this way. The result turns out to be given by [$\bar{\omega} = \omega/W_b$; Kita *et al.*, 1987a]

$$P_{\text{main}}(\omega) = 2\pi p_m \bar{\omega}^{\sigma-1} \{1 + \bar{\omega}[\eta_0 + \eta_1(-2\ln|\bar{\omega}| + B_p)]\} \\ \simeq 2\pi p_m \exp[\sigma_1(\omega)\ln|\bar{\omega}| + \sigma_2(\omega)], \quad (10.27)$$

$$I(\omega) = 2\pi N(0) |\omega|^2 \mu_m \bar{\omega}^\beta \{1 + \bar{\omega}[\eta_0 + \eta_1(-2\ln|\bar{\omega}| + B_A)]\} \\ \simeq 2\pi N(0) |\omega|^2 \mu_m [\beta_1(\omega)\ln|\bar{\omega}| + \beta_2(\bar{\omega})]. \quad (10.28)$$

Here the second lines are obtained from the first in the form of a generalized power law, with

$$\sigma_1(\omega) = -1 + \sigma - 2\eta_1 \bar{\omega}, \\ \sigma_2(\omega) = (\eta_0 + \eta_1 B_p) \bar{\omega}; \quad (10.29)$$

$$\beta_1(\omega) = \beta - 2\eta_1 \bar{\omega}, \\ \beta_2(\omega) = (\eta_0 + \eta_1 B_A) \bar{\omega}. \quad (10.30)$$

In Eqs. (10.27)–(10.30), η_0 and η_1 are constants related linearly to $\delta'(0)$, and B_p and B_A are written solely in terms of $\delta(0)$ (their expressions are, unfortunately, too lengthy to be given here). It is also shown that Eq. (10.28) may be used in the case of XES without any modification, if we use it only in the range $\omega < 0$, in accordance with the remark made in Sec. III.B.2 on the analyticity of the ω -dependent exponent (Ohmura *et al.*, 1974).

The validity of expressing the ω series by an exponential function that simply puts it on the shoulders of the exponential was examined by Kita (1987), who derived the next terms of the order of ω^2 . His conclusion is that the new terms to be included in the first line of $P(\omega)$ in Eq. (10.27) contain the term $\omega^2[\eta_0 + \eta_1(-\ln|\bar{\omega}| + B_p)]^2/2!$. The same thing holds for $I(\omega)$. This feature of the ω series strongly suggests the validity of the exponential form. Kita also demonstrated that the relation between photoemission and absorption expressed by the rule of thumb (Sec. III.D.2) hold precisely for the expression of the ω -dependent exponents used in the generalized power law.

The results Eqs. (10.27) and (10.28) may be regarded as an extension, applicable for a wide class of V , of the treatments of Ohmura *et al.* (1974; see Sec. III.B.2), which were based on perturbation theory with respect to V . In Sec. XI.H, we shall compare Eqs. (10.27) and

(10.28) with the exact numerical results and see that they reproduce the true spectra surprisingly well.

XI. NUMERICAL RESULTS

Some numerical results obtained by means of the theoretical formulas presented in Secs. IV–X will be given in this section. First, however, we have one remark to make in relation to the existing numerical results in the literature.

For most of the topics listed in our table of contents, that is, for topics other than those covered in Sec. III.B, D, F, and H, there have been no attempts comparable to ours in the literature, and our results are thus the first ones. On the other hand, for the topics covered in Secs. III.B, D, and F, all related to the exact intensity curves of the MND model, there are a number of references in which the curves presented are claimed to be exact. For example, some of the XAS and XES spectra given by Grebennikov *et al.* (1977a, 1977b) and von Barth and Grossmann (1979, 1982), as well as the photoemission curve obtained by Feldkamp and Davis (1980), all quoted in Sec. III.F, would seem comparable with our results. We are not claiming in Sec. XI.B or D that our approach is the only one capable of yielding an exact spectrum for the MND model. Those spectra cited above are sufficiently correct that a detailed comparison would yield information on the quality of the numerical methods those authors adopted. However, in the interesting near-edge range of $\omega < 0.05$, best suited for this purpose simply because it is the most difficult frequency range, we need numerical values with a precision of, say, two or three decimal places to test them against our analytical intensity formula. [See Table I of Ohtaka and Tanabe (1986) in which our data in the range $0.01 < \omega < 0.1$ were tested along these lines. See also the discussion in Sec. XII of Figs. 31 and 32, which shows the need for a very careful treatment of divergent spectra in extracting a reliable critical exponent.] Unfortunately, the divergent curves in that frequency range have very often been given in arbitrary units, with figures too small for a close scrutiny; there have been none, indeed, except those using the renormalization-group formalism, in which the numerical values are available. This is one of the reasons for not trying to make a comparison. Another reason is that the existing data are obtained for a model often more realistic than the original MND model, whereas all our numerical results are based on the latter. For example, the calculation of von Barth and Grossmann (1982) used the conduction band of Na and made use of a realistic core-hole potential. If we remember that the critical amplitude is determined by information concerning the band as a whole, not solely by the phase shift at the Fermi level, a direct comparison between their figures and ours looks rather meaningless. The same comment applies to the curves of the generalized power law discussed in Sec. XI.H, for which the

curves given by the perturbative treatment of Ohmura and Ishikawa (1980b) will be sufficiently correct.

The only exception is the numerical data obtained by means of the renormalization-group formalism by Oliveira and Wilkins (1981, 1985) and Cox *et al.* (1985). We shall carry out a detailed comparison with their results for the critical amplitude and try to evaluate the effectiveness of the renormalization-group formalism.

Now let us begin by specifying the model for numerical analysis. Our formulation presented so far shows that once the profile $N(\varepsilon)$, the parameter V , w , and the position ε_F of the Fermi level are specified, we may obtain everything else we need for the soft-x-ray problem. Since the XAS and XES intensities are simply proportional to $|w|^2$, we put $|w|^2 = 1$ hereafter.

For $N(\varepsilon)$, we consider the following two conduction bands: Band A with a constant density of states

$$\text{Band A: } N(\varepsilon) = 0.5 \quad (-1 \leq \varepsilon \leq 1), \quad (11.1)$$

and Band B with a semielliptical density of states

$$\text{Band B: } N(\varepsilon) = \frac{2}{\pi} (1 - \varepsilon^2)^{1/2} \quad (-1 \leq \varepsilon \leq 1). \quad (11.2)$$

Here we take the center of the conduction band as the origin $\varepsilon = 0$ of energy and assume the band to spread in the energy range $-1 \leq \varepsilon \leq 1$. We thus take $W_b = 2$, choosing half the bandwidth $W_b/2$ as a unit of energy. The position of the Fermi energy is varied in the range $-1 \leq \varepsilon_F \leq 1$. The profiles Eqs. (11.1) and (11.2) are normalized by \mathcal{N} , the total number of states of the conduction band, so that

$$\int_{-1}^1 N(\varepsilon) d\varepsilon = 1. \quad (11.3)$$

The phase shift $\delta(\varepsilon)$ is then obtained from Eq. (7.15) with the prescription for the continuum version as in Eqs. (3.26) and (7.35):

$$\text{Band A: } \tan \delta(\varepsilon) = (\pi V / 2) / \left[1 + \frac{V}{2} \ln \left| \frac{\varepsilon + 1}{\varepsilon - 1} \right| \right], \quad (11.4)$$

$$\text{Band B: } \tan \delta(\varepsilon) = 2V(1 - \varepsilon^2)^{1/2} / (1 + 2V\varepsilon). \quad (11.5)$$

In the following, a dimensionless quantity, $V\mathcal{N}/(W_b/2)$ in actual units, will be denoted simply as V .

The position of the bound state is obtained from the continuum version of the eigenvalue equation (7.2):

$$\text{Band A: } \varepsilon_\lambda = -\coth(1/V), \quad (11.6)$$

$$\text{Band B: } \varepsilon_\lambda = -1/2V. \quad (11.7)$$

For Band B, the bound state is present only when $V > V_c$, while it is always present for any value of V in Band A. The critical value of the potential strength is calculated to be $V_c = 0.5$.

A. Magnitude of C_0 [Eq. (8.43) in the absence of a bound state and Eq. (9.53) in the presence of one]

We show C_0 for Band A in Fig. 13(a) with $V=1.0$ and $V=4.0$ and for Band B in Fig. 13(b) with $V=0.4$ and $V=4.0$, as a function of the position of the Fermi level. Table I shows the value of C_0 together with that of $\exp(-\xi)$, which in the expression for C_0 requires a bit of numerical manipulation. From these results we may conclude that when the Fermi level lies well inside the band, the magnitude of C_0 will be $0.5 < C_0 < 1.0$, and with decreasing V , C_0 approaches unity. We may also conclude that the factor $\exp(-\xi)$ may safely be dropped for the values of V chosen in our calculation. Judging from the values of $\delta(0)$ listed in Table I, we may say that the values for V adopted here are apt to be encountered very often in actual systems.

For an extremely large or small band filling ($\epsilon_F \approx -1.0$ or ≈ 1.0), C_0 changes rapidly as a function of ϵ_F . However, even for a small band filling, for example, an actual phase shift at the Fermi level cannot deviate very much from the value $\pi/2$ to satisfy the Friedel sum rule. The change of C_0 with $\epsilon_F \approx -1.0$ shown in Fig. 13 reflects the behavior $\delta(\epsilon) \rightarrow \pi$ [$\delta(\epsilon) \rightarrow 0$] in the presence [absence] of a bound state below the band bottom. Thus we

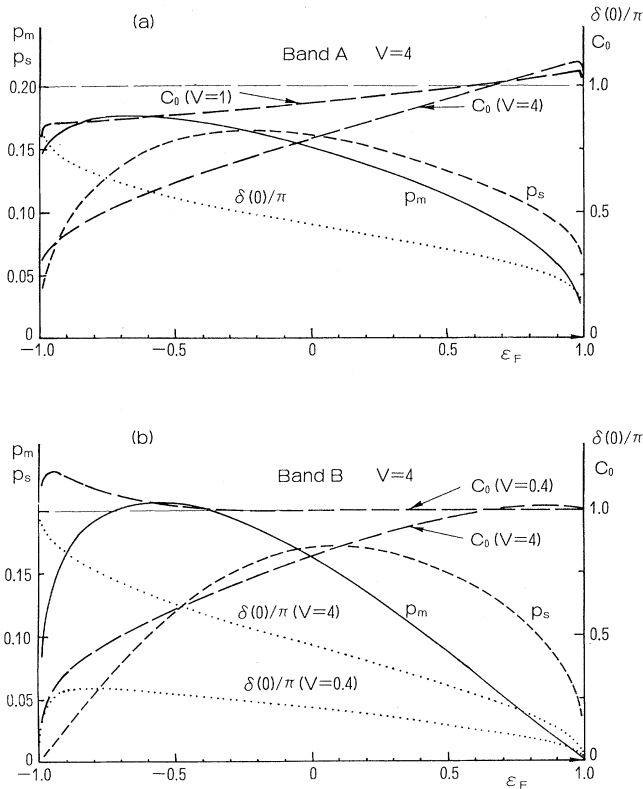


FIG. 13. Photoemission amplitudes p_m , p_s and the prefactor of the orthogonality theorem C_0 as functions of the Fermi energy E_F for $V=4$: (a) for Band A; (b) for Band B. In (a) the curve of C_0 for $V=1$ is also shown, and in (b) that for $V=0.4$ is drawn.

TABLE I. Some numerical values for the Fermi level at the band center. For $\delta(0)/\pi=0.2$ in Band B, there is only the main band.

	$\delta(0)/\pi$	C_0	p_m	p_s	$e^{-\xi}$
Band A	0.20	0.986	0.039	0.017	0.996
	0.40	0.861	0.133	0.146	0.998
	0.450 ($V=4.0$)	0.7917	0.152	0.161	1.003
Band B	0.20	0.998	0.040		1.008
	0.40	0.901	0.139	0.147	1.008
	0.460 ($V=4.0$)	0.8147	0.163	0.170	1.061

feel that the rapid change of C_0 for a very small band filling should not be taken too seriously as a typical behavior to be observed actually.

We wish to emphasize that the present C_0 is defined by the ratio $|\Delta|^2/\mathcal{N}_{\text{eff}}^{-\sigma}$ with $\mathcal{N}_{\text{eff}}=N(0)W_b=W_b/\Delta\epsilon$, as Eq. (2.13) or Eq. (8.42) shows. If we are to redefine it as the ratio $|\Delta|^2/N^{-\sigma}$, where N is the number of states below the Fermi level, its magnitude will be modified by the factor $(\mathcal{N}_{\text{eff}}/N)^{-\sigma}$, which introduces an additional dependence on the band filling.

In Fig. 14, we attempt to obtain the value of C_0 from an analysis of a finite system. We divide the energy region $-1 \leq \epsilon \leq 1$ into \mathcal{N} sections, so that the sections are distributed according to $N(\epsilon)$ given by Eq. (11.1) or Eq. (11.2). The section defines the positions for $\{\epsilon_k\}$, the unperturbed energy levels in the ground configuration. The energies $\{\epsilon_\kappa\}$ in the excited configuration are then calculated by numerically solving Eq. (7.2), which then yields

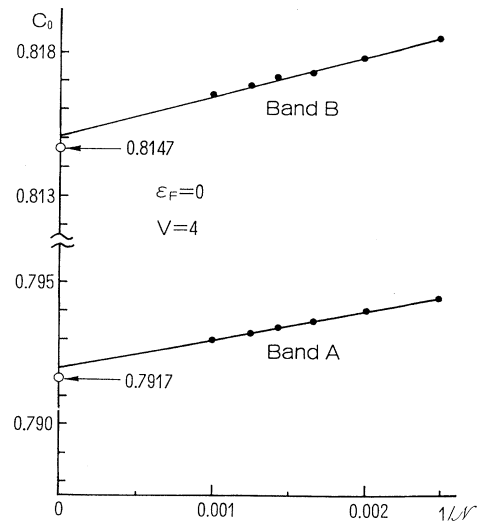


FIG. 14. Numerical estimate of the value of C_0 for Band B. The values obtained from the analytical expression (9.53) are shown on the ordinate. The straight lines show the extrapolations of the numerical values. The result is for the case $V=4$ with the Fermi level at the band center.

$|\Delta|^2$ from Eq. (8.37) and finally $|\Delta|^2 \mathcal{N}_{\text{eff}}^\sigma$. Figure 14 shows the value of $|\Delta|^2 \mathcal{N}_{\text{eff}}^\sigma$ calculated in this way. Comparing it with the theoretical values shown in the ordinate, we see that the extrapolation from the data obtained with $\mathcal{N} < 1000$ yields a good value of C_0 with an accuracy of three decimal places. Note that once the phase shift is known as a function of energy, $\{\varepsilon_k\}$ may be related to $\{\varepsilon_k\}$ through Eq. (7.14). Equation (8.37), which expresses $|\Delta|$ solely in terms of the energy eigenvalues $\{\varepsilon_k\}$ and $\{\varepsilon_k\}$, is thus useful in obtaining an approximate value for C_0 , even, perhaps, in the case of a non-contact-type core-hole potential.

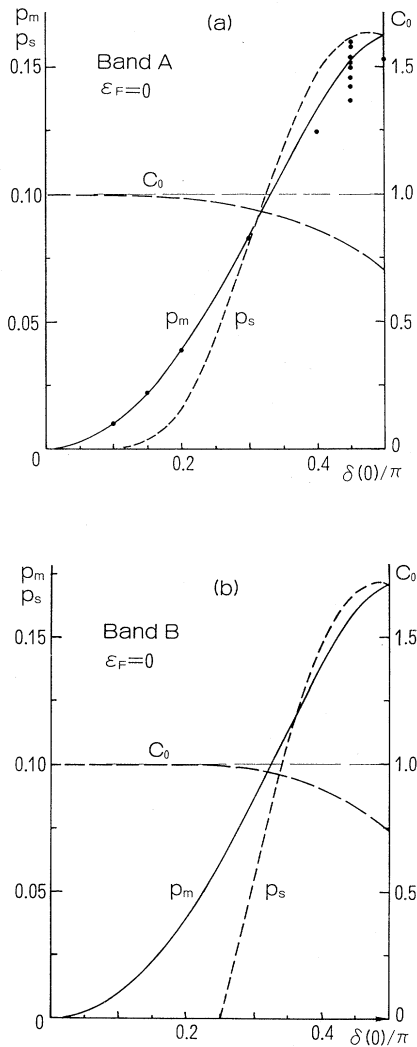


FIG. 15. The photoemission amplitudes p_m , p_s and the coefficient C_0 of the orthogonality theorem as functions of the phase shift at the Fermi level: (a) Band A; (b) Band B. The dots in (a) are the values obtained numerically for p_m by Cox *et al.* (1985). The Fermi level is at the band center. In Band A, a bound state exists irrespective of the value of V , while a bound state appears in Band B when V exceeds 0.5, which corresponds to $\delta(0)/\pi = 0.25$.

B. Critical amplitudes for x-ray photoemission and absorption [Eqs. (9.49)–(9.52)]

The critical amplitudes for photoemission, p_m and p_s , are given in Fig. 13 as a function of ε_F , the position of the Fermi level, and in Fig. 15 as a function of the phase shift with the Fermi level kept fixed just at the band center, $\varepsilon_F = 0$ (in Fig. 15, C_0 is also given for comparison). From the figures, we conclude that the amplitudes p_m and p_s have comparable magnitudes. This will be one of the reasons for the secondary photoemission bands having a strength comparable to that of the main band, as will be shown in Sec. IX.C, in marked contrast to the XAS case summarized below. It is also shown that the $\delta(0)$ and ε_F dependences of the amplitudes p_m and p_s have not much to do with those of C_0 . We have given several values for p_m and p_s in Table I.

The critical XAS amplitudes μ_m and μ_s are plotted in Fig. 16 for Band A. We see at once that μ_s is negligibly small. The secondary XAS band is hardly observable. It is interesting to note that μ_m reflects the $\delta(0)$ dependence of C_0 more closely than p_m and p_s .

Numerical values for p_m and p_s to be compared with ours have been given by Oliveira (1981), Oliveira and Wilkins (1981), and Cox *et al.* (1985) through the renormalization-group (RG) formalism. The values for p_m are plotted in Fig. 15 by dots (Cox *et al.*, 1985). There are several points corresponding to the choices of parameter Λ and l , explained in Sec. III.F.7. We see that for small $\delta(0)$ the RG formalism yields very good values for the critical amplitude of the main photoemission band. For $\delta(0) \sim \pi/2$, the agreement becomes worse because the correct expression of p_m involves integrals over a wide energy range through the dispersion integrals in Eq. (9.52) with Eq. (9.54) for $X(\varepsilon_\lambda)/X(\bar{D})$: Information from throughout the whole band is required to determine p_m . In view of the coarse graining employed in the RG formalism away from the Fermi level, the disagreement is understandable. One should rather say that the disagree-

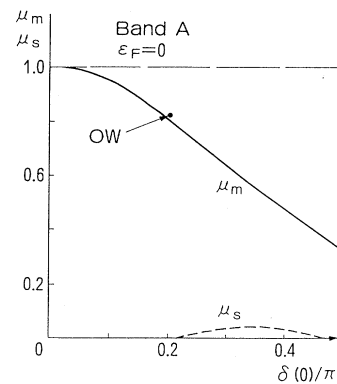


FIG. 16. The amplitudes of XAS, μ_m for the main band and μ_s for the secondary, as functions of the phase shift at the Fermi level chosen at the band center. The point OW shows the value obtained by Oliveira and Wilkins (1981).

ment in Fig. 15 is unexpectedly small. Use of a smooth density of states will obviously be one of the reasons for such a small discrepancy.

The RG result for μ_m is given in Fig. 16. There is only one set of data in the literature provided by Oliveira and Wilkins (1981). The agreement is again satisfactory. We may thus conclude that the RG formalism is powerful with respect to determining the photoemission and absorption critical amplitudes, as in the case of critical exponents demonstrated in Fig. 12.

Mahan (1982) calculated Ξ_m numerically. His value is $0.910D^{-\sigma}|X(0)|^2$, while the analytical expression (9.52) yields $0.9102D^{-\sigma}|X(0)|^2$ for his parameter [Band A with $\delta(0)=\pi/5$], indicating the high precision of Mahan's calculation.

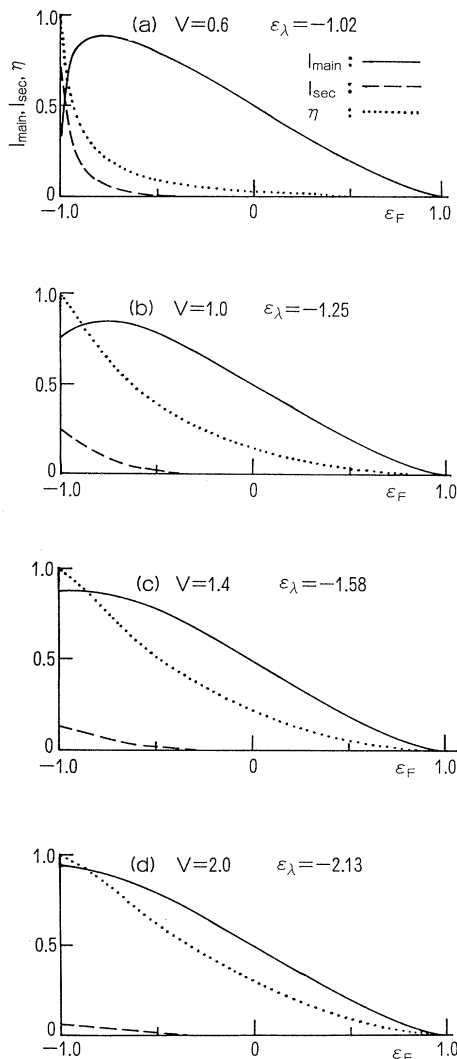


FIG. 17. Integrated intensities I_{main} and I_{sec} of optical absorption ($|\omega|^2$ is put to unity) and the probability η for the bound state to be empty, as functions of the position of the Fermi energy. The results are given for Band B for $V=0.6-2.0$ in the presence of a bound state at energy ϵ_λ .

C. Integrated intensities [Eq. (9.22) for x-ray photoemission and Eq. (9.31) for x-ray absorption spectra]

Figure 17 shows the integrated XAS intensities, with I_{main} and I_{sec} given by Eq. (9.31), for Band A with several values of V . It is found that I_{sec} is always small except when the band filling is very small ($\epsilon_F \simeq -1.0$). The quantity η defined by Eq. (9.28) is also shown by a dotted line. When $\eta \simeq 0.5$, Eq. (9.22) shows that the main and secondary photoemission bands are comparable in magnitude. Thus it is found that a strong secondary band, comparable with the main one, will be observable more often in photoemission than in XAS.

As V increases, the wave function for the bound state shrinks, yielding a smaller b dependence of the overlap $a_{\lambda b}$. Since the positiveness of I_{sec} is guaranteed by the Schwarz inequality in Eq. (9.31), we conclude that a larger V leads to a smaller I_{sec} . Conversely, in the case $V \simeq 0.5 (=V_c)$ for Band B, a shallow bound state exists ($\epsilon_\lambda \simeq -1.0$), leading to a strongly b -dependent $a_{\lambda b}$, especially for the states b near the band bottom. Therefore, in the case of $\epsilon_F \simeq -1.0$, the probability η for the bound state to be empty is expected to depend strongly on the position of the Fermi level. The rapid change of I_{sec} with ϵ_F ($\simeq -1.0$) in Fig. 17 corresponds to this situation.

The comment made concerning Fig. 13 for the case of a small band filling with $\epsilon_F \simeq -1.0$ will be equally applicable here, and the result shown in Fig. 13 for the extreme case of $\epsilon_F \simeq -1.0$ should be modified in an actual case. Indeed, we shall encounter a situation in Sec. XI.I in which the secondary XAS band is negligible in spite of very small band filling.

D. Exact line shape at $T=0$ [Eqs. (4.12), (4.24), (4.25), and (7.30) for photoemission and Eqs. (4.28), (4.42), and (7.31) for XAS]

We restrict ourselves to the case in which the Fermi level is positioned just at the band center ($\epsilon_F=0$). The procedure for obtaining spectra for all ranges of frequency is as follows: We first calculate the phase shift by way of Eqs. (11.4) and (11.5), put it into the dispersion integral Eq. (7.25), substitute the resulting $|X_{\gamma+}|$, $|\bar{X}_{\mu+}|$ into Eq. (7.29) to obtain $\phi(t)$ and $\bar{\phi}(t)$, and then obtain $\Lambda(t+\sigma, t+\rho)$ through Eq. (7.33). Each step so far may be carried out in a straightforward manner. To check the accuracy of $\phi(t)$ and $\bar{\phi}(t)$, we examine their values for $t \simeq \infty$ and compare them with the analytical asymptotes given by Eq. (8.4). We actually calculated $\phi(t)$ and $\bar{\phi}(t)$ in the range $0 < t < 200$ and checked their values for $t \simeq 200$.

In obtaining $\Lambda(t+\sigma, t+\rho)$ from Eq. (7.33), we use the asymptotic-in-time form of Eq. (8.4) for the large- ξ region. After constructing it, we must solve the integral equation (7.32). If we could truncate the integral at a finite time region, the solution would be obtained by inverting the finite-dimensional matrix $(1-\Lambda)$. However,

we find that the numerical data obtained in this way contain rather a large error. For an accurate numerical procedure, the ρ integration in Eq. (7.32) must be carried out systematically to $\rho = \infty$. To put it another way, we must treat $F(t + \sigma, t + \tau)$ as an infinite-dimensional matrix. We refer the reader to the original paper for the procedure necessary to take account of this feature.

The result for photoemission is given in Fig. 18(a) and that for absorption is shown in Fig. 18(b) and for comparison, the asymptotic spectra $P_{\text{main}}(\omega)$ and $I_{\text{main}}(\omega)$ given by Eqs. (9.49) and (9.50), respectively, are superimposed with the label ND (Nozières and DeDominicis). Also shown is $I^{(0)}(\omega)$, the spectrum due to the first term of the pairwise series for $I_0(t)$ given by Eq. (10.9), which, when Fourier transformed, is given by Eq. (10.14).

Our numerical treatment reproduces both the critical exponent and the amplitudes quite accurately with an error less than 1%. For $P_{\text{main}}(\omega)$, Fig. 18(a) shows that the asymptotic formula Eq. (9.49) is fairly good over a wide range of ω , not restricted to the edge region. The situation is worse in the case of XAS: only in the range $\omega < 0.05$ does the asymptotic curve agree with the exact one to within an error of 10%. Except in this near-edge region, the ND formula grossly overestimates the actual x-ray absorption spectrum.

We see that $I^{(0)}(\omega)$ agrees fairly well with the true spectrum. We note that the case with $V = 1.0$ corre-

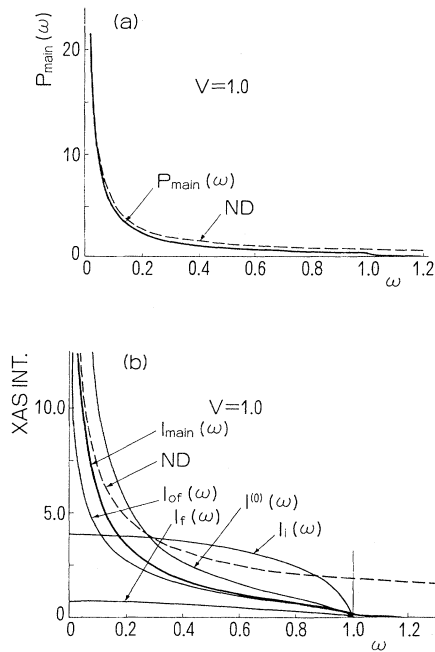


FIG. 18. Photoemission and absorption intensities for the case $V = 1.0$ as a function of the frequency ω measured from the threshold: (a) for $P_{\text{main}}(\omega)$ of photoemission; (b) for $I_{\text{main}}(\omega)$ of absorption. The dashed curve marked ND (Nozières and DeDominicis) shows the asymptotic formulas (9.49) and (9.50) for photoemission and absorption, respectively. The thin solid curves in (b) represent approximate absorption intensities obtained by various formulas defined by Eqs. (10.18)–(10.20).

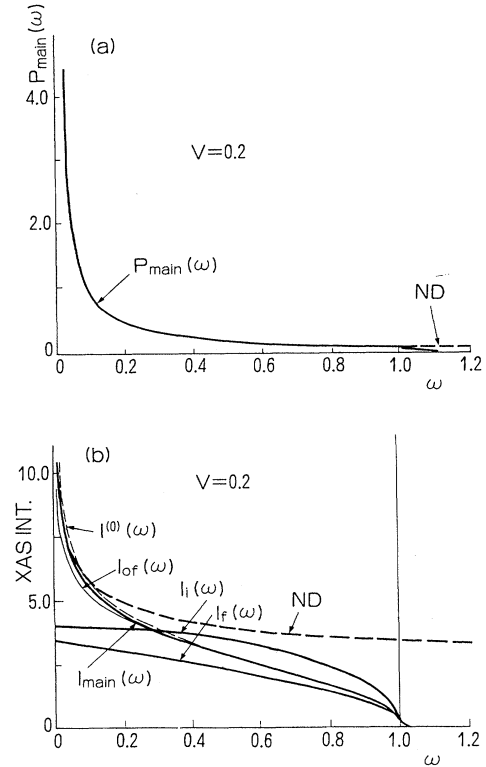


FIG. 19. Photoemission and absorption intensities for the case of $V = 0.2$. For the symbols, see Fig. 18.

sponds to $\alpha = 0.70(\pi/2)$ and that the pairwise iteration series diverges, according to the criterion of Eq. (10.13). Figure 18(b) thus implies that, in spite of the divergence, the term $I^{(0)}(\omega)$ of the series has a practical meaning as a first approximation to the absorption spectra.

In Figs. 19(a) and 19(b), the case with a smaller V is

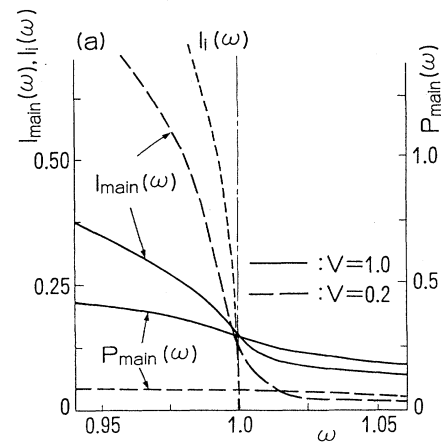


FIG. 20. Intensities of photoemission and absorption near the band edge $\omega = 1.0$ of Band B for the two cases of $V = 0.2$ and $V = 1.0$. $I_i(\omega)$ shows 2π times the semielliptic density of states [Eq. (10.15) with Eq. (11.2)].

shown. We observe that for $\omega > 0.1$, $I^{(0)}(\omega)$ practically coincides with $I(\omega)$.

Figure 20 shows the spectra near the upper band edge $\omega = 1.0$. If we include the excitation of many shakeup pairs, the excitation energy of the conduction band increases indefinitely. Since any single-particle excitation from a core level terminates at $\omega = D = 1.0$, the nonzero value of $I(\omega)$ at $\omega = 1.0$ is a measure of the contribution from shakeup excitations. It is remarkable that the square-root behavior of $N(\epsilon)$ is rather hard to recognize in the true spectrum for a large V .

E. Pairwise series expansion [Eqs. (10.8) and (10.9)]

Figure 21 shows

$$\sum_{k=0}^n a^{(k)} / \sum_{k=0}^{\infty} a^{(k)} \tag{11.8}$$

and

$$\sum_{k=0}^n b^{(k)} / \sum_{k=0}^{\infty} b^{(k)} \tag{11.9}$$

of Eqs. (10.8) and (10.9), which take account of asymptotic photoemission and absorption up to the n th term of the pairwise series. We have plotted two curves for the values of $\alpha = [2\delta(0)/\pi]$, $\alpha = 0.49$ and $\alpha = 0.51$, because the radius of convergence of the series is $\alpha_c = 0.5$, as shown by Eq. (10.13). Unfortunately, it is hard to see a meaningful difference between these two cases. However,

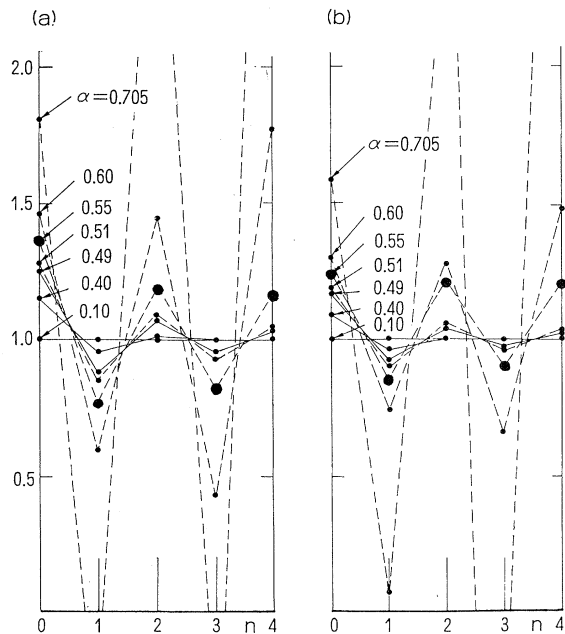


FIG. 21. Convergence of the pairwise series. In (a) the sum of $a^{(k)}$ [Eq. (10.8)] and in (b) that of $b^{(k)}$ [Eq. (10.9)] are plotted as functions of n . The parameter α is defined by $\alpha = 2\delta(0)/\pi$, and the critical value of convergence is $\alpha = 0.5$. As a guide to the eyes, the values for $\alpha = 0.55$ are shown by large solid circles.

for $\alpha = 0.40$ the series converges very quickly at $n = 2$, while in the case of $\alpha = 0.6$ it oscillates badly with n . This feature convinces us of the correctness of the present value for α_c .

F. Single-particle formulas for XAS [Eqs. (10.14)–(10.20) and Eq. (10.23)]

In Figs. 18 and 19, we have plotted $I_i(\omega)$, $I_f(\omega)$, and $I_{of}(\omega)$, the initial-state rule, final-state rule, and orthogonalized final-state rule formulas. We see that $I_{of}(\omega)$ coincides with the true spectrum very well. Its agreement for a smaller value of V is especially impressive. In contrast, it is hard to determine whether $I_i(\omega)$ or $I_f(\omega)$ provides a better approximation to the true spectrum. This is because the Fermi level lies at the center of the band. For a larger or smaller band filling, the difference between $I_i(\omega)$ and $I_f(\omega)$ shows up clearly, as the analysis of Sec. X.B shows. Figure 22 shows the situation for five positions of the Fermi level. In considering the case of $V = 0.3$, we have plotted $I^{(0)}(\omega)$ as given by Eq. (10.14) in place of the exact $I(\omega)$, for simplicity. We see that $I_f(\omega)$ works at a small band filling, while $I_i(\omega)$ is good at a large band filling, as discussed in Sec. X.B.

G. Temporal development of $\mathcal{A}(t)$ and $I_0(t)$ [Eqs. (7.30) and (7.31)]

Figures 23(a) and 23(b) show the function $\mathcal{A}(t)$ defined by

$$\mathcal{A}(t) = \int_0^t A(\tau) d\tau, \tag{11.10}$$

with $A(\tau)$ given by Eq. (7.30) and $I_0(t)$ defined by Eq. (7.31). Results are shown for the case of $\epsilon_F = 0$ for Band B. {In the case of $V = 1.0$, a bound state exists in the excited configuration, and $\mathcal{A}'(t)$ [Eq. (9.32)] and $I_0'(t)$ [Eq. (9.14)] are used.} The asymptotic t dependences are

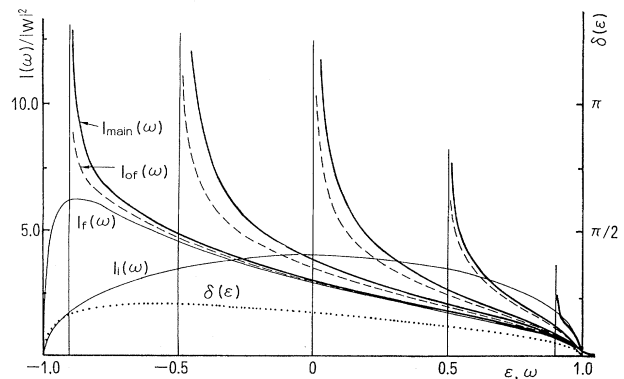


FIG. 22. Change of XAS intensities with band filling for the case of $V = 0.3$. The absorption intensities are plotted for five positions of the Fermi level. The spectra $I_f(\omega)$, $I_i(\omega)$, and $I_{of}(\omega)$ are defined by Eqs. (10.18)–(10.20). The phase shift is also plotted as a function of energy ϵ .

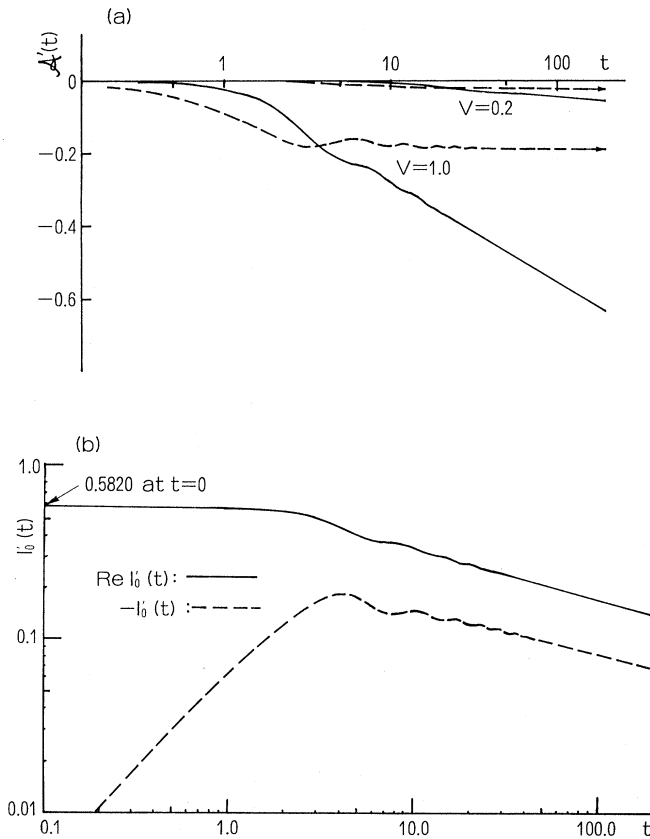


FIG. 23. The time developments of $\mathcal{A}(t)$ and $I_0(t)$ for Band B (t in units of $1/D$): (a) for $\mathcal{A}(t)$ and (b) for $I_0(t)$. The real (imaginary) part is shown by the solid (dashed) curve.

given by Eqs. (8.15) and (8.16), respectively. The figures thus show how these quantities evolve into their asymptotic forms.

The most striking feature of Fig. 23 is that even for $t > 1.0$ ($t > 1/D$ in actual units) the asymptotic form can be perceived. For $1.0 < t < 10.0$ oscillations with the period 2π are only superimposed on the asymptotic behavior. For $t < 10$, $\mathcal{A}(t)$ is less than 0.2 for $V=1.0$, implying that for absorption in the spectral range $\omega > 0.1$ we may take $P(t)$ as unity to a good approximation. This is what we have done in analyzing the single-particle formula in Sec. X.B. In addition to being used for comparison of numerical results with the analytical asymptotes (8.15) and (8.16), the value $I_0(0)$ is also used to see the accuracy of our numerical procedures, because we know its analytical value related to the integrated intensity of absorption [Eq. (6.2)]. We thus have estimated the error to be less than 1%, as stated before.

H. Generalized power-law formula [Eq. (10.27) for photoemission and Eq. (10.28) for XAS and XES]

The approximate spectra given by the intensity formula with ω -dependent exponents are given in Fig. 24 for

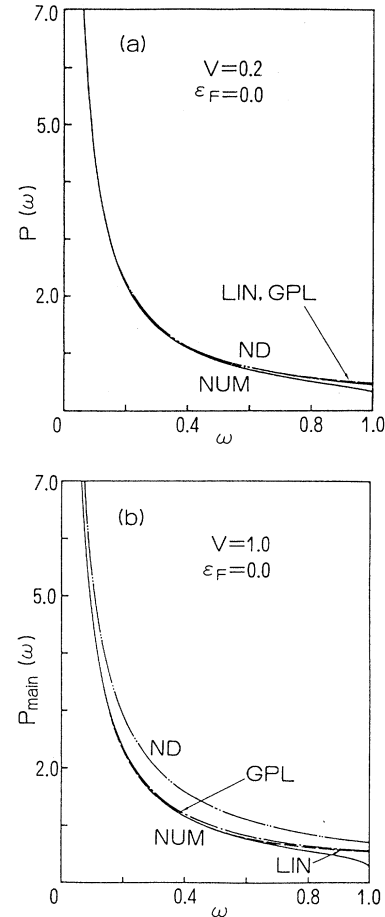


FIG. 24. Generalized power-law formulas compared with the exact and asymptotic curves for x-ray photoemission: (a) for $V=0.2$ and (b) for $V=1.0$. The curves labeled ND (Nozières and DeDominicis) show the asymptotic formula given by Eq. (9.49). The curves labeled GPL are the second expressions of Eq. (10.27), and the curves labeled LIN (linearized) are the first expressions. The curves marked NUM show the exact numerical line shapes.

photoemission and Fig. 25 for absorption, for Band B with $\epsilon_F=0$. The curves are drawn with the ω -dependent exponent calculated to $O(\omega)$. The curves marked LIN are for the first of the two expressions, Eqs. (10.27) and (10.28). In Fig. 26, we show the result of Kita (1987) for XAS and XES. The label GPL- n indicates that the curve was obtained with the generalized power law (GPL) calculated to $O(\omega^n)$ ($n=0,1,2$). The GPL-0 is thus the asymptotic expression $I_{\text{main}}(\omega)$ given by Eq. (9.50). The GPL-1 is given by Eq. (10.28), and the GPL-2 is the result of generalization to higher order (although its explicit form is not shown here).

From the figures we see that GPL formulas reproduce the exact spectra quite well except near the band edge, where the band-edge effect alters the line shape strongly. It is natural that a Taylor expansion at the Fermi level,

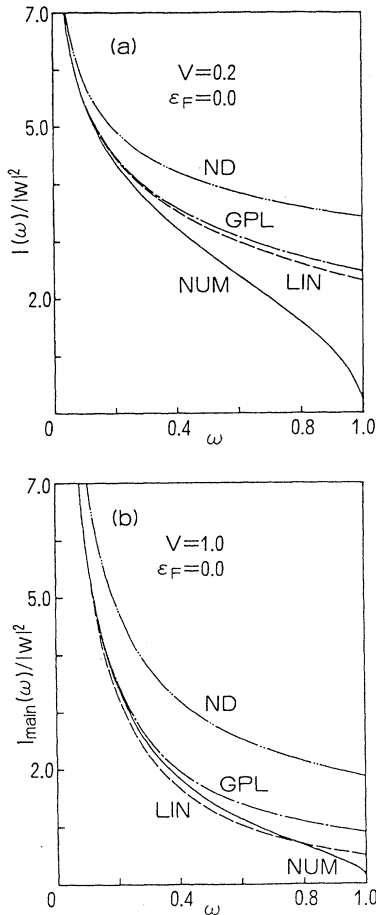


FIG. 25. Generalized power-law formulas compared with the exact and asymptotic curves for x-ray absorption. The curves LIN and GPL are the first and second expressions of Eq. (10.28), respectively. The curves NUM are the exact line shapes.

upon which the GPL expressions are based, fails to cover the square-root termination of $N(\epsilon)$ at $\epsilon = 1.0$. With increasing V , many-body effects become dominant and the band-edge effect is less appreciable. This means that the GPL formula is more accurate for a larger V , as is, in fact, revealed by the two curves with different V in Figs. 24 and 25.

With a small value for V , the difference between LIN and GPL formulas is not appreciable in Fig. 25. For a larger V , it seems that GPL is better than LIN. This is indeed the trend shown analytically by Kita, as discussed in Sec. X.C.

In Fig. 26, we observe that XES and XAS intensities are not symmetrical with respect to the edge $\omega = 0$. The intensities expressed by the curve GPL-0 have a mirror-image relationship. The improvement in the XES curve obtained by GPL-1 is striking. This is because the presence of an ω -linear term in the generalized power law is indeed the principal origin of the breakdown of the

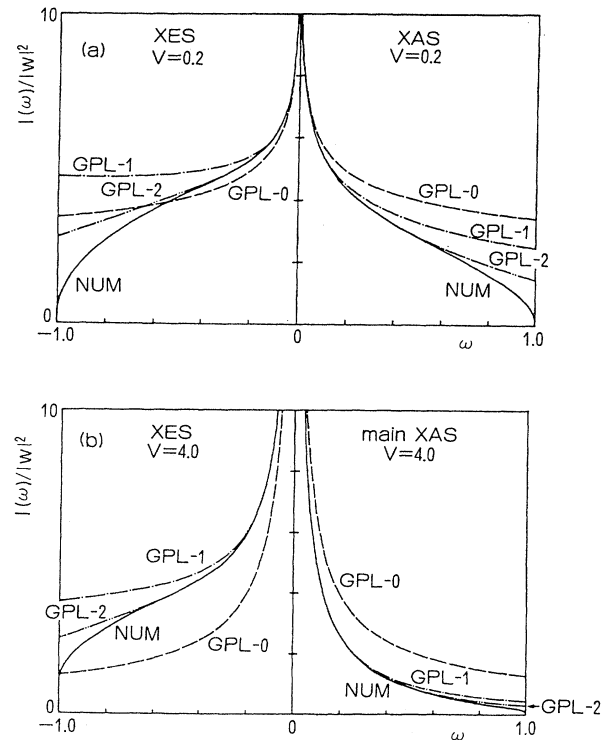


FIG. 26. Generalized power-law formulas compared with the exact XAS and XES intensities: (a) $V = 0.2$; (b) $V = 4.0$ (Kita, 1987). For the curve labeled GPL- n , see the text.

mirror-image relation between XAS and XES (Sec. III.B.2).

In summary, the Taylor expansion at the Fermi level and a few terms of the order of ω and ω^2 in the ω -dependent power yield strikingly good intensity curves both for photoemission and for absorption over a very wide frequency range. Of course, the agreement with exact curves depends upon the smoothness of the band profile $N(\epsilon)$, so we must admit that the present calculation based on the model of Band B with the Fermi level chosen at the band center is likely to favor the GPL formula. The phase shift $\delta(\epsilon)$ calculated for Band B is shown in Fig. 13 by dotted curves, which indicate that the approximation (10.26), upon which the GPL formulas were based, holds well except for ϵ near the band edge.

I. Thermal broadening and comparison with experiments on quantum wells [Eqs. (7.38) and (7.39)]

Edge anomalies have been observed recently in the emission and absorption spectra to and from the top of the valence band in n -type quantum wells, such as $\text{In}_x\text{Ga}_{1-x}\text{As}$ -GaP and GaAs- $\text{Al}_x\text{Ga}_{1-x}\text{As}$. The electrons in conduction bands are doped by a modulation-

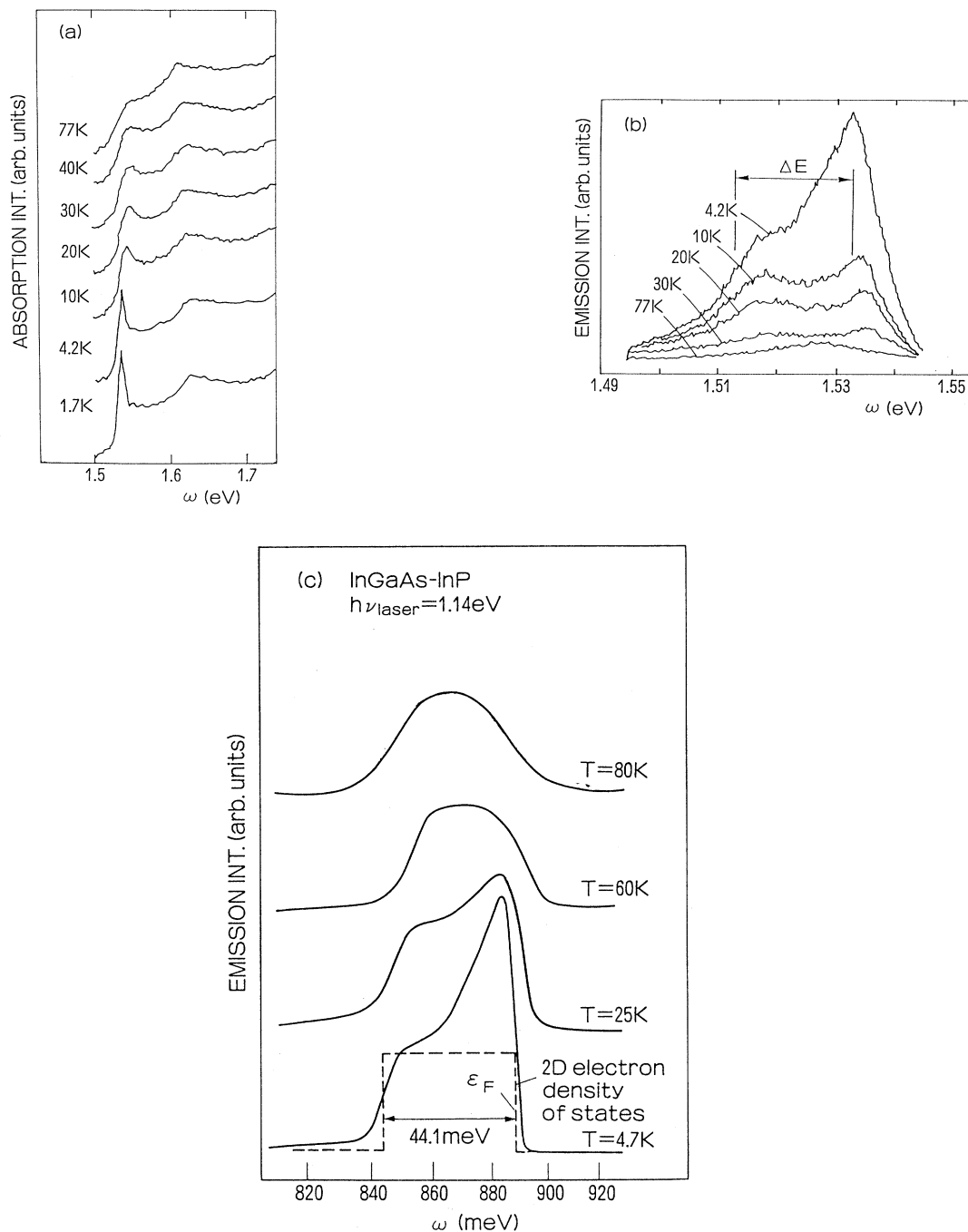


FIG. 27. Experimental absorption (a) and emission (b) intensities as functions of photon energy, obtained by Lee *et al.* (1987a, 1987b) for a GaAs-Al_xGa_{1-x}As quantum well. ΔE in (b) is the Fermi energy. In (c) the emission spectrum obtained by Skolnick *et al.* (1987a, 1987b) for In_xGa_{1-x}As-GaP is shown.

doping technique and considered to be free from the random potentials due to dopants. The conduction band may thus be regarded as a free quasi-two-dimensional band having constant density of states. The Fermi energy is usually of the order of 100–200 K for a carrier concentration of $n \approx 10^{11} \text{ cm}^{-2}$. Thus it is easy to observe

the temperature effect experimentally.

Typical absorption and emission spectra observed by Lee, Iwasa, and Miura (1987a, 1987b, 1988) are shown in Fig. 27. In the case of absorption, a prominent peak near the threshold characterizes the spectrum, which is asymmetric with a very sharp rise in the lower-energy side as

compared with gradual decay in the higher-energy side. The striking thermal smearing of the peak profile also attracts our attention. Indeed, it is very easily blurred by temperature effects, in marked contrast to the exciton peak in an undoped system, which is independent of temperature even at room temperature. The emission band is strongly temperature dependent as well, with a width roughly equal to E_{Fermi} . The data for $\text{In}_x\text{Ga}_{1-x}\text{As-GaP}$ of Skolnick *et al.* (1987a, 1987b, 1988), who observed an emission band that reflects more clearly the two-dimensional density of states, are given in Fig. 27(c).

These peculiarities shown in Fig. 27 are all to be expected naturally if the peak is really due to infrared divergence. The system thus serves as a good test for our treatment of the infrared divergence at $T \neq 0$.

In applying our theory to this system, we note that an important effect will result from possible motion of the hole created optically in the valence band. We assume here that the hole in the valence band is at rest throughout the optical process. One justification for this assumption is the heavy hole mass relative to that of electrons ($m_h \sim 7m_e$ in GaAs). Several other considerations lend support to this assumption, as well (Ohtaka and Tanabe, 1989). Another factor to be taken into account in attempting the fitting is the finite lifetime of the hole. We also need to know a reasonable value for the strength of the hole potential. The line shape will depend critically on both.

In the two-dimensional density of states $N(\epsilon)$, the final state always has a bound state, as in Band A treated previously, which leads to a slight adjustment in the treatment of Sec. VII.C. We use here a separable form for the matrix elements of the hole potential and optical matrix element. Taking the Fermi level as the origin of energies and using the Fermi energy E_{Fermi} as the scale of energy (i.e., $|\bar{D}|=1$), we set

$$V_{kk'} = -Vu_k u_{k'}, \quad (11.11)$$

$$w_{kc} = -wu_k, \quad (11.12)$$

where the following form is assumed for u_k :

$$u_k = \exp[-(\epsilon_k + 1)/\Gamma] \quad (11.13)$$

with $\Gamma=10$. The parameter Γ serves as a cutoff energy of the final-state interaction, and the value $\Gamma=10$ is chosen so that the result for $-2 < \omega < 2$ will not depend much on the value of Γ . We can show that the separable form of Eqs. (11.11) and (11.12) simply introduces the shape function u_k into the summands of Eqs. (7.36) and (7.37), so that no serious modification is necessary.

Photon energy ω is measured from the threshold in the absence of a final-state interaction. We put $|\omega|^2=1$ as before. Since the conduction band is assumed to extend to infinity, the constant density of states is normalized by N , the total number of electrons, so that the parameter V used in what follows is $VN(0)$ in an unnormalized unit. Figure 28 shows the results for three values of V , $V=0.15$, $V=0.37$, and $V=0.5$. Various quantities cal-

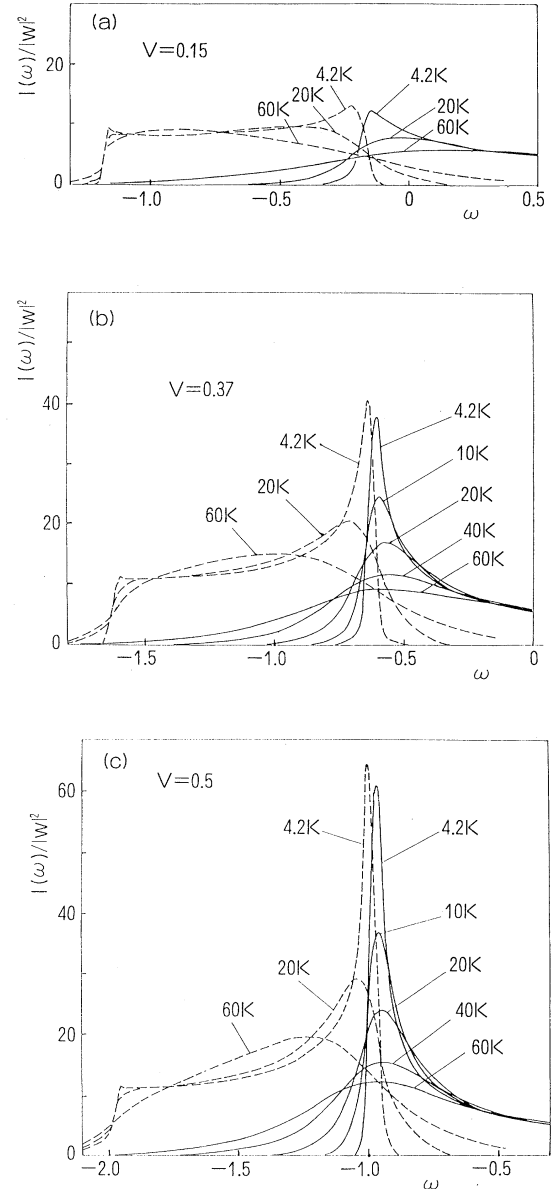


FIG. 28. Calculated absorption (solid curves) and emission (dashed) spectra for (a) $V=0.15$, (b) $V=0.37$, and (c) $V=0.50$, as functions of ω in units of $|\bar{D}|$, the Fermi energy, for several values of temperature.

culated for these values of V are listed in Table II. The quantity ΔE^0 therein, the relaxation shift at $T=0$, is calculated from Eq. (9.20) with the existence of a bound state taken into account. Figure 28 shows that the threshold actually shifts downwards by nearly ΔE^0 relative to the unperturbed threshold. The values of $\delta(0)$ listed show that the magnitudes chosen for V are not bad. Note that we are adopting a V that yields $\delta(0)$ near $\pi/2$, though the band filling is very small.

Figure 29 shows how the ideal line shapes given above are modified by taking account of the spins and the life-

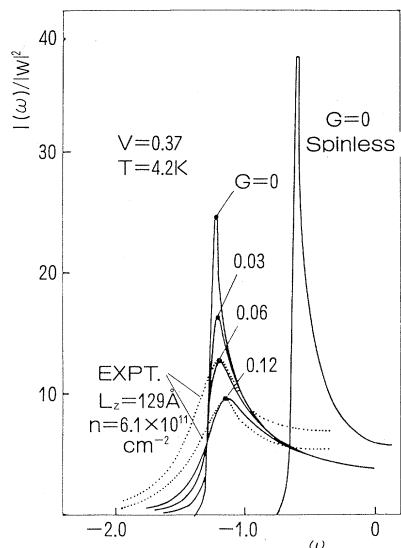


FIG. 29. Modification of theoretical absorption curve for the case of $V=0.37$ and $T=4.2$ K. The curve marked “ $G=0$, spinless” is reproduced from Fig. 28(b). The group of solid curves on the left-hand side show the curves with spin taken into account together with the lifetime of the hole, expressed by the parameter G . The dotted curves are the experimental ones reproduced from Fig. 27(a), drawn so that the top of the peak coincides with the theoretical curve.

time of the hole, which is parametrized by the factor G . The effect of spins appears in two ways, producing a relaxation shift twice as large as that of Fig. 28 and changing the critical exponent from $2\delta(0)/\pi - [\delta(0)/\pi]^2$ to $2\delta(0)/\pi - 2[\delta(0)/\pi]^2$, thus suppressing the edge anomalies. The hole lifetime is incorporated by the factor $\exp(-Gt)$ in the Fourier transform. The experimental (dotted) curves are reproduced so that their peak height coincides with the theoretical curve. We find that $G=0.12$ gives a good fit to the observed peak breadth.²

Figure 30 shows the absorption and emission curves, the theoretical curve for $V=0.37$ and $G=0.12$, in (a) and experimental ones in (b) and (c). Note that the unit of energy in (a) is 200 K, that is, 0.02 eV. We find reasonable agreement in view of the idealized model adopted for the system, which neglects the finite thickness of the well, electron correlation, etc.

As for the emission spectrum, the curves shown in Fig. 30(a) do not agree at all with those observed in Fig. 27(b). They are, however, similar, to Fig. 27(c) of $\text{In}_x\text{Ga}_{1-x}\text{As-GaP}$. Since the integrated intensity of Fig. 27(b) depends critically upon T , we shall have to introduce some unknown relaxation mechanism to obtain good agreement

²A part of G certainly takes account of the broadening due to the finite hole mass, nonparabolicity of bands, etc.

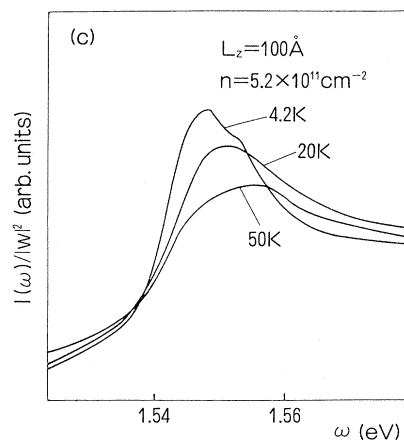
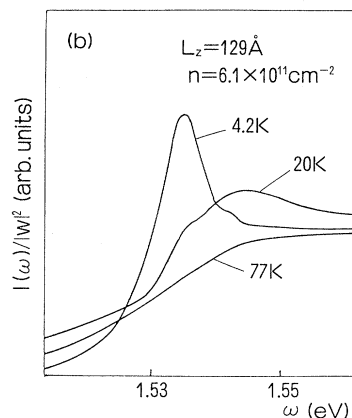
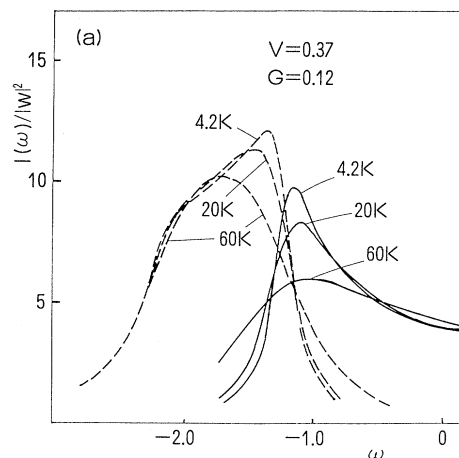


FIG. 30. Absorption and emission for a quantum well: (a) theoretical absorption (solid curves) and emission (dashed curves) for $V=0.37$ and $G=0.12$ in a quantum well with $L_z=129$ Å, $n=6.1 \times 10^{11}$ cm⁻² (L_z is the well thickness and n the density of electrons); (b) experimental absorption curves for the same quantum well; (c) experimental absorption for a quantum well with $L_z=100$ Å, $n=5.2 \times 10^{11}$ cm⁻². In (a), ω is measured in units of $|D|=200$ K.

TABLE II. Three calculated values of the potential V . ϵ_λ and ΔE^0 are given in units of the Fermi energy E_{Fermi} .

	$V=0.15$	$V=0.37$	$V=0.50$
ϵ_λ	-1.004	-1.221	-1.509
$\delta(0)$	0.258 ($\pi/2$)	0.575 ($\pi/2$)	0.697 ($\pi/2$)
β	-0.241	-0.492	-0.575
ΔE^0	-0.180	-0.624	-0.970

with the emission curve observed by Lee *et al.*

Finally, we should like to comment on the correlation effect. Electron correlation manifests itself in several ways, as discussed in Sec. II. The most important is that it causes electron screening, which in turn determines the parameter V . For x-ray photoemission, we have an approximate formula due to Langreth (1970) by which to obtain the spectrum, taking into account the screening due to correlation. A calculation of spectra using the random-phase approximation (RPA) dielectric function (Nishimura and Ohtaka, 1989) shows that the phase shift obtained by our choice, $V=0.37$, is quite reasonable; here we, quote only the values of $2[\delta(0)/\pi]^2$. From Table II, we have 0.165 for $V=0.37$, while the RPA treatment (no fitting parameter) of the Langreth formula yields 0.150. In addition, the Debye-Waller factor due to plasmon excitation is not so large because the value of the effective r_s is less than unity. The RPA result shows that there will be approximately a 40% suppression due to plasmon excitation. For more about the effect of the correlation, see Sec. XII.

Altogether, we may conclude that the theoretical curves obtained based on the solution of the soft-x-ray problem describe the real situation fairly well.

XII. APPLICATION OF THE MND MODEL TO REAL SYSTEMS

Before ending this review, we should like to discuss the applicability of the MND model. This section is intended mainly to show that the model has indeed been a powerful tool in explaining the experimental data. References are cited in this section only for this purpose, not with any intent of providing a comprehensive survey of the experiments and related theories.

In the early 1970s there were some doubts about the usefulness of the MND model in explaining the edge anomalies of actual simple metals. However, this was due to a number of complexities involved in real systems, which obscured the ideal aspects of the physics, essentially well described by the MND model. We have at present sufficient evidence to support the validity of the model, and its usefulness is well established not only theoretically, in the Kondo problem, for example, but also experimentally in explaining optical properties of simple metals.

The MND model predicts a sharp or rounded edge de-

pending upon the sign of the critical exponent β in Eq. (1.2). Since usually $\beta(l_0=0) < 0$ and $\beta(l_0=1) > 0$, a sharp edge peak is predicted in the case of L absorption (p hole left behind) and a rounded edge in K absorption (s hole). All the alkali metals, Li, Na, K, Rb, Cs, and other simple metals such as Mg and Al that have been examined extensively to date follow this rule without exception. To support this statement we cite here only a number of experiments: XAS and XES measurements obtained by Neddermeyer (1976) and Callcott *et al.* (1978) for light alkali metals, and the absorption spectra taken by Ishii *et al.* (1977) and Miyahara *et al.* (1980) for heavy alkali metals. In particular, in the case of L absorption, power-law behavior was demonstrated unambiguously in these data. For example, the log-log plot of Ishii *et al.* (1977), attempted for Rb, after eliminating the effects of instrumental resolution, clearly shows the reliability of the value of the critical exponent of Rb obtained experimentally. Thus the applicability of the MND model is not merely qualitative.

The observed magnitudes of the critical exponents in absorption and photoemission spectra are generally in agreement with those obtained from the calculation of phase shifts. It is interesting here to note that the theoretical values of the phase shifts, reliable enough to be adopted as confirmation of the exactness of the Nozières and DeDominicis (ND) formula for the critical exponent, are not obtained from such a simplified core-hole-conduction-electron interaction as was assumed in the MND model. We must actually incorporate the s or p character of the spatial extent of the hole, the Bloch character of the conduction electrons, the realistic screening of the hole potential by electron correlation, and so on. Strictly speaking, the spin of the core hole brings about an exchange interaction with the conduction electrons, which causes a difference in the phase shifts of up- and down-spin conduction electrons. Moreover, the core-hole potential obtained with all these factors taken into account is required to be such that leads to phase shifts satisfying the Friedel sum rule.

If reliable phase shifts are employed, the ND form of the critical exponent is correct. This fact shows the power of the simple MND model, which neglects all these complexities as irrelevant, and justifies the effort of seeking an exact MND solution. For elaborate procedures to obtain the phase shifts, a few pioneering papers are cited here: Ausman and Glick (1969), Almladh and von Barth (1976), Ohmura and Sano (1977), Bryant and Mahan (1978), and Bryant (1979).

We have at present reliable theoretical values for the phase shifts at the Fermi level and thus for the critical exponent, in the sense that those obtained by different authors and different schemes agree well. This situation will easily be seen in Table III, where we give some experimental and theoretical data from the literature. We mention here only one convincing example to illustrate the present status of the phase-shift calculations. Since the magnitude of $\beta(l_0=0)$ (hereafter denoted simply as

TABLE III(a). Some of the experimental and theoretical critical exponents in the literature for L absorption of XAS, with values for $-\beta(l_0=0)$ of Eq. (1.2). The notation "ex" shows that the value is obtained by taking account of the exchange effect; "em" indicates data from emission; "vb" means that it takes account of the presence of a virtual bound state.

Na	K	Rb	Cs	Al	Mg
XAS (experiment)					
0.26±0.04 ^a	0.23 ^b	0.19 ^b	0.06 ^b	0.2±0.06 ^{c,em}	0.3±0.07 ^{c,em}
0.24 ^d	0.28±0.02 ^e	0.26±0.02 ^e	0.07±0.02 ^e	0.15±0.04 ^a	0.18±0.04 ^a
0.37 ^{f,ex}				0.12 ^g	0.21 ^g
				0.18 ^f	0.23 ^f
XAS (theory)					
0.40 ^h	0.27 ⁱ	0.25 ⁱ	0.05 ^{i,vb}	0.24 ^j	0.25 ^j
0.38 ^k	0.28 ^l	0.29 ^l	0.23 ^l	0.06 ^k	0.27 ^m
0.34 ^m				0.13 ⁿ	0.19 ⁿ
0.38 ^o				0.23 ^m	0.28 ^o
				0.25 ^o	

^a Dow and Sonntag, 1973; Dow *et al.*, 1974.

^b Ishii *et al.*, 1977.

^c Neddermeyer, 1976.

^d Callcott *et al.*, 1978.

^e Miyahara *et al.*, 1980.

^f Citrin *et al.*, 1979.

^g Citrin *et al.*, 1975.

^h Ausman and Glick, 1969.

ⁱ Ohmura and Ogiwara, 1989.

^j Mahan, 1977.

^k Almladh and von Barth, 1976.

^l Bryant, 1979.

^m Ohmura and Sano, 1977.

ⁿ Bryant and Mahan, 1978.

^o Minnhagen, 1976, 1977.

β) is dominated by the s -wave phase shift, one would expect $-\beta$ ($=|\beta|$) to become large as the screening becomes less dominant. This is indeed the trend observed in light metals, where a metal with a smaller carrier density (i.e., with a larger r_s) has a larger $-\beta$; the empirical relation $-\beta=0.068 r_s$ has been found for light metals such as Na, Mg, and Al (Dow, 1975). In contrast, for heavier alkali metals, such as K, Rb, and Cs, the observed data do not follow this rule (Ishii *et al.*, 1977; Mi-

yahara *et al.*, 1980). In Cs, in particular, a very small value of the critical exponent is observed. As shown in Table III, however, the recent theory is successful in reproducing the observed critical exponents of heavier alkali metals, in which the anomaly of Cs is attributed to the presence of a virtual bound state (Ohmura and Ogiwara, 1989).

In a strictly quantitative sense, there are still some unexplained disagreements between theory and experiment. One is the lack of mirror-image symmetry between the XAS and XES spectra. For example, Callcott *et al.* (1978) obtained $-\beta=0.24$ for Na from the XAS data and $-\beta=0.15$ from the XES. In XES the spin-orbit doublet is not observed, and the peak looks much less prominent than that in XAS. The situation is more or less the same in other metals (Citrin *et al.*, 1979). The asymptotic behavior predicted by the ND theory has a strict mirror-image relationship, while the exact solution of the MND model shows that mirror symmetry no longer exists. In the calculated emission spectra we have an edge peak slightly larger in magnitude than that in absorption, as demonstrated in our numerical results of Figs. 26, 28, and 30 and in the spectra of Fig. 19 obtained by Grebennikov *et al.* The theory thus predicts an edge peak slightly larger in XES than in XAS. The actual situation is the converse of this. Therefore, the experimental asymmetry with respect to the position of the threshold is not to be ascribed to the frequency dependence of the critical exponent, which was shown to be responsible for the asymmetric edge properties of the exact solution, as discussed in Sec. III.B.2. One possible reason for the lack of mirror symmetry is incomplete relaxation of the

TABLE III(b). Some of the experimental and theoretical critical exponents in the literature for L absorption of XPS, with values for σ of Eq. (1.4).

Na	Al	Mg
Photoemission (experiment)		
0.20 ^a	0.16 ^b	0.13 ^b
	0.12 ^a	0.13 ^a
Photoemission (theory)		
0.19 ^c	0.13 ^d	0.10 ^e
0.20 ^d	0.08 ^e	0.12 ^f
0.14 ^e	0.10 ^f	0.13 ^g
0.19 ^g	0.11 ^g	

^a Citrin *et al.*, 1975.

^b Ley *et al.*, 1975.

^c Ausman and Glick, 1969.

^d Almladh and von Barth, 1976.

^e Ohmura and Sano, 1977.

^f Bryant and Mahan, 1978.

^g Minnhagen, 1976, 1977.

system before photon emission, as analyzed by Almladh (1977a, 1977b) and Mahan (1977, 1988). Another possibility is the presence of a nonradiative decay channel in the emission case, as discussed in Sec. XI.I for the relative magnitude of the observed absorption and emission spectra in a 2-D quantum well.

Another aspect that still remains to be clarified is the rather poor agreement between theory and experiment on the values of the critical exponent in Na, the most typical simple metal yielding an edge peak. When we look at Table III, we at once become aware of this unhappy situation in Na as compared with other heavier alkali metals. There are two conceivable reasons for this. Since the observed relative intensities of L_2 and L_3 peaks do not agree with the prediction based on a simple spin-orbit interaction, a spin-dependent coupling between the conduction electrons and core hole must be complicating the situation, as analyzed first by Onodera (1975) for exchange mixing of the L_2 and L_3 spectra and later by Kaga (1977) and Yoshimori and Okiji (1977) for electron scattering of the Kondo type. The presence of an exchange coupling is the first possible reason. Citrin *et al.* (1979), in fact, found a better fit for Na using the Onodera theory (see Table III). With regard to the effect of core-hole spin, we refer the reader to the original papers and to the review by Almladh and Hedin (1983). We discuss here the second possibility of a generalized power-law, which seems to dominate the first effect.

We note that the range of frequency in which the simple MND power-law formula is valid is rather limited. Let us return to Figs. 25 and 26, which demonstrate how the MND result is improved by using an ω -dependent critical exponent. For ω (the frequency scaled by half the bandwidth) less than unity, $\omega^{\beta_1} < \omega^{\beta_2}$ for the two exponents $0 < -\beta_1 < -\beta_2$ (i.e., a smaller $-\beta$ follows from a smaller intensity). Figure 26 thus implies that the curve GPL-1, which has a smaller magnitude than the ND value (curve GPL-0) in the absorption case, has a critical exponent smaller than that predicted by the ND theory. Therefore, if the experiments are assumed to be described by the exact solution of the MND model, the fitting procedure for the XAS intensity using only an ω -independent exponent will necessarily give a critical exponent $-\beta$ smaller than the true one. The trend shown in Table III appears to be in accord with this situation. To see the generality of this tendency, the calculation of Ohmura and Ishikawa (1980b) will be helpful, where a perturbational treatment of the core-hole potential leads to the result that the GPL-1 generally gives rise to a smaller absorption intensity and a greater emission intensity than the ND prediction (this contrast between XAS and XES is well demonstrated in Fig. 26). According to Ohmura and Ishikawa, the correction due to ω dependence is larger for a larger ratio of the core-hole potential to the bandwidth. The better fit shown in Table III for heavy alkali metals is expected to be explained within this context, though the size of the correction due to the generalized power law has not yet been determined.

Figures 31 and 32 show how the exact XAS and photoemission intensities deviate from the predictions of the asymptotic theory as frequency deviates from the edge. The results are reproduced from Fig. 18 (for a square-root band with total bandwidth 2 and the position of the Fermi level at the band center). Figures 31(a) and 31(b) show the log-log plot of the intensities for XAS and XPS, respectively, in the frequency range $0.01 < \omega < 0.4$. The dashed straight line shows the intensity of the asymptotic formula (9.50) expressed in terms of the ND exponent $-\beta$ and the critical amplitude μ given by Eq. (9.51), and the solid curve shows the exact intensity. For the two cases of $V=1.0$ [$\delta(0)=0.705(\pi/2)$] and $V=4.0$ [$\delta(0)=0.921(\pi/2)$], we find $-\beta=0.581$, $\mu=1.880$, and $-\beta=0.709$, $\mu=1.274$, respectively. Figure 32(a) shows the XAS critical exponent defined by the tangent at ω to the log-log plot of the exact intensity curve of Fig. 31(a) (called the curvature exponent) and the generalized power

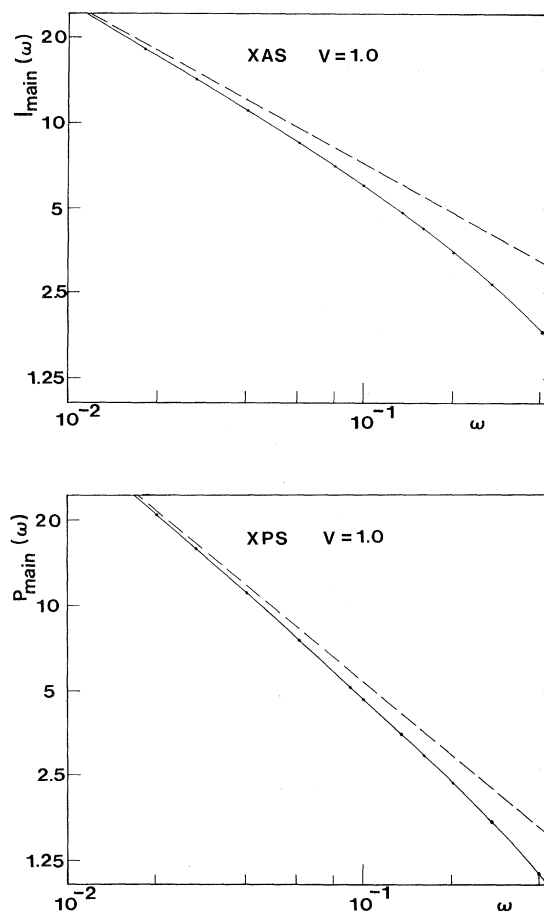


FIG. 31. Comparison of the Nozières-DeDominicis and MND models: (a) Log-log plot of the XAS intensity reproduced from Fig. 18; (b) plot of the photoemission intensity. The dashed straight line shows the ND prediction, and the solid curve is the exact curve of the MND model. The frequency ω is scaled by half the bandwidth (see the caption of Fig. 18).

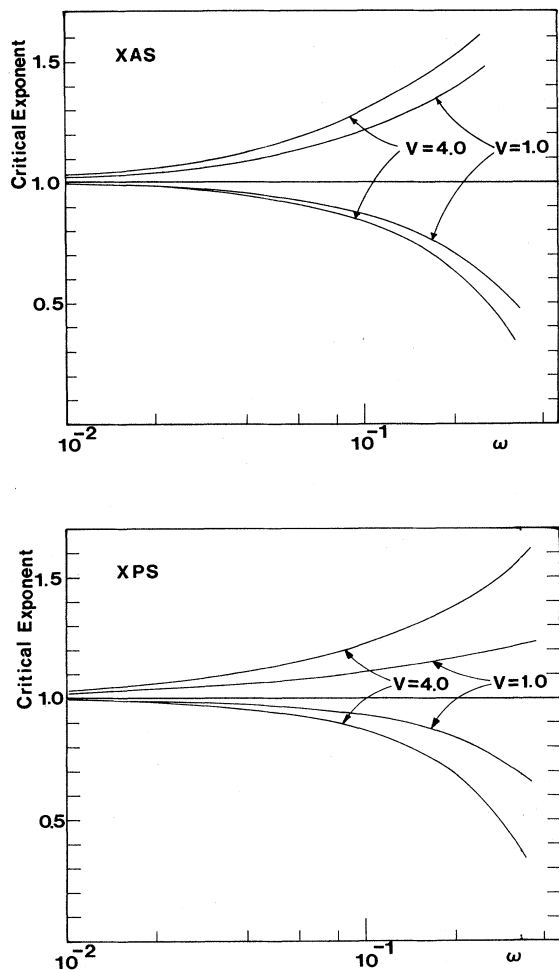


FIG. 32. Curvature and generalized power-law exponents: (a) for $-\beta$ of XAS; (b) for $(1-\sigma)$ of x-ray photoemission. The exponents normalized by the ND value are shown for the two cases of $V=1$ and $V=4$. The curves larger than unity are the curvature exponents because the exact intensity varies more rapidly with ω than does the ND prediction, as seen in Fig. 31. Curves smaller than unity show the generalized power-law exponent. They are less than unity because the exact intensity is smaller than that of the ND prediction. See the text for the definitions of the two exponents.

$-\beta(\omega)$ obtained by fitting the intensity at ω to $\mu\omega^{\beta(\omega)}$ (called the GPL exponent). They are both normalized by $-\beta$, the ND value of the critical exponent. The curves for $V=4$ are drawn using a log-log plot (not shown here). As mentioned above, the values for the GPL exponent are smaller than those for the ND. Figure 32(b) shows the case of photoemission for the curvature and GPL exponents for the quantity $(1-\sigma)$, normalized by its ND value (0.886 for $V=1$ and 0.781 for $V=4$).

We see from Fig. 32 that the asymptotic formula in photoemission has a wider range of applicability than in the XAS case. This trend, already pointed out in relation

to Fig. 18, is reflected in Table III in that the experimental photoemission values agree with the ND value better than do those for absorption. We see also that over rather a wide frequency range of $0.01 < \omega < 0.04$ it is possible to fit the exact curve of absorption or photoemission to a straight line; from this we might conclude that the asymptotic formula has a frequency range of applicability of, say, one-third of the total bandwidth. In reality, however, what applies in a strict sense is the GPL formula, not the ND formula. At $\omega=0.2$, for example, both the curvature and the GPL exponents are seen to deviate from the ND value by more than 30%. Therefore, if we aim at a precision of 10%, it is important to employ intensity data for ω less than $\omega=0.05$. In the photoemission case the situation is better, as can be seen in Fig. 32. Judging from the values of $\delta(0)$, the phase shift at the Fermi level, the case of $V=1.0$ does not differ very much from that of actual simple metals. The above consideration therefore shows an obvious difficulty with the experimental determination of the critical exponent. Moreover, the fitting for Na made by Citrin *et al.* (1979) over a wide 1-eV frequency range with an ω -independent exponent (but with the exchange effect taken into account) seems to the present authors rather audacious.

The raw experimental data involve the lifetime effect of the core hole (Doniach and Sunjić, 1970; Almladh and Minnhagen, 1978a), phonon effect (Flynn, 1976; Hedin and Rosengren, 1977), and temperature effect (Almladh and Minnhagen, 1978b, for the quasiboson approximation and Ohtaka and Tanabe, 1984, for the exact treatment discussed in Secs. V and VII.C), all of which manifest themselves in an otherwise divergent edge region. We thus need to convolute the theoretical curve with Gaussian and Lorentzian spectra in order to incorporate these effects (Callcott *et al.*, 1978), or, conversely, we need to deconvolute the observed data to eliminate them (Ishii *et al.*, 1977). These processes inevitably introduce additional errors to the derived critical exponent. Furthermore, the ω dependence of the transition matrix element and density of states near the Fermi level and the d -character ($l_0=2$) feature of the excited configuration state in the L absorption spectrum can certainly affect the edge property. These factors more or less mask the ideal features of the MND model in the observed spectra.

The failure to observe a power law in the electron energy-loss spectrum from K electron excitation of Li (Ritsko *et al.*, 1974) may be partly attributed to ambiguity of this sort, in addition to the presence of an exchange coupling. It does not imply the breakdown of the MND model in Li. It is true that the experiment of Ritsko *et al.* for Li and that of Slusky *et al.* (1976) for Mg tested negatively the prediction of Doniach *et al.* (1971) that an edge peak would be observed, even in the K excitation spectrum, if the momentum transfer q of an incident electron were large enough to relax the selection rule. But Slusky *et al.* (1979) showed later that in the case of Na, K, and Mg, the q dependence of the loss spectrum was not contradictory to the MND theory. Theoretically,

Ohmura (1981) shows that the observed spectra, including those of Li, could be understood naturally within the context of the MND model when one took account of instrumental resolution and the deviation of the spectral shape due to the generalized power law.

Overall, the predicted critical exponents agree in general with the theory; there are some discrepancies that may presumably be attributed to the ω dependence of the generalized critical exponent. Although experimental confirmation poses a challenge, the improved techniques of today will certainly shed some light on the problems listed above as unsettled. The data available are becoming obsolete, all obtained about 10 or more years ago. Since an optical apparatus with $\Delta\Omega/\Omega=2.5\times 10^{-5}$ is now available (Ishii, 1990), where $\Delta\Omega$ is the energy resolution and Ω the photon energy used—as compared to $\Delta\Omega/\Omega=5\times 10^{-3}$ at best in those days—we do hope that renewed experiments will be carried out to collect better data through present-day techniques.

Next we turn to the correlation effect. This topic, extensively examined by Minnhagen (1976, 1977), making use of the lowest-order cumulant approximation of Langreth (1970), has been reviewed by Almladh and Hedin (1983), and we actually have little to add to their review. The correlation effect is evident in the spectrum in the ranges $\omega\simeq 0$ and $\omega\simeq 1.0$. In the region $\omega\simeq 1.0$ the effect manifests itself most prominently in the form of sidebands due to plasmon excitation. In the near-edge region, on the other hand, the correlation effect appears in two ways. One is the screening of the core-hole potential through correlation, as mentioned at the end of Sec. X. As discussed above, a core-hole potential cannot lead to a reliable value of the phase shift unless properly screened. An interesting question concerning the dynamical nature of the screening is whether or not an additional ω dependence of the critical exponent arises from the correlation. Minnhagen (1976) showed that in the case of photoemission the ω dependence was practically negligible over a very wide range of the order of the plasma frequency and that the values of the critical exponent calculated taking dynamic screening into account were in good agreement with those obtained from, say, an orthogonalized plane-wave pseudopotential (see Table III). This suggests that the ND prediction of the critical exponent and the ω dependence of the generalized power law in the threshold region will persist even if the correlation effects are fully taken into account somehow.

Evidently this reflects the success of the Fermi-liquid theory in describing the dynamics near the Fermi level. We saw that the exact solution could be given solely in terms of the product of the differences between the unperturbed energy ε_m and perturbed energy ε_μ [see Eqs. (7.12) and (7.13) or Eq. (8.37) with Eqs. (7.8) and (7.9); see also Sec. VIII.E]. The point is that the critical exponent is determined by the factor $1/(\varepsilon_\mu - \varepsilon_m)$, with both ε_μ and ε_m near the Fermi energy. The important quantity here is how much ε_μ is shifted from ε_m by the core-hole attraction. We know that in normal Fermi liquids the en-

ergy shift near the Fermi level is properly expressed by the phase shift, or the eigenphase shift of the S matrix, which fully incorporates the correlation effect (Langer and Ambegaokar, 1961). Thus, even if the correlation is taken into account, the key role of the factor $1/(\varepsilon_\mu - \varepsilon_m)$ with $\varepsilon_\mu, \varepsilon_m \simeq 0$ and the expression of the critical exponent in terms of phase shifts will remain valid, only if we regard the phase shifts to be those of quasiparticles. Here we note that the conclusion is drawn from the Fermi-liquid picture not only in the ground but also in the excited configuration with the help of the expressions involved in the exact solution. In the context of, for example, a perturbation treatment of the core-hole potential in terms of initial-state bases, it is rather hard to derive this conclusion because the role of the states of the excited configuration is unclear in building up the infrared peak, and it is impossible in this treatment to construct a state near the Fermi level in the excited configuration without having the ground-configuration states far away from the Fermi level, where the Fermi-liquid picture breaks down.

As the second effect of correlation on the edge spectrum, let us consider the critical amplitude. The factors $(\varepsilon_\mu - \varepsilon_m)$ with a large energy separation are equally important in the critical amplitude, as is obvious in Eq. (9.52) with Eq. (8.3), which involves the integral of the phase shift over the entire conduction band. This means that the critical amplitude will necessarily be affected by the breakdown of the Fermi-liquid picture away from the edge. In fact, we know that in the simple case of core-hole-boson interaction the intensity of a zero-boson line (i.e., the intensity near the edge) is governed by the sum rule for the intensity over the entire absorption band (Mahan, 1975). Therefore, if the intensity of multiboson satellites increases, the intensity of the zero line decreases accordingly. The effect is usually described by the Debye-Waller factor. The vanishing overlap between many-body ground states described by the orthogonality theorem is, in other words, an indirect indication of the strength of the excitation away from the edge (Kotani, 1987). By the reasoning given above we are sure that the exponent of the orthogonality theorem remains valid, while the amplitude, whose exact form of the MND model is given in Sec. IX, will be affected by the correlation. The Debye Waller factor estimated in the cumulant expansion approximation will provide a good estimate of the change due to the correlation. According to Hedin *et al.* (1971), the intensity of the zero line of photoemission in simple metals is reduced by 30% to 50% depending upon the value of the parameter r_s . In the two-dimensional case of the GaAs heterojunction analyzed in Sec. X, we have seen that the reduction is estimated to be 40%.

The validity of the ND expression for the critical exponent even in the presence of the correlation effect was indicated in the paper by Vendrinskii and Richter (1972) and shown by Yamada and Yosida in the case of the orthogonality theorem discussed in Sec. V. If we have no

recourse to the quasi-boson approximation or to a lowest-order cumulant approximation, it is interesting to consider how the critical amplitude is modified by the correlation. Experimentally, there seem to be no data that indicate unambiguously the effect of correlation upon the critical amplitude. Obviously this is due only to the difficulty of measuring the absolute intensity of the spectrum.

XIII. SUMMARY

This article deals with soft-x-ray absorption and emission problems, concentrating on the theoretical developments after Mahan's paper, which related for the first time the observed edge anomalies to the final-state interaction. In reviewing the topic, we have restricted ourselves to problems related to infrared divergence in simple metals. Subjects such as the effect of electronic correlation on the x-ray spectra and the final-state interaction involving a d or f level in the excited configuration were mostly omitted. One justification for these omissions is that extensive review articles are available by Almladh and Hedin (1983) on the correlation effect and by Kotani and Toyozawa (1979) and Kotani (1987) on the problem of an incomplete d or f shell. Another reason is the fact that treatments of the latter topic which take into account the electronic correlation are now under development (Müller *et al.*, 1982; Gunnarsson and Schönhammer, 1983; Fujimori and Minami, 1984; Jo and Kotani, 1988; Bianconi *et al.*, 1989). In any case, neither of these topics seems to have much to do with the infrared divergence in the x-ray problem.

In the first half of this article (Secs. II and III) a historical survey is given, and in the second half (Secs. IV–XI) recent work of the present authors is outlined.

The theory of the soft-x-ray problem was first addressed twenty years ago by the pioneering work of Mahan. Through the use of the MND Hamiltonian, the nature of the infrared divergence has since been clarified. Before the papers of the present authors, several exact results had already been derived separately by the application of several different techniques. We can cite as examples the critical exponents found by Nozières and DeDominicis and by Combescott and Nozières, the orthogonality theorem as given by Anderson, the critical amplitude for photoemission proposed by Feldkamp and Davis, several generalizations accomplished by Yamada and Yosida of the orthogonality theorem, the pairwise series expansion obtained by Mahan, and so on. We have completed or generalized some of these topics here from a unified point of view. For example, we have given analytical expressions for the prefactor of the orthogonality theorem and for the critical amplitudes of XAS and XES; we have provided a rigorous proof of the proposed form for the critical amplitude for photoemission; we have analyzed the convergence of the pairwise series, etc. As to other topics, we have added new information on

the separate contributions of the main and secondary bands with respect to the critical amplitudes and integrated intensities. We have also treated fully the effect of temperature on the infrared divergence and obtained frequency-dependent exponents of the generalized power law, which reproduce almost exactly the true spectra over a very wide frequency range.

As many authors have pointed out with regard to the value of the critical exponents, comparison of the theoretical predictions with experiment has been a difficult task, because a number of factors neglected in the MND model inevitably affect the spectra in actual situations. Recent discovery of an edge peak in artificially fabricated materials appears to have aroused a renewed interest in the edge problem. According to the analysis made in the literature, these materials offer a near-ideal medium in which to explore the problem. Since the theoretical aspects of the edge problem are not simple, we hope the present review will be of some help to those interested in undertaking new optical experiments.

ACKNOWLEDGMENTS

The authors gratefully thank Professor T. Ishii for valuable information on the experimental side of the soft-x-ray edge problem.

REFERENCES

- Aitken, A. C., 1964, *Determinants and Matrices* (Interscience, New York), p. 97.
- Almladh, C.-O., 1977a, *Solid State Commun.* **22**, 339.
- Almladh, C.-O., 1977b, *Phys. Rev. B* **16**, 4343.
- Almladh, C.-O., and L. Hedin, 1983, in *Handbook on Synchrotron Radiation*, edited by E.-E. Koch (North-Holland, Amsterdam), Vol. 1b, p. 607.
- Almladh, C.-O., and P. Minnhagen, 1978a, *Phys. Rev. B* **17**, 929.
- Almladh, C.-O., and P. Minnhagen, 1978b, *Phys. Status Solidi B* **85**, 135.
- Almladh, C.-O., and U. von Barth, 1976, *Phys. Rev. B* **13**, 3307.
- Anderson, P. W., 1967a, *Phys. Rev. Lett.* **18**, 1049.
- Anderson, P. W., 1967b, *Phys. Rev.* **164**, 352.
- Anderson, P. W., and G. Yuval, 1969, *Phys. Rev. Lett.* **23**, 89.
- Anderson, P. W., G. Yuval, and D. R. Hamann, 1970, *Phys. Rev. B* **1**, 4464.
- Ausman, G. A., and A. J. Glick, 1969, *Phys. Rev.* **183**, 687.
- Azóroff, L. V., 1974, Ed., *X-ray Spectroscopy* (McGraw-Hill, New York), p. 1.
- Bassani, F., and M. Altarelli, 1983, in *Handbook in Synchrotron Radiation*, edited by E.-E. Koch (North-Holland, Amsterdam), Vol. 1a, p. 463.
- Bauer, G. E., and T. Ando, 1985, *Phys. Rev. B* **31**, 8321.
- Bianconi, A., T. Miyahara, A. Kotani, Y. Kitajima, T. Yokoyama, H. Kuroda, M. Funabashi, and A. Arai, 1989, *Phys. Rev. B* **39**, 3380.
- Brown, F. C., 1975, in *Solid State Physics*, edited by H. Ehren-

- reich, F. Seitz, and D. Turnbull (Academic, New York), Vol. 29, p. 1.
- Brown, G. S., 1980, in *Synchrotron Radiation Research*, edited by H. Winick and S. Doniach (Plenum, New York), p. 61.
- Brown, G. S., and S. Doniach, 1980, in *Synchrotron Radiation Research*, edited by H. Winick and S. Doniach (Plenum, New York), p. 353.
- Bryant, G. W., 1979, *Phys. Rev. B* **19**, 2801.
- Bryant, G. W., and G. D. Mahan, 1978, *Phys. Rev. B* **17**, 1744.
- Callcott, T. A., E. T. Arakawa, and D. L. Ederer, 1978, *Phys. Rev. B* **18**, 6622.
- Chang, Y. C., and G. D. Sanders, 1985, *Phys. Rev. B* **32**, 5521.
- Citrin, P. H., G. K. Wertheim, and Y. Baer, 1975, *Phys. Rev. Lett.* **35**, 885.
- Citrin, P. H., G. K. Wertheim, and M. Schlüter, 1979, *Phys. Rev. B* **20**, 3067.
- Combescott, M., and P. Nozières, 1971, *J. Phys. (Paris)* **32**, 913.
- Compton, A. H., and S. K. Allison, 1935, *X-rays in Theory and Experiment*, 2nd ed. (D. van Nostrand, New York), p. 1.
- Courant, R., and D. Hilbert, 1966, *Methods of Mathematical Physics* (Wiley, New York), Vol. 1, p. 112.
- Cox, D. L., H. O. Froto, L. N. Oliveira, and J. W. Wilkins, 1985, *Phys. Rev. B* **32**, 555.
- Davis, L. C., and L. A. Feldkamp, 1981, *Phys. Rev. B* **23**, 4269.
- Doniach, S., P. M. Platzman, and J. T. Yue, 1971, *Phys. Rev. B* **4**, 3345.
- Doniach, S., and M. Sunjić, 1970, *J. Phys. C* **3**, 285.
- Dow, J. D., 1975, *Comments Solid State Phys.* **6**, 71.
- Dow, J. D., and C. P. Flynn, 1980, *J. Phys. C* **13**, 1341.
- Dow, J. D., J. E. Robinson, J. H. Slowik, and B. F. Sonntag, 1974, *Phys. Rev. B* **10**, 432.
- Dow, J. D., and B. Sonntag, 1973, *Phys. Rev. Lett.* **31**, 1461.
- Feldkamp, L. A., and L. C. Davis, 1980, *Phys. Rev. B* **22**, 4994.
- Ferrel, R. A., 1969, *Phys. Rev.* **186**, 339.
- Flynn, C. P., 1976, *Phys. Rev. Lett.* **37**, 1445.
- Fowler, R. H., 1936, *Statistical Mechanics*, 2nd ed. (Cambridge University Press, Cambridge, England), p. 36.
- Friedel, J., 1952, *Philos. Mag.* **43**, 153.
- Friedel, J., 1954, *Adv. Phys.* **3**, 446.
- Friedel, J., 1969, *Comments Solid State Phys.* **2**, 21.
- Fujimori, A., and F. Minami, 1984, *Phys. Rev. B* **30**, 957.
- Fumi, F. G., 1955, *Philos. Mag.* **46**, 1007.
- Gell-Mann, M., and F. Low, 1951, *Phys. Rev.* **84**, 350.
- Grebennikov, V. I., Yu. A. Babanov, and O. B. Sokolov, 1977a, *Phys. Status Solidi B* **79**, 423.
- Grebennikov, V. I., Yu. A. Babanov, and O. B. Sokolov, 1977b, *Phys. Status Solidi B* **80**, 73.
- Gunnarsson, O., and K. Schönhammer, 1983, *Phys. Rev. B* **28**, 4315.
- Hamann, D. R., 1971, *Phys. Rev. Lett.* **26**, 1030.
- Hänsch, W., and W. Ekardt, 1981, *Phys. Rev. B* **24**, 5497.
- Hänsch, W., and P. Minnhagen, 1982, *Phys. Rev. B* **26**, 2772.
- Hedin, L., 1974, in *X-ray Spectroscopy*, edited by L. V. Azároff (McGraw-Hill, New York), p. 226.
- Hedin, L., B. I. Lundqvist, and S. Lundqvist, 1971, in *Electronic Density of States*, edited by L. H. Bennet, NBS Spec. Publ. No. 323 (U.S. GPO, Washington, D.C.), p. 233.
- Hedin, L., and A. Rosengren, 1977, *J. Phys. F* **7**, 1339.
- Hopfield, J. J., 1969, *Comments Solid State Phys.* **2**, 40.
- Ishii, T., 1990, private communication.
- Ishii, T., Y. Sakisaka, S. Yamaguchi, T. Hanyu, and H. Ishii, 1977, *J. Phys. Soc. Jpn.* **42**, 876.
- Ishikawa, K., Y. Ohmura, and Y. Mizuno, 1973, *J. Phys. Soc. Jpn.* **34**, 324.
- Jo, T., and A. Kotani, 1988, *Phys. Rev. B* **38**, 830.
- Kaga, H., 1977, *J. Phys. Soc. Jpn.* **43**, 1144.
- Kita, T., 1987, *J. Phys. Soc. Jpn.* **56**, 387.
- Kita, T., K. Ohtaka, and Y. Tanabe, 1987a, *J. Phys. Soc. Jpn.* **56**, 387.
- Kita, T., K. Ohtaka, and Y. Tanabe, 1987b, *J. Phys. Soc. Jpn.* **56**, 4609.
- Kleinmann, D. A., and R. C. Miller, 1985, *Phys. Rev. B* **32**, 2266.
- Kondo, J., 1984a, *Physica B* **125**, 279.
- Kondo, J., 1984b, *Physica B* **126**, 377.
- Kondo, J., 1988, in *Fermi Surface Effects*, edited by J. Kondo and A. Yoshimori (Springer, Berlin), p. 1.
- Kotani, A., 1987, in *Handbook on Synchrotron Radiation*, edited by G. V. Marr (North-Holland, Amsterdam), Vol. 2, p. 611.
- Kotani, A., and Y. Toyozawa, 1973a, *J. Phys. Soc. Jpn.* **35**, 1073.
- Kotani, A., and Y. Toyozawa, 1973b, *J. Phys. Soc. Jpn.* **35**, 1082.
- Kotani, A., and Y. Toyozawa, 1974, *J. Phys. Soc. Jpn.* **37**, 912.
- Kotani, A., and Y. Toyozawa, 1979, in *Synchrotron Radiation*, edited by C. Kunz (Springer, Berlin), p. 169.
- Langer, J. S., and V. Ambegaokar, 1961, *Phys. Rev.* **121**, 1090.
- Langreth, D. C., 1970, *Phys. Rev. B* **1**, 471.
- Lee, J. S., Y. Iwasa, and N. Miura, 1987a, *Semicond. Sci. Technol.* **2**, 675.
- Lee, J. S., Y. Iwasa, and N. Miura, 1987b, *Solid State Commun.* **64**, 597.
- Lee, J. S., N. Miura, and Y. Iwasa, 1988, *Surf. Sci.* **196**, 534.
- Ley, L., F. R. McFeely, S. P. Kowalczyk, J. G. Jenkin, and D. A. Shirley, 1975, *Phys. Rev. B* **11**, 600.
- Lloyd, P., 1967, *Proc. Phys. Soc. London* **90**, 207.
- Madden, R. P., 1974, in *X-ray Spectroscopy*, edited by L. V. Azároff (McGraw-Hill, New York), p. 338.
- Mahan, G. D., 1967a, *Phys. Rev.* **153**, 882.
- Mahan, G. D., 1967b, *Phys. Rev.* **163**, 612.
- Mahan, G. D., 1975, in *Solid State Physics*, edited by H. Ehrenreich, F. Seitz, and D. Turnbull (Academic, New York), Vol. 29, p. 771.
- Mahan, G. D., 1977, *Phys. Rev. B* **15**, 4587.
- Mahan, G. D., 1980, *Phys. Rev. B* **21**, 1421.
- Mahan, G. D., 1981, *Many-Particle Physics* (Plenum, New York), p. 771.
- Mahan, G. D., 1982, *Phys. Rev. B* **25**, 5021.
- Mahan, G. D., 1988, in *Fermi Surface Effects*, edited by J. Kondo and A. Yoshimori (Springer, Berlin), p. 41.
- Miller, R. C., and D. A. Kleinman, 1985, *J. Lumin.* **30**, 520.
- Minnhagen, P., 1976, *Phys. Lett. A* **56**, 327.
- Minnhagen, P., 1977, *J. Phys. F* **7**, 2441.
- Miyahara, T., S. Sato, T. Hanyu, A. Kakizaki, S. Yamaguchi, and T. Ishii, 1980, *J. Phys. Soc. Jpn.* **49**, 194.
- Mizuno, Y., and K. Ishikawa, 1968, *J. Phys. Soc. Jpn.* **25**, 627.
- Müller, J. E., O. Jepsen, and J. W. Wilkins, 1982, *Solid State Commun.* **42**, 365.
- Muskhelishvili, N. I., 1953, in *Singular Integral Equations*, edited by J. M. R. Radok (Noordhoff, Groningen), p. 1.
- Neddermeyer, H., 1976, *Phys. Rev. B* **13**, 2411.
- Nishimura, K., and K. Ohtaka, 1989, unpublished.
- Nozières, P., and C. T. DeDominicis, 1969, *Phys. Rev.* **178**, 1097.
- Nozières, P., J. Gavoret, and B. Roulet, 1969, *Phys. Rev.* **178**, 1084.
- Oguchi, A., and K. Yosida, 1986, *Prog. Theor. Phys.* **75**, 1048.
- Ohmura, Y., 1981, *J. Phys. Soc. Jpn.* **50**, 1807.

- Ohmura, Y., and K. Ishikawa, 1973, *Bull. Tokyo Institute of Technology* **114**, 1.
- Ohmura, Y., and K. Ishikawa, 1980a, *J. Phys. Soc. Jpn.* **48**, 1176.
- Ohmura, Y., and K. Ishikawa, 1980b, *J. Phys. Soc. Jpn.* **49**, 1829.
- Ohmura, Y., K. Ishikawa, and Y. Mizuno, 1974, *J. Phys. Soc. Jpn.* **36**, 370.
- Ohmura, Y., and A. Ogiwara, 1989, *J. Phys. Soc. Jpn.* **58**, 4635.
- Ohmura, Y., and H. Sano, 1977, *J. Phys. Soc. Jpn.* **43**, 875.
- Ohtaka, K., and Y. Tanabe, 1983, *Phys. Rev. B* **28**, 6833.
- Ohtaka, K., and Y. Tanabe, 1984, *Phys. Rev. B* **30**, 4235.
- Ohtaka, K., and Y. Tanabe, 1986, *Phys. Rev. B* **34**, 3717.
- Ohtaka, K., and Y. Tanabe, 1989, *Phys. Rev. B* **39**, 3054.
- Oliveira, L. N., 1981, Ph.D. thesis (Cornell University).
- Oliveira, L. N., and J. W. Wilkins, 1981, *Phys. Rev. B* **24**, 4863.
- Oliveira, L. N., and J. W. Wilkins, 1985, *Phys. Rev. B* **32**, 696.
- Onodera, Y., 1975, *J. Phys. Soc. Jpn.* **39**, 1482.
- Paratt, L. G., 1959, *Rev. Mod. Phys.* **31**, 616.
- Pardee, W. J., and G. D. Mahan, 1973, *Phys. Lett. A* **45**, 117.
- Penn, D. R., S. M. Girvin, and G. D. Mahan, 1981, *Phys. Rev. B* **24**, 6971.
- Richtmeyer, R. D., 1936, *Phys. Rev.* **49**, 1.
- Ritsko, J. J., S. E. Schnatterly, and P. C. Gibbons, 1974, *Phys. Rev. B* **10**, 5017.
- Rivier, N., and E. Simanek, 1971, *Phys. Rev. Lett.* **26**, 435.
- Rorison, J. M., 1987, *J. Phys. C* **20**, L311.
- Roulet, B., J. Gavoret, and P. Nozières, 1969, *Phys. Rev.* **178**, 1072.
- Schmitt-Rink, S., C. Ell, and H. Haug, 1986, *Phys. Rev. B* **33**, 1183.
- Schönhammer, K., and O. Gunnarsson, 1977, *Solid State Commun.* **23**, 691.
- Schönhammer, K., and O. Gunnarsson, 1978a, *Solid State Commun.* **26**, 399.
- Schönhammer, K., and O. Gunnarsson, 1978b, *Solid State Commun.* **26**, 147.
- Schönhammer, K., and O. Gunnarsson, 1978c, *Z. Phys. B* **30**, 297.
- Schönhammer, K., and O. Gunnarsson, 1978d, *Phys. Rev. B* **18**, 6606.
- Schotte, K. D., and U. Schotte, 1969, *Phys. Rev.* **182**, 479.
- Schotte, K. D., and U. Schotte, 1971, *Phys. Rev. B* **4**, 2228.
- Skolnick, M. S., J. M. Rorison, K. J. Nash, D. J. Mowbray, P. R. Tapster, S. J. Bass, and A. D. Pitt, 1987a, *Phys. Rev. Lett.* **58**, 2130.
- Skolnick, M. S., K. J. Nash, D. J. Mowbray, P. R. Tapster, S. J. Bass, and A. D. Pitt, 1987b, *Phys. Rev. B* **35**, 5925.
- Skolnick, M. S., J. M. Rorison, K. J. Nash, and S. J. Bass, 1988, *Surf. Sci.* **196**, 507.
- Slusky, S. G., P. C. Gibbons, S. E. Schnatterly, and J. R. Fields, 1976, *Phys. Rev. Lett.* **36**, 326.
- Slusky, S. G., S. E. Schnatterly, and P. C. Gibbons, 1979, *Phys. Rev. B* **20**, 379.
- Smirnov, V. I., 1965, *A Course of Higher Mathematics* (Addison-Wesley, Reading, Mass.), Vol. IV, p. 1.
- Swarts, C. A., J. D. Dow, and C. P. Flynn, 1979, *Phys. Rev. Lett.* **43**, 158.
- Tanabe, Y., 1986, *Phys. Rev. B* **33**, 2806.
- Tanabe, Y., and K. Ohtaka, 1984, *Phys. Rev. B* **29**, 1653.
- Tanabe, Y., and K. Ohtaka, 1985, *Phys. Rev. B* **32**, 2036.
- Tanabe, Y., and K. Ohtaka, 1986, *Phys. Rev. B* **33**, 2806.
- Tombouliau, D. H., 1957, in *Handbuch der Physik*, (Springer, Berlin/Göttingen/Heidelberg) **30**, 246.
- Tombouliau, D. H., and P. L. Hartman, 1956, *Phys. Rev.* **102**, 1423.
- Vendrinskii, R. V., and J. Richter, 1972, *Izv. Akad. Nauk SSSR, Ser. Fiz.* **36**, 339.
- von Barth, U., and G. Grossmann, 1979, *Solid State Commun.* **32**, 645.
- von Barth, U., and G. Grossmann, 1982, *Phys. Rev. B* **25**, 5150.
- Watson, K. M., 1954, *Phys. Rev.* **95**, 228.
- Wentzel, G., 1925a, *Z. Phys.* **31**, 445.
- Wentzel, G., 1925b, *Z. Phys.* **34**, 730.
- Wertheim, G. K., and P. H. Citrin, 1978, in *Photoemission in Solids*, Topics in Applied Physics, No. 26, edited by M. Cardona and L. Ley (Springer, Berlin), p. 197.
- Wilkins, J. W., 1982, in *X-ray and Atomic Inner-Shell Physics*, AIP Conference Proceedings No. 94, edited by B. Crasemann (AIP, New York), p. 687.
- Yamada, K., 1984, *Prog. Theor. Phys.* **72**, 195.
- Yamada, K., 1986, *Prog. Theor. Phys.* **75**, 1044.
- Yamada, K., A. Sakurai, and S. Miyazima, 1985, *Prog. Theor. Phys.* **73**, 1342.
- Yamada, K., A. Sakurai, and M. Takeshige, 1983, *Prog. Theor. Phys.* **70**, 73.
- Yamada, K., and K. Yosida, 1978a, *Prog. Theor. Phys.* **59**, 1061.
- Yamada, K., and K. Yosida, 1978b, *Prog. Theor. Phys.* **60**, 353.
- Yamada, K., and K. Yosida, 1979, *Prog. Theor. Phys.* **62**, 363.
- Yamada, K., and K. Yosida, 1982, *Prog. Theor. Phys.* **68**, 1504.
- Yoshimori, A., and A. Okiji, 1977, *Phys. Rev. B* **16**, 3838.
- Yosida, K., and A. Yoshimori, 1973, in *Magnetism*, edited by H. Suhl (Academic, New York), Vol. V, p. 253.
- Yuval, G., and P. W. Anderson, 1970, *Phys. Rev. B* **1**, 1522.